DISCLAIMER:

This document does not meet the
current format guidelines of
the Graduate School at
The University of Texas at Austin.

It has been published for
informational use only.

The Thesis Committee for Soros Chitsiripanich
Certifies that this is the approved version of the following thesis:

Field Application of Capacitance-Resistance Models to Identify Potential Location for Infill Drilling

APPROVED BY
SUPERVISING COMMITTEE:

Supervisor:

Larry W. Lake

Sanjay Srinivasan

Field Application of Capacitance-Resistance Models to Identify Potential Location for Infill Drilling

by

Soros Chitsiripanich, B.E.

Thesis

Presented to the Faculty of the Graduate School of

The University of Texas at Austin

in Partial Fulfillment

of the Requirements

for the Degree of

Master of Science in Engineering

The University of Texas at Austin

May 2015

Acknowledgements

Foremost, I would like to acknowledge PTT Exploration and Production Plc. (PTTEP) for granting me the scholarship to pursue my interest in petroleum engineering. The opportunity to study here at the University of Texas at Austin fully equipped me with the skills necessary to advance my career and broaden my perspectives to achieve my academic goals.

The first individual that I would like to express my sincere gratitude to is my advisor, Dr. Larry W. Lake. I owe a debt of gratitude to him for his persistent supervision, useful advice, and motivation. It has been an honor and pleasure to know and to work with the distinguished professor and petroleum engineer like him. I deeply appreciate his time and effort reviewing the thesis. Besides my advisor, I would like to thank my thesis committee: Dr. Sanjay Srinivasan for his insightful comments.

My sincere thanks also go to Fei Cao for her support on the way. Without her helpful advice especially in the application of the Capacitance-Resistance Model to field data, I would not have successfully completed this research. In addition, I would like to thank Mr. Emilio Nunez and staff of the Petroleum and Geosystems Engineering Department at the University of Texas at Austin for providing me with all the necessary facilities for the research for their help and support. Thanks are also due to General Algebraic Modeling System (GAMS) Development Corporation and Computer Modeling Group (CMG) for providing the software used in this research.

Last but not least, I am grateful for the love and support of my family and friends who have supported me throughout entire process, both by keeping me harmonious and helping me putting pieces together.

Abstract

Field Application of Capacitance-Resistance Models to Identify Potential Location for Infill Drilling

Soros Chitsiripanich, M.S.E.

The University of Texas at Austin, 2015

Supervisor: Larry W. Lake

A significant amount of bypassed oil often remains in a mature waterflooded reservoir because of non-uniform sweep. Infill drilling is one of the most attractive options to increasing oil recovery in consequence of its operational simplicity, low risk and promising results. Targeting proper infill location is a complex task and conventionally requires a comprehensive reservoir characterization program such as the streamline simulation (SLS). Achieving a good and reliable model, however, requires massive effort. This inspired the establishment of an alternative method, the Capacitance-Resistance Model (CRM), which is fast, cheap, yet robust.

The CRM was applied to an oil field in Southeast Asia, leading to the identification of several key challenges and the emphasis of the input data examination. These challenges are field operations, existence of free gas, and unavailability of flowing bottomhole pressures, in which all of them cause the violation to the CRM assumption and will be addressed appropriately. In addition, this is the first time that the two-phase flow coupled CRM was used with field data. The key additional input required by this

model is the reservoir pore volume associated with each producer, which is determined from matching each well's historical water cut with Koval's equation. Nevertheless, dealing with field data is more complicated as the trend often did not follow the theory because of early water breakthrough in a thief zone or poorly managed waterflood.

The results indicated that the CRM is able to give a good fit for both field and well levels. The quality of well by well matching seems to depend on the available number of data points of that well as all wells with low r-square values have very limited available data for matching. The gain results also reveal the good efficiency of the waterflood strategy as there are only 2 injectors having injection loss. It can also be geologically inferred from the gain that the field is anisotropic; there is no obvious preferential flow path in any specific direction. Moreover, field evidence such as the tracer tests, the RFT pressures and the wells' production history support the CRM results.

The hypothesis made for the identification of the potential infill locations is that areas with low normalized gain, high oil saturation and high pore volume are attractive for new infill producers. This was successfully validated with the actual infill wells' performance of this field. The combination of maps consisting of the connectivity, the saturation, the thickness, the porosity and the permeability maps, are analyzed simultaneously to see whether the potential areas identified by them correspond with the performance of the infill wells.

Generally, the integrated examination of these data is theoretically expected to help locate the bypassed oil and provide an insight to the reservoir characterization and the waterflood performance. However, it was observed with this set of field data that using more properties actually does not guarantee a more accurate result, especially when there are some properties that considerably mislead the interpretation. All in all, the combination of the relevant input parameters should increase the accuracy because they

help each other to mitigate the errors caused from a single parameter. In other word, the potential area needs to have both poor reservoir continuity and good rock quality so that it is likely to yield a satisfying infill performance.

Table of Contents

List of Tables

List of Figures

Chapter 1: Introduction

1.1 Problem Statement

A significant amount of bypassed oil often remains in a mature waterflooded reservoir. This is attributed to non-uniform sweep because of natural complexities of a reservoir including heterogeneity, poor continuity, permeability and porosity variations. Infill drilling is considered to be one of the most attractive options to increasing oil recovery because of its operational simplicity, low risk and promising results. According to Driscoll (1974), the important mechanisms that provided incremental recovery, which are easily defined but very difficult to evaluate in a real field situation, can be classified as improved reservoir continuity, and improved areal and vertical sweep efficiency.

Targeting proper infill locations requires a comprehensive reservoir characterization program integrating both geological and engineering data to identify areas with a large volume of remaining mobile oil-in-place and good reservoir properties. Streamline simulation (SLS) has been used extensively for this purpose. Its strengths are the ability to quantify the distribution of injected water to associated producers and the amount of oil produced because of each supporting injector. Combined with a good reservoir description, SLS allows heterogeneities to be handled appropriately and thus it can model fluid flow and displacement accurately. This information is used to determine volumetric sweep efficiency in each region throughout the field so that the poorly swept and drained areas can be identified.

Despite encouraging and robust output obtained from SLS, achieving a good and reliable model requires massive effort. Firstly, detailed rock and fluid properties must be modeled every part of the reservoir; few of these are clearly known. Therefore, multiple realizations of both static and dynamic models must be constructed to capture

uncertainty. In addition, history matching, which is part of the SLS process, is an exhausting task that is frequent non-unique because of the uncertain nature of subsurface data. Particularly for a field with long production history and many wells, the simulation is expensive and time-consuming. Consequently, SLS might not be practically applicable and it is necessary to look for a fast, cheap yet robust approach to identify a highly probable infill location.

The capacitance-resistance model (CRM) is a potential alternative method for this purpose. The model was developed by considering material balance combined with Darcy's flow equations. It is based on a multi-linear regression technique solving for interwell connectivity, which makes it a point-to-point model. It does not require three-dimensional geological and reservoir engineering models. Primary inputs are only the well production and injection rates, which are generally available for any oil field. The model is computationally fast and relatively cost-effective compared to finite difference reservoir simulation. Despite its simplicity, the model's capability to characterize the reservoir has been successfully validated by several researchers (i.e. Yousef, 2006; Sayarpour, 2008; Weber, 2009; Nguyen, 2012; Cao, 2014).

This research focuses on applying the CRM to a mature waterflooded field in Southeast Asia, validating the results with field evidence and measurements, evaluating the results for targeting infill locations and checking using the actual performances of infill wells drilled in this field. In addition, the secondary task of this work is to attempt to estimate interwell permeability from one of the output from CRM, the time constant.

1.2 Objectives

The objectives of this research are as follows:

1. To identify key challenges in applying the CRM to actual field data and address them properly
2. To evaluate the effectiveness of CRM for characterizing a reservoir by validating the results with field evidences and measurements.
3. To initiate a new method of using CRM output combined with reservoir properties distribution maps to determine potential location for infill producers.
4. To analyze the relationship between the CRM time constant and interwell permeability.

1.3 Outline

This thesis consists of 5 chapters.

Chapter 1 is the introduction that describes the background and motivation of this research.

Chapter 2 is the literature review focusing on the development and application of both the original and the coupled CRM, the factors contributing to incremental recovery after infill drilling, the use of SLS to determine infill location and the relationship between SLS and CRM.

Chapter 3 discusses the field application of the original and the coupled CRM to a Southeast Asian oil field and the validation of the results.

Chapter 4 presents a novel method of using the CRM to identify proper infill drilling locations. The validation of this method is determined by actual performances of the infill wells drilled in this field.

Chapter 5 provides conclusions and recommendation for future work.

Chapter 2: Literature Review

The background of previous research and traditional practices related to the work in this thesis are discussed here. This work studies the feasibility of using the Capacitance- Resistance Model (CRM) as a key reservoir engineering tool to characterize reservoir connectivity and evaluate waterflood performance. Ultimately, once the reservoir is better understood, infill locations will be identified. Therefore, the literature related to this research is divided into 2 parts. Firstly, the CRM will be explained including a summary of the development, theory and application in characterizing reservoirs.

The second section of this chapter presents the general ideas and how the infill locations have been identified conventionally. Application of streamline simulation (SLS) will be the main focus here as the technique has been widely used and related to the CRM.

2.1 THE CAPACITANCE-RESISTANCE MODEL (CRM)

The Capacitance- Resistance Model (CRM) is a signal processing tool that takes injection and production rates as an input and output, and uses a multivariate nonlinear regression to analyze the relationship between them and determine model parameters. Its fundamental equations are derived from the continuity principle combined with Darcy's law. It is based on some assumptions such as two-component immiscible displacement, stabilized flow, constant productivity index, no aquifer and slightly compressible fluids. Practically, many mature waterflood fields can satisfy these assumptions. Therefore, the CRM is a data-driven model that is based on analytical principles.

While traditional finite-difference simulation requires constructing three-dimensional static and dynamic models, the CRM, a point-to-point model, does not require estimation of physical reservoir properties. It automatically history-matches the rate data using a nonlinear programming (NLP) optimization algorithm, which is relatively fast, inexpensive and effortless compared to the traditional simulation. Two types of model parameters, gains and time constants are obtained as output that characterizes waterflood reservoirs. The gains or connectivities (see Figure 2.2) quantify the communications between each injector-producer pair while the time constants represent attenuation and dissipation of the injection signal traveling through the reservoir before arriving at producers. The latter indicates the effect of compressibility, pore volume and productivity index of a reservoir control volume of that pair. Figure 2.1 below is a diagram representing an overview of the CRM.

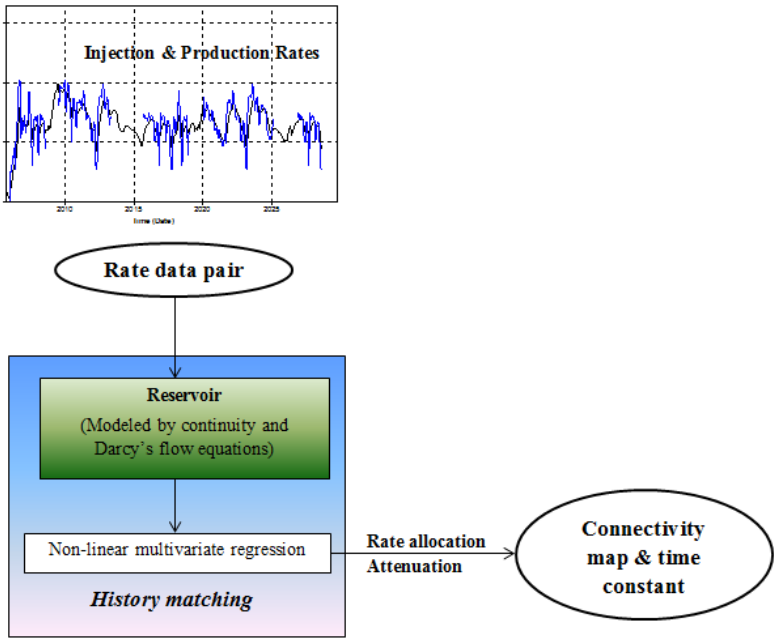

Figure 2.1 Overview of the CRM

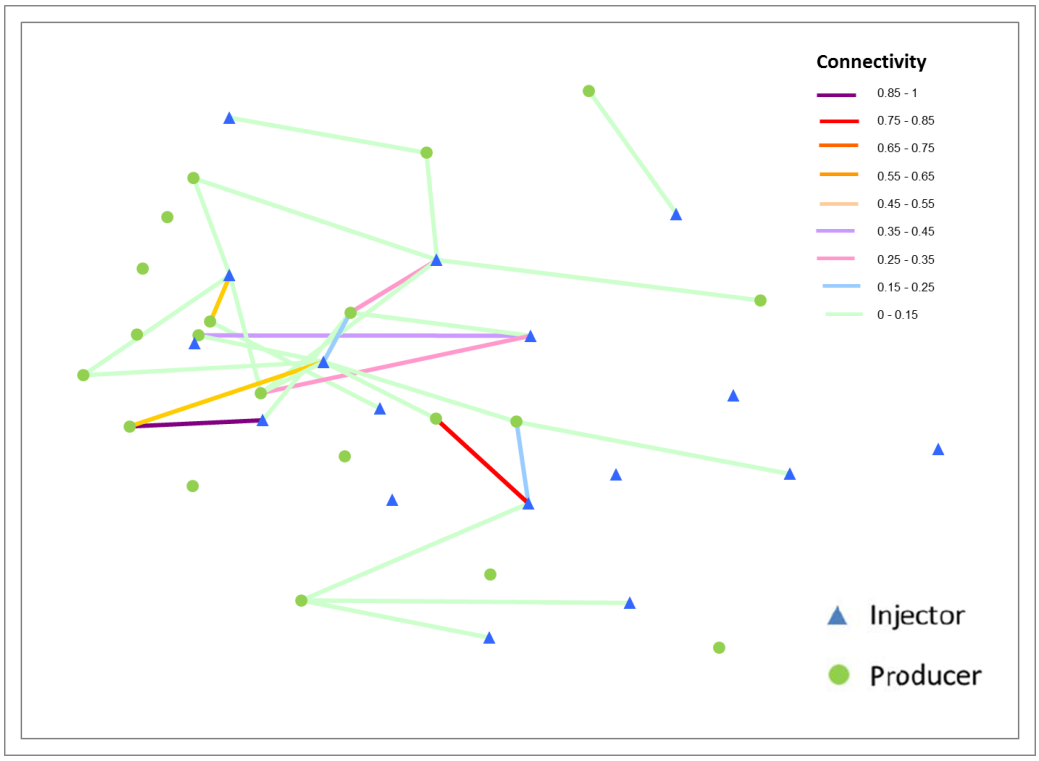

Figure 2.2 Example of connectivity map obtained from CRM analysis

2.1.1 Background and History

Early works that introduced the concept of capacitor-resistor network to reservoir flow modeling could be traced back to the 1940s. At that time, these works concentrated on constructing real electrical networks to represent oil reservoirs. Recently in 2003, a mathematical model that adopts the same analogy was firstly proposed by Albertoni and Lake. The main idea is to infer an inter-well connectivity from injection and production rate fluctuations using multivariate linear regression (MLR) with diffusivity filters to account for dissipation of a signal while traveling through a reservoir. Gentil (2005) explained a physical relationship between the CRM connectivity and reservoir transmissibility.

Yousef (2006) significantly advanced the existing model by incorporating the material balance concept. He analytically derived the CRM from the continuity equation and solved the problem by numerical integration. He proposed a new complete model that includes the effects of both compressibility and transmissibility. The diffusivity filters were replaced by intrinsic filters, which introduced time constants, accounting for time lag and attenuation between wells. He also extended the model to account for fluctuating bottom-hole pressures. The model was successfully validated with both synthetic and actual field data.

Instead of a numerical solution, Sayarpour (2008) further improved the CRM by analytically integrating the differential equations of the CRM using superposition in time. He developed solutions for three different control volumes, a single tank (CRMT), a producer-based (CRMP) and a well pair-based (CRMIP) drainage volume. The analytical solution is simpler than the numerical one previously proposed by Yousef and, thus, results in faster computational time. This makes the model much more practical when applying to actual field data, especially with many data points. He also firstly applied the model, combined with an oil fractional flow model, to optimize oil production by manipulating injection rates. For the study purpose of this work, CRMP is the most appropriate form to be used, together with CRMIP. Their detailed equations will be described in the following section.

Weber (2009) continued Sayarpour's work by applying the analytical solutions of the CRM to large fields. He introduced algorithms that make the technique practical such as outlier classification, data cleaning and model parameters reduction. Additionally, the CRM was extended to apply in the time period before water breakthrough, i.e. immature waterflood, and a reservoir with aquifer by Izgec and Kabir (2009, 2010). The author validated the results by comparing the CRM to a streamline simulation (SLS) and

discovered that their outputs were related. Also, Delshad et al. (2009) broadened the application by analyzing the obtained inter-well connectivity to model the fracture distribution at each section of the reservoir.

The extension of CRM application was further done by Nguyen (2011) and Kim (2011), who developed a new form of the CRM equations called the integrated CRM (ICRM) which enables the analysis of reservoirs under primary recovery and water-CO_2 flood (WAG). She also used the optimized injection scheme obtained from the CRM to be applied in a West Texas field and the field successfully gained a considerable amount of incremental oil after 1 year. Concentrating on real field application, Cao (2011) established a novel procedure to clean and quality-control production data using the CRM. She validated the algorithm with several synthetic fields and demonstrated how poor data quality misleads the characterization of a reservoir. Laochamroonvorapongse (2013) integrated the CRM with the existing analytical methods, the reciprocal productivity index (RPI) and the water-oil ratio (WOR) plots, to evaluate a miscible flood performance in a West Texas field. She also incorporated the effect of producer-producer interaction into the CRM leading to more accuracy in parameter estimation.

Not only at the University of Texas at Austin (UT) where the CRM research began, the technique inclines to achieve more acceptance from petroleum industry all over the world. At the University of Calgary, Kaviani et al. (2012) proposed modifications to the simple CM so that it can tolerate deviations in two critical assumptions that are common field conditions. The segmented CM is applied when BHP data are unavailable and fluctuating. The compensated CM is used when there are producer shut-in periods and new producers added. The new models have been validated with both simulated and actual field data. Soroush (2014) conducted a sensitivity analysis on the results to determine the applicable ranges of properties when applying the CRM to

field data. He firstly applied the technique to a heavy oil field and found a good agreement of the results with known geological and reservoir engineering features.

At the University of Southern California (USC), Jafroodi and Zhang (2011) allowed the CRM to have time-varying parameters by applying the ensemble Kalman filter (EnKF), a real-time updating scheme. Also, they introduced an algorithm called Enopt to optimize the net present value of the reservoir by controlling well injection. The Monte Carlo nature of Enopt allows for both the uncertainty in reservoir characterization and nonlinear nature of the optimization objective to be incorporated. The technique is validated by numerical simulated data. Additionally, Moreno (2013), from YPF-Technologia, Buenos Aires, proposed a multilayer CRM combined with a simple dynamic model representing the evolution of connectivities with time. The model is able to consider all changes in well completions or reservoir with large heterogeneity among layers. Both synthetic and real field data were analyzed with this model which all shows a good agreement. Similarly, a CRM research was conducted at the University of Tehran where Mamghaderi (2013) extended the simple CRM modeling of a single layer reservoir to a layered reservoir. Additional input data are measurements from Production Logging Tools (PLT). An effect of cross-flow between layers is also considered to determine productions for each layer separately. The results has been validated with both synthetic and real reservoir and found that the model accuracy is improved.

Recently, Cao (2014)'s work advanced the CRM one step further. She introduced the saturation equation (an oil material balance) into the model and resolved them before finally came up with a two-phase flow model that can be used during an early period of waterflood (immature waterflood). With this new model, oil saturations at each time step can be determined together with the drainage volume of each producer. The validation was successfully done through several synthetic fields with different imposed geological

features. Other applications of the CRM can be found in the work of Liang, et al., 2007, Dinh and Djebbar, 2007, Lee et al., 2009, Kim, 2011, Wang, 2011.

2.1.2 Equations

2.1.2.1 The original CRM, numerical solution

The development of the CRM originated from a macroscopic tank material balance of fluids at reservoir condition. Considering a single well pair, a producer and an injector, in an arbitrary drainage volume and assuming slightly compressible system, the governing continuity equation is given by:

$$c_t V_p \frac{d\bar{P}}{dt} = i(t) - q(t) \tag{2.1}$$

where c_t is the total compressibility, V_p is the drainage pore volume, $\bar{P}$ is the average reservoir pressure, $i(t)$ is the injection rate and $q(t)$ is the production rate. This equation indicates that a change in an average reservoir pressure is solely attributed to the net rate of mass accumulation to the volume.

It is more useful to describe the equation based entirely on routinely measured field parameters, i.e. rates and flowing bottomhole pressure (FBHP); thus, a linear productivity model is used to eliminate the average pressure from the equation:

$$q = J\left(\bar{P} - P_{wf}\right) \tag{2.2}$$

where J is the productivity index and P_{wf} is the FBHP. Combining Eq. 2.1 and 2.2 yields:

$$\tau \frac{dq}{dt} + q(t) = i(t) - \tau J \frac{dP_{wf}}{dt} \tag{2.3}$$

where τ, the time constant of the drainage volume, is defined as:

$$\tau = \frac{c_t V_p}{J} \tag{2.4}$$

Following Yousef (2006), integrating the equation numerically gives the solution:

$$q(t) = q(t_0)e^{\frac{-(t-t_0)}{\tau}} + \frac{e^{-t/\tau}}{\tau}\int_{\xi=t_0}^{\xi=t} e^{\xi/\tau} i(\xi)d\xi + J\left[P_{wf}(t_0)e^{\frac{-(t-t_0)}{\tau}} - P_{wf}(t) + \frac{e^{-t/\tau}}{\tau}\int_{\xi=t_0}^{\xi=t} e^{\xi/\tau} P_{wf}(\xi)d\xi\right] \quad (2.5)$$

where t_0 is the initial time and ξ is a variable of integration. Eq. 2.5 is the fundamental CRM equation expressing that a well's total production rate consists of 3 components, as shown on the right side of the equation, which are a primary depletion from a previous time step, an effect of injection rates and a change in FBHP of a producer respectively.

Because a total production rate at one producer is generally supported by several injectors and the nature of rates and pressure data is discrete, the integral terms in Eq. 2.5 must be discretized and, by applying the principle of superposition in space, the equation can be extended to multiple producers and injectors. Additionally, the effect of interaction among producers can be taken into account. Yousef addressed this issue by incorporating the FBHP's of other producers in the FBHP term. Finally, according to these modifications, the generalized CRM for producer j and I injectors is given by:

$$q_j(n) = q_{0_j} + \lambda_p q(n_0)e^{\frac{-(n-n_0)}{\tau_p}} + \sum_{i=1}^{i=I}\lambda_{ij}\left[\sum_{m=n0}^{m=n}\frac{\Delta n}{\tau_{ij}}e^{\frac{m-n}{\tau_{ij}}} i_{ij}(m)\right] + \sum_{k=1}^{k=K}\nu_{kj}\left[P_{wf_{kj}}(n_0)e^{\frac{-(n-n_0)}{\tau_{kj}}} - P_{wf_{kj}}(n) + \sum_{m=n_0}^{m=n}\frac{\Delta n}{\tau_j}e^{\frac{m-n}{\tau_j}} P_{wf_j}(m)\right] \quad (2.6)$$

where q_{0_j} is an extra rate accounting for an unbalance between injection and production, n is a time-like variable, Δn is the selected time interval depending on the availability of the data, λ_p and τ_p are the weighing factor and time constant for the contribution from an

exponential decline of the previous time step rate, λ_{ij} is the weighted connectivity between injector i and producer j, τ_{ij} is the time constant of the medium between that well pair, ν_{kj} is a coefficient that determines the effect of changing the FBHP of producer k on the production rate of producer j.

There are two main output parameters obtained from the CRM, the gains (λ_{ij}) and the time constants(τ_{ij}). The gain between injector i and producer j represents the fraction of water injected in injector i that contributes to the total production of producer j at steady-state; thus, it can be inferred as a quantitative expression of inter-well connectivity of that well pair. The analysis of inter-well connectivities throughout the field will provide an insight to the waterflood performance and reservoir characterization leading to further optimization plans. On the other hand, the time constant is a direct measure of the dissipation of pressure accounting for attenuation and time lag between each pair. A small value means small dissipation, less attenuated and delay. Regardless of distance, a change in injection rate would cause a nearly instantaneous and equal change at a producer. Both parameters are determined by adjusting them with the objective to minimize the square errors between measured and calculated (from Eq. 2.6) production rates.

2.1.2.2 The original CRM, analytical solution

Because of current field measurement methods, both rates and pressure data obtained are discrete in nature. To enhance the CRM's applicability to field data, three CRM's analytical solutions were proposed by Sayarpour (2008). Compared to the numerical solution previously developed by Yousef, this analytical one allows faster computational time. As this work mainly used the CRMP, the producer-based

representation of the reservoir, one of the three analytically integrated forms, only the equations for CRMP will be explained in detail below.

Figure 2.3 represents the CRMP volume, which is an arbitrary control volume around a given producer (j), with several possible supporting injectors (N_i).

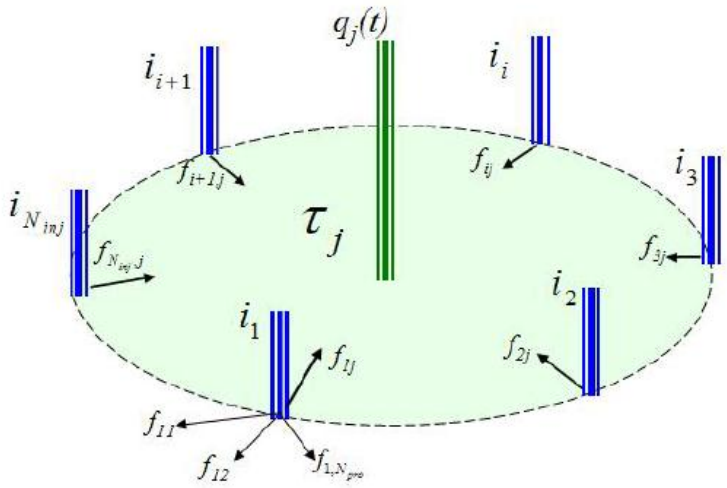

Figure 2.3 Schematic representation of a control volume used in the CRMP (Sayarpour, 2008)

Liang et al. (2007) introduced the continuity equation under such a control volume:

$$\frac{dq_j(t)}{dt} + \frac{1}{\tau_j} q_j(t) = \frac{1}{\tau_j} \sum_{i=1}^{N_i} f_{ij} i_i(t) - J_j \frac{dP_{wf,j}}{dt} \tag{2.7}$$

where f_{ij} is exactly identical to the λ_{ij} previously defined. To solve this equation analytically, Sayarpour assumed a linear variation of FBHP and stepwise changes in injection rates. This assumption is consistent with the discrete nature in which field data are reported as shown in Fig 2.4.

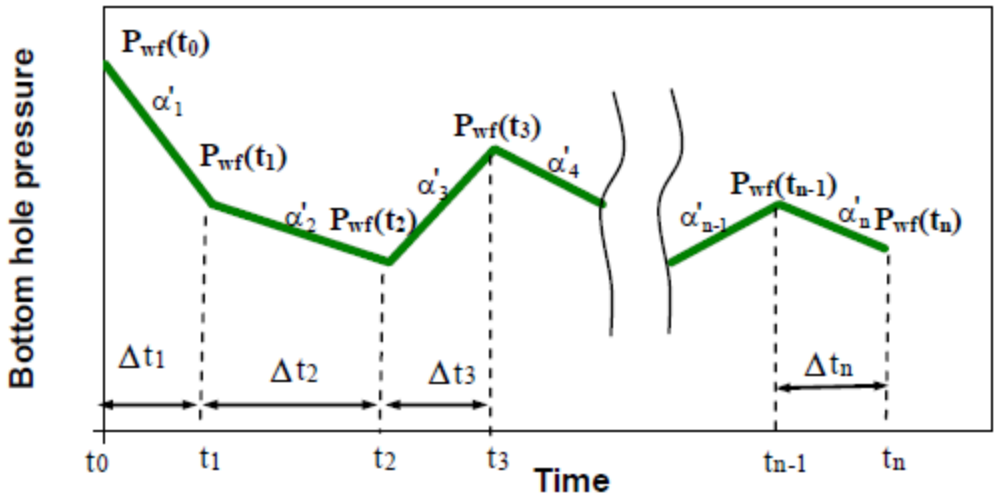

Figure 2.4 Example of linearly varied FBHP within each time interval (Sayarpour, 2008)

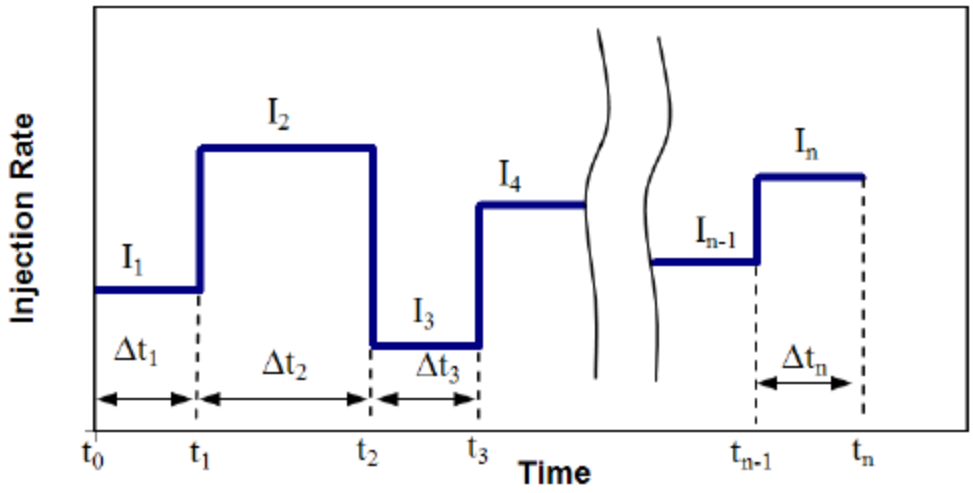

Figure 2.5 Example of fixed injection rate within each time interval (Sayarpour, 2008)

Additionally, assuming a known initial production rate, a constant productivity index for all producers and integrating Eq. 2.7 over a discrete time period, Δt_k, the total production rate of producer j can be written as:

$$q_j(t_k) = q_j(t_{k-1})\left(e^{-\frac{\Delta t_k}{\tau_j}}\right) + \left(1 - e^{-\frac{\Delta t_k}{\tau_j}}\right)\left[\sum_{i=1}^{N_i}\left[f_{ij} I_i^{(k)}\right] - J_j \tau_j \frac{\Delta P_{wf,j}^{(k)}}{\Delta t_k}\right] \quad (2.8)$$

where k is the interested time interval, $I_i^{(k)}$ is the injection rate of injector i at time step k and $\Delta P_{wf,j}^{(k)}$ is the change in FBHP at that producer during time interval t_{k-1} to t_k. This equation suggests that the total production rate of producer j during any interested time interval is a weighted average of the previous time step's production rate, the effect of injection and the FBHP change at that producer as shown on the right side of the equation, respectively. To have the solution written from the first time interval (t_0) to the last time interval (t_n), a principle of superposition in time is imposed to obtain:

$$q_j(t_n) = q_j(t_0)\left(e^{-\frac{(t_n - t_0)}{\tau_j}}\right) + \sum_{k=1}^{n}\left\{e^{-\frac{(t_n - t_k)}{\tau_j}}\left(1 - e^{-\frac{\Delta t_k}{\tau_j}}\right)\left[\sum_{i=1}^{N_i}\left[f_{ij} I_i^{(k)}\right] - J_j \tau_j \frac{\Delta P_{wf,j}^{(k)}}{\Delta t_k}\right]\right\} \quad (2.9)$$

The model described by Eq. 2.9 can be fitted for a selected time horizon to the data. Model parameters (f_{ij}, τ_j) are again estimated using multivariate nonlinear regressions with the objective function:

$$\min z = \sum_{k=1}^{n}\sum_{j=1}^{N_p}\left(q_j^{obs}(t_k) - q_j^{cal}(t_k)\right)^2 \quad (2.10)$$

and the following additional constraints:

$$f_{ij}, \tau_j \geq 0 \; for \; all \; i \; and \; j \quad (2.11)$$

$$\sum_{j=1}^{N_p} f_{ij} \leq 1 \; for \; all \; i \quad (2.12)$$

Apart from the CRMP, another analytical form, the CRMIP, is also used in this work and will be presented in detail in Chapter 5. In this case, a control volume is defined to be an arbitrary drainage volume between an injector-producer pair as shown in Fig 2.6.

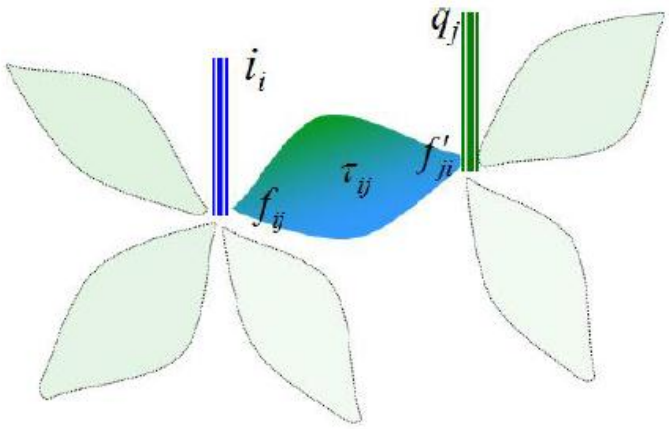

Figure 2.6 Schematic representation of a control volume used in the CRMIP (Sayarpour, 2008)

A final model equation of CRMIP (analogous to Eq. 2.9 of CRMP) is given by:

$$q_j(t_n) = \sum_{i=1}^{N_i} q_{ij}(t_0) e^{-\left(\frac{t_n - t_0}{\tau_{ij}}\right)} + \sum_{i=1}^{N_i}\left\{\sum_{k=1}^{n}\left[\left(1 - e^{\frac{-\Delta t_k}{\tau_{ij}}}\right)\left(f_{ij} I_i^{(k)} - J_{ij}\tau_{ij}\frac{\Delta P_{wf}^{(k)}}{\Delta t_k}\right) e^{-\left(\frac{t_n - t_k}{\tau_{ij}}\right)}\right]\right\} \quad (2.13)$$

where q_{ij} is the production rate of producer j contributed from injector i and τ_{ij} is the time constant of the defined control volume.

2.1.2.2 The two-phase flow coupled CRM

In an immature waterflooded field where a water cut is small, the assumption of constant oil and water mobilities used in the original CRM will be less valid since fluid saturations change considerably. This motivated the development of the coupled CRM (Cao, 2014), in which oil mass balance equation is, for the first time, used. The derivation begins with total fluid and oil material balances, assuming no aquifer, no free gas and

two-phase (oil and water) immiscible displacement. With the selected control volume is the drainage volume around a given producer with injectors, which is identical to that for the CRMP, the governed equations are given by:

$$V_p c_t \frac{d\bar{P}}{dt} = i(t) - q(t) \tag{2.14}$$

$$V_p \left(\frac{d\bar{S}_o}{dt} + \bar{S}_o (c_f + c_o) \frac{d\bar{P}}{dt} \right) = -q_o \tag{2.15}$$

where $\bar{S}_o$ is the average oil saturation in the control volume, c_f and c_o are the rock and oil compressibility, q_o is the oil production rate. Recalling the relationship between rate and pressure:

$$q = J\left(\bar{P} - P_{wf}\right) \tag{2.2}$$

In the original CRM, J is assumed to be constant which is valid for single-phase flow and acceptable for high-water cut production. For two-phase flow, in which the definition of J is given by:

$$J = \frac{2\pi kh}{\left[\frac{1}{2}\ln\left[\frac{4A}{\gamma C_A r_w^2}\right]\right]}\left[\frac{k_{ro}}{\mu_o} + \frac{k_{rw}}{\mu_w}\right] \tag{2.16}$$

where k is the single-phase permeability, h is the average thickness of the reservoir within the control volume, A is the drainage area, r_w is the wellbore radius, C_A is the shape factor, γ is the Euler constant, k_r is the relative permeability and μ is the fluid viscosity. Because relative permeability depends strongly on saturations, it is immediately apparent that the productivity index is a function of saturations and will be no longer constant in an immature waterflood since saturations change during that period. This makes Eq. 2.14 depend on the saturation and it has to be solved together with Eq.2.15. Assuming a constant FBHP, the analytical solution to Eq. 2.14 is similar to Eq. 2.8 except the disappearance of the FBHP term and it is given by:

$$q_j(t_k) = q_j(t_{k-1})\left(e^{-\frac{\Delta t_k}{\tau_j(t)}}\right) + \left(1 - e^{-\frac{\Delta t_k}{\tau_j(t)}}\right)\left[\sum_{i=1}^{N_i}\left[f_{ij}I_i^{(k)}\right]\right] \tag{2.17}$$

where the time constant now changes for each time step as the productivity index changes. The semi-analytical solution to Eq. 2.15 is:

$$\bar{S}_{oj}{}^{k} = \bar{S}_{ij} - \frac{\Delta t}{V_{pj}}\sum_{n=1}^{k}\left[\frac{\bar{S}_{oj}{}^{n-1}(c_f + c_o)}{c_t}\left(\sum_{i=1}^{N_i} f_{ij}I_i^{(n)} - q_j^n\right) + q_{oj}^n\right] \tag{2.18}$$

where k is the time of interest, $\bar{S}_{ij}$ is the average oil saturation around producer j measured at the time the well was drilled, V_{pj} is the pore volume of producer j, q_{oj}^n is the oil production rate of producer j at time step n. Equations 2.17 and 2.18 will be referred to as a pressure and a saturation equation, respectively. Neglecting the pressure dependency of variables, there are 2 parameters (k_{ro} and k_{rw}) in Eq. 2.17 that depend on saturations. These must be iterated and updated at each time step. To determine the key parameters from both equations, we used an empirical relationship to relate and calculate the relative permeability.

Considering an empirical relationship of oil-water relative permeability proposed by Corey (1954), the independent variable is the saturation at the outlet or the producer. Welge's equation (1952) relating the outlet saturation to the average saturation is given by:

$$S_{o2} = \bar{S}_o + W_i\left(1 - f_{w,x_D=1}\right) \tag{2.19}$$

where S_{o2} is the outlet oil saturation, W_i is the cumulative pore volume of water injected and $f_{w,x_D=1}$ is the producing water cut measured at that well. The water cut is simply calculated from production data while W_i is determined from:

$$W_i = \frac{\sum_k \sum_i f_{ij}I_i^k}{V_p} \tag{2.20}$$

where V_p is the dynamic pore volume associated with each producer and can be determined using the Koval (1963) equation:

$$f_{w,x_D=1} = \frac{K_v - \sqrt{\frac{K_v}{t_d}}}{K_v - 1}, \qquad \frac{1}{K_v} < t_d < K_v \tag{2.21}$$

where K_v is the Koval factor and t_d is the dimensionless time, which is the ratio of the cumulative injection and the dynamic pore volume. The plot of water cut versus time can be obtained for each producer. An example is shown in Figure 2.7. The red line is determined using Eq. 2.21 through nonlinear regression to match with the measured data. The pore volume and Koval factor are obtained from history matching.

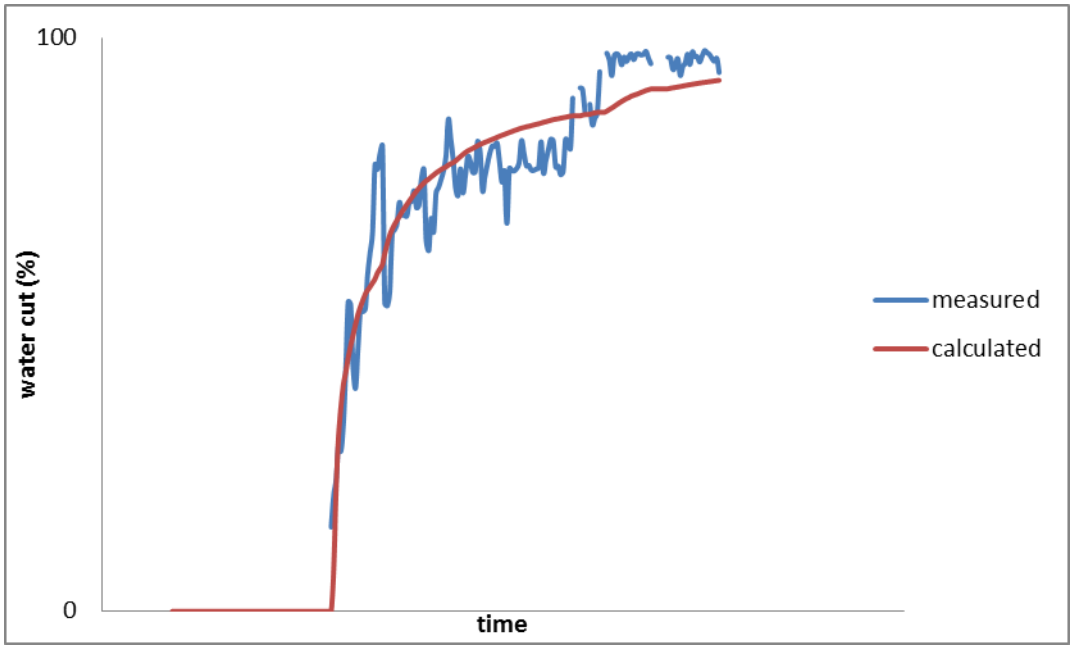

Figure 2.7 A plot of measured and calculated water cut versus time for a producer

The flow chart below (Figure 2.8) demonstrates a procedure to determine the optimized model parameters by solving the pressure and saturation equations. For each time step, the first step is to calculate $q_j(t_k)$ by guessing f_{ij}, τ_j and $\bar{S}_{ij}$. Then, the oil

production rate can be directly calculated from measured water cut at that time step and, thus, the average saturation, $\bar{S}_{oj}{}^{k}$, can be determined using the saturation equation. The next step is to update the outlet saturation so that the time constant can be re-evaluated and the new $q_j(t_k)$ is determined. This procedure is done simultaneously for all producers and all time steps to minimize the difference between the measured and calculated production rates.

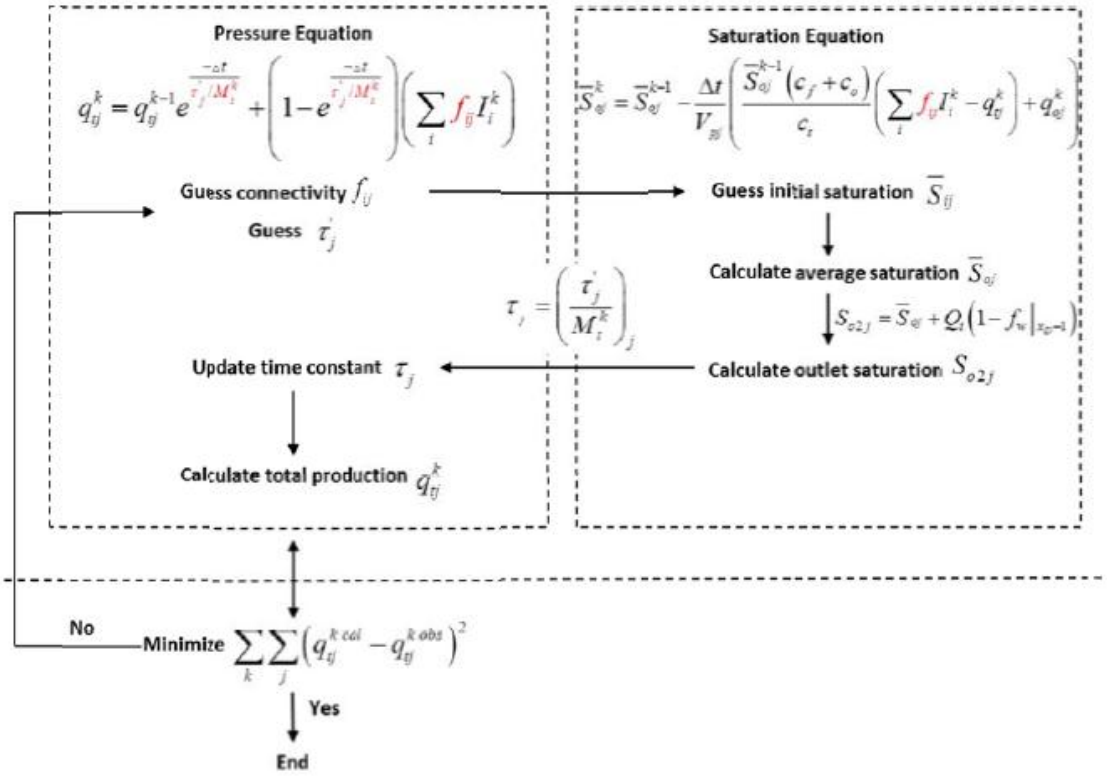

Figure 2.8 Flow chart summarizing the procedure to obtain the model parameters of the coupled CRM (Cao, 2014)

The additional output obtained from the coupled CRM contains the average saturations within each producer's drainage volume that change with time. This should be a key parameter to determine a prospective infill location.

2.2 INFILL DRILLING

2.2.1 General ideas

In this research, infill drilling will be defined as the drilling of additional producers with an objective to recover bypassed oil in a field that has already completed primary depletion and has been undergoing waterflooding. Driscoll (1974) described factors that contribute to incremental recovery after infill drilling, which may be summarized as follows: (1) improved areal sweep efficiency, (2) areal heterogeneity, (3) improved vertical sweep efficiency, (4) improved lateral pay continuity, (5) recovery of wedge edge oil, (6) reduced economic limits.

The areal sweep efficiency is increased by reversing the original streamline and sweeping across the previously unswept areas, especially for patterns with poor streamline balance because of poor geometric alignment. This is illustrated in Figure 2.9.

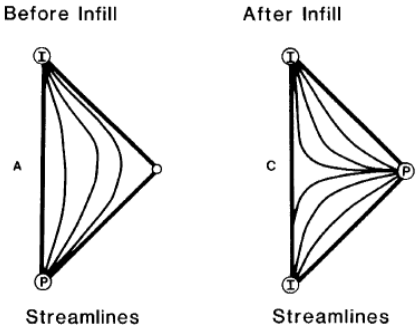

Figure 2.9 Effect of adding new producer on streamline arrangement

(Adapted from Gould and Munoz, 1982)

Areal heterogeneity (i.e. anisotropy, fractures) leads to injection imbalance creating early water breakthrough (WBT) and a preferential sweep of specific part of a pattern. As demonstrated in Figure 2.10, a directional permeability variation of 30 results in large water saturation along the highly permeable direction (y) and significant

bypassed oil is observed along the low permeability direction (x). Incremental recovery is attributed to rotating the pattern after infilling and flooding across the x-direction. Reservoirs with significant areal anisotropy can exhibit considerable incremental infill recoveries.

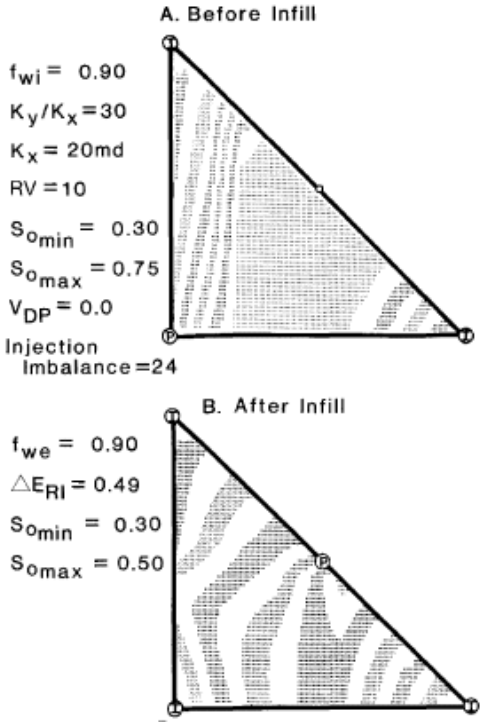

Figure 2.10 Effect of areal heterogeneity on saturation distribution

(Gould and Munoz, 1982)

Drilling a new well also provides an opportunity for recompletion, which will improve the vertical injection profile and isolate previously swept zones mechanically. Generally, the most permeable zones are preferentially swept. Furthermore, a new well can enhance reservoir continuity by penetrating more sands and making them connected to existing injectors resulting in an increase in floodable pay. Both the areal and vertical sweep efficiencies constitute the volumetric sweep efficiency, which is an indication of

the fraction of reservoir which has been swept by injected water and that additional oil recovery exists in the unswept portion.

In an ideal and homogeneous reservoir, infill drilling only accelerates production; however, all real reservoirs always have heterogeneities. Good infill performance can result from: (1) unusually poor reservoir continuity in some specific part of the reservoir, (2) good reservoir deliverability and quality. Favorable characteristics include reservoirs with poor initial waterflood recovery, complex geology such as many stringers, lateral permeability and porosity variation and poor continuity, which could be overcome by closer well spacing.

There are several indicators reflecting a non-uniform sweep that suggest that a reservoir is a good candidate for infill drilling. For instance, repeat formation tester (RFT) pressure measurement reflects highly different reservoir pressure in various layers, production logging tool (PLT) indicate poor vertical water distribution for many injectors, static BHPs reflected significant variation in areal pressure distribution and measured chloride content of produced water confirmed that some up-dip wells, away from injector, were producing injected water while down-dip well were not.

2.2.2 Determination of an infill location

The determination of an infill location is a complicated task because it is affected by several uncertain factors such as reservoir and fluid properties and localized sweep efficiency. Most previously published research on bypassed oil identification technique relied mainly on a combined analysis of the distribution of petrophysical and reservoir properties including permeability, porosity, saturation and net sand thickness, in which most of these data are obtained from well logging. Nevertheless, under waterflooding,

those static properties have recently found insufficient to accurately model the reservoir performance. It is essential to incorporate the dynamic effect of sweep efficiency into the process. Poor waterflood sweep is attributed to significant anisotropy, unmatched perforation intervals and, most importantly, poor interwell connectivity, thus, resulting in large volumes of bypassed oil. Therefore, targeting infill drilling requires a reservoir characterization program to identify areas of field with good quality rock and the largest volume of oil in place.

Streamline simulation (SLS) is recognized as one of the most powerful tools for this purpose. Valuable information obtained from SLS are the well allocation factors (WAF) reflecting the interwell connectivity. The WAF is used to determine the distribution of injected water to associated producers, water loss to aquifer and also percentage of oil produced because of each supporting injector. The phase rates are obtained by solving the transport problem along each streamline (SL).

Injection efficiency (IE) is another parameter widely used to analyze waterflood performance. It is defined as:

$$IE = \frac{offset\ oil\ production\ rate\ (Q_o)}{water\ injection\ rate\ (Q_{inj})} \tag{2.22}$$

where water injection rate is obviously known and offset oil production rate is the summation of oil rate associated with bundles of streamline that start in that injector and end in connected offset producers at that instant time and must be calculated from WAFs. As time increases, IE is expected to decrease as more water breakthrough occurs. A powerful way to display IE is by using a crossplot (Thiele and Batycky, 2006) as shown in the Figure 2.11.

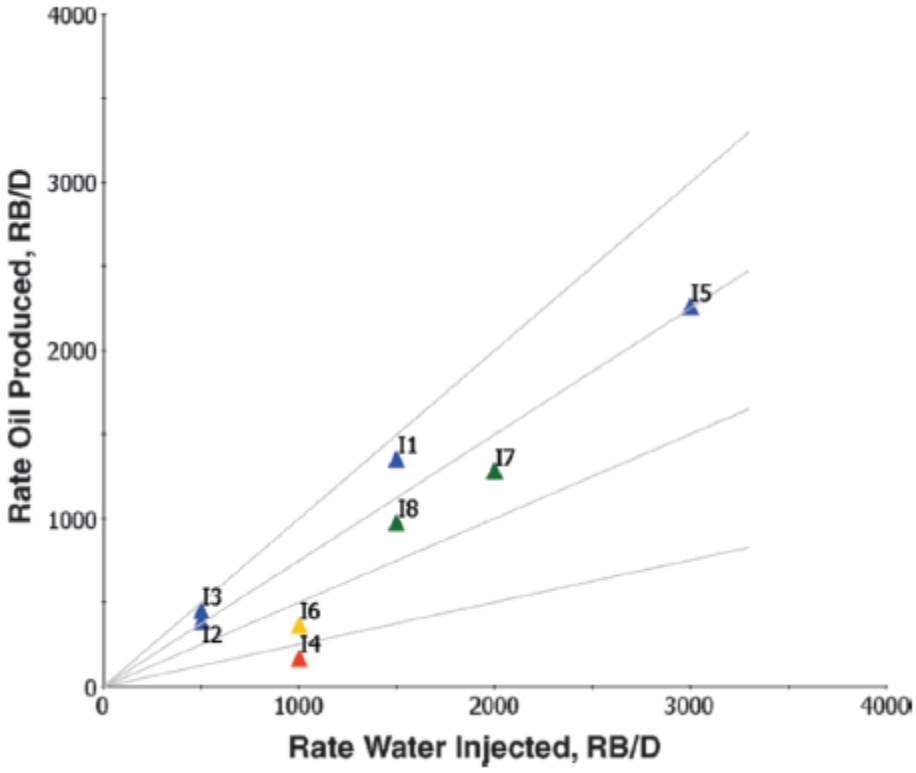

Figure 2.11 Crossplot displaying IEs for all injectors (Thiele and Batycky, 2006)

The plot is an effective way to assess the efficiency of a waterflood. The IE of an injector is determined by the slope of the straight line connecting the origin point and the point labeled its name. The 4 straight lines in the plot represent slopes of 0.25, 0.5, 0.75 and 1. I4 is located below the quarter-slope line meaning that its IE is less than 25%. Wells with less than 25% IE and a large injection rate are obvious indications of water cycling occurring. Similarly, a well that loses water to, for example, an aquifer will see a lower IE while the most efficient injector will have a 100% IE meaning that every barrel of injected water produces an equal volume of oil. Hence, SLS can help us quantify water cycling, reduce unnecessary injection, reallocate water to efficient injectors and identify fully swept zone. An unswept portion of a reservoir, which will be a potential location for

infill drilling, is illustrated by lack of streamline as shown in Figure 2.12. The dark blue area in the south, which has relatively lower porosity, also has small streamline density indicating poor sweep and, thus, high remaining bypassed oil.

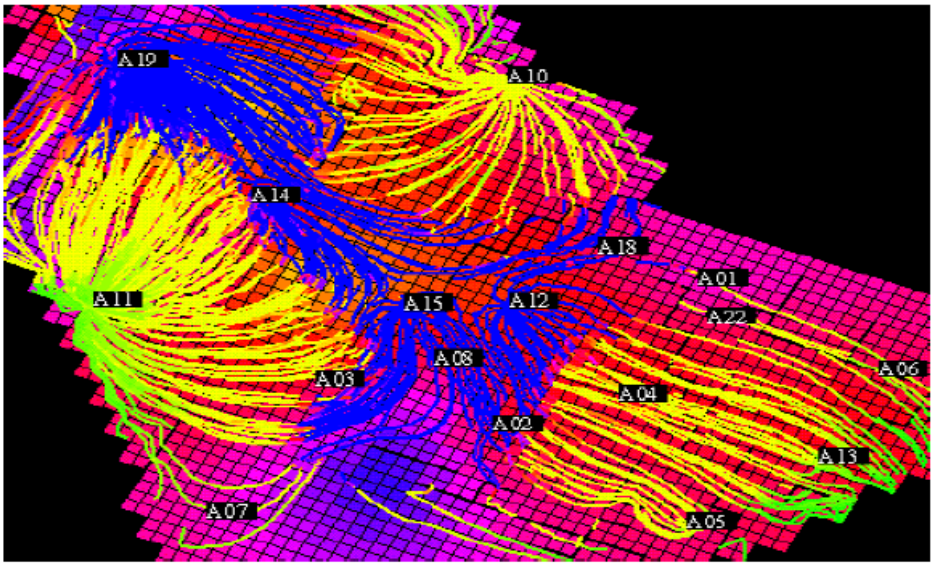

Figure 2.12 Example of streamline simulation results superimposed on porosity map (Lolomari et al., 2000)

Numerous authors have already demonstrated the application of SLS combined with reservoir characteristic maps to determine proper infill locations. Dehdari et al. (2008) stated that if streamline do not pass through one part of a reservoir, that only means less sweep efficiency and it is risky to jump to the conclusion that this part is suitable for infilling. On the other hand, a set of reservoir characteristic maps consisting of permeability, porosity, thickness, saturation and productivity index should be used together to find the best location. These maps can be generated from finite-difference simulation as well as kriging interpolation from petrophysical data. An example of

thickness map is shown in Figure 2.13. The results in this work were validated experimentally through the simulation.

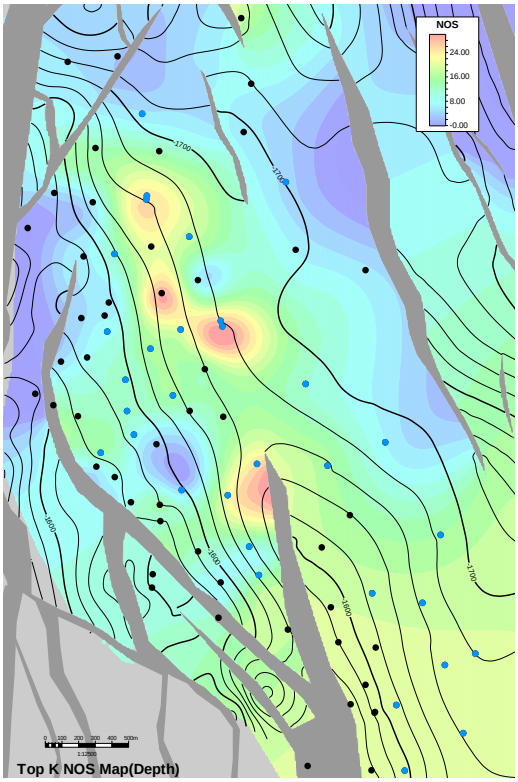

Figure 2.13 Net oil sand thickness map obtained from kriging interpolation of well logging data

According to Sayyafzadeh et al. (2010), new producers should be drilled in sections of reservoir where the streamline density is low and oil saturation is high. One of the most important effects of infill drilling is to improve areal sweep efficiency by changing the streamline within pattern. A low streamline density in a region means poor flow and putting new wells there will cause the sweep to improve. They also pointed out that for regions that have wells with high density SLs must be converted to injectors

because these wells have good connections with the whole reservoir. Grid-based simulation was used to verify the outcomes and the results show that the ultimate oil recovery increases around 70 percent by infilling and switching the producers to injectors. Al-Mudhafer (2013) proposed an infill criterion using 5 parameters obtained from a reservoir modeling including pressure, permeability, oil saturation, porosity and thickness. The net present value (NPV) of the project was specified as the objective function and an optimization approach performed via spreadsheet.

Taware et al. (2012) also came up with an identical concept. They suggested that previous screening approaches, relying on reservoir quality maps, which are both static such as permeability, porosity and thickness, and dynamic, such as remaining oil, pressure, productivity index, have limited application. The approach does not account for the drainage and swept volumes from existing wells. Therefore, they proposed a novel method incorporating the streamline time of flight (TOF) into the analysis. The TOF from the injectors (TOFI) represents swept volumes for injectors whereas streamline TOF from the producers (TOFP) provides drainage volumes for producers. These two quantities can be effectively combined to a total time of flight (TOFT). A region with high value of TOFT is poorly drained and poorly swept. They proposed one single parameter, called "dynamic measure", as a grid property that takes all these effects into account and can be used to rank infill locations quantitatively:

$$Dynamic\ Measure\ (DM) = \left(TOFT_{RN} \cdot So_{RN} \cdot PV_{RN} \cdot k_{RN} \cdot k_{ro_{RN}}\right) \tag{2.23}$$

where the subscript RN denotes rank normalization of the property, which is done for each grid cell. It is based on a combination of streamline attributes and reservoir properties. The DM map can be generated and areas with high DM are attractive for new wells.

In conclusion, according to these studies, the combination of the streamline simulation and the reservoir characteristic maps can be considered to be one of the most widely used method to identify potential infill locations. This systematic procedure is essential because the determination of infill locations is a complicated task as it is affected by several elements such as reservoir connectivity leading to the interference between wells, and rock and fluid properties. Most of the previous studies, however, validated their proposed methods only with the synthetic reservoirs. This weakness inspired this work to validate its recommended approach with actual infill wells' performance, which will be more justifiable.

Chapter 3: Application of the CRM in a Southeast Asian field

This chapter discusses the application of both the original and the coupled CRM to actual field data. The first section will begin with field's background, and then the preparation of the input data will be described. Several related issues will be identified and examined for the compromising solutions. The second section is about the results and discussions. The topics include the fitting quality, the gain, the time constant and the saturation.

3.1 GENERAL INFORMATION OF THE FIELD

The field is a conventional oil reservoir (40^{o} API) producing from a set of prograding deltaic sandstone sequences that interfingered with a lacustrine shale at a depth from 1,400 to 2,200 m. This has resulted in thin, stacked but laterally extensive sand cycles that restrict vertical communication within the formation and has a low net-to-gross (5-23%) series of fair quality reservoirs. The structure is a half graben tilted towards the east and bounded on the west by faults striking NNW-SSE and dipping predominantly west. Most of the oil is trapped in mouth-bar sands that are well connected laterally but have shale breaks vertically. The structural depth map of the reservoir is presented in the Figure 3.1.

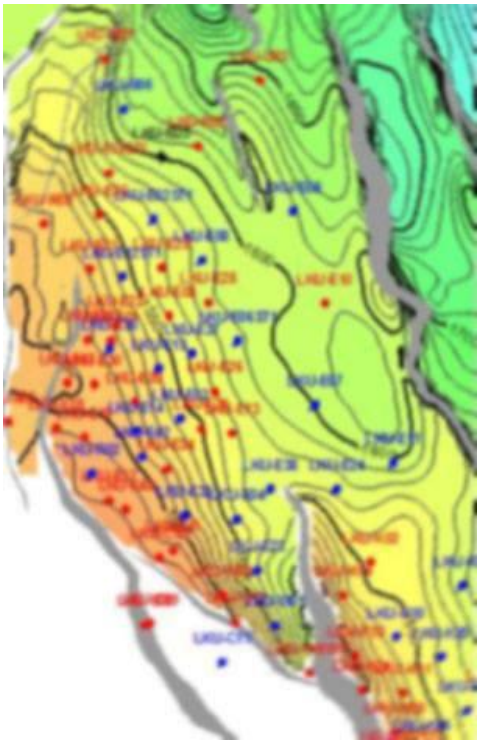

Figure 3.1 Structural depth map of the reservoir

As obviously seen in the map, wells are highly dense on the left side, which is the up-dip location, as the structure is dipping toward the east. The average porosity and permeability are approximately 20% and 15 md, respectively. The original-oil-in-place is about 115 MMSTB. Initially, the reservoir is saturated with the pressure equal to the bubble point pressure.

The summary of production and development history of the field is illustrated in Figure 3.2. In 1982, the production started naturally under solution gas and gas cap drive mechanisms, with weak aquifer support. The production characteristic obviously exhibited these mechanisms, with a gradual decline in both gross and oil production rates, a slight amount of produced water, an increase in producing gas-oil ratio (GOR) and a considerable drop in reservoir pressure. The reservoir has been depleted continuously for

13 years leading to a decline in reservoir pressure to significantly below the bubble point. Significant quantities of free gas have come out of the solution and to form a gas cap, signifying a necessity of a pressure maintenance program.

After that, a full-field waterflood was implemented in 1995 with 6 injectors at a well spacing of 500 m under an inverted 5-spot pattern. As expected, after injecting for 5 years, the field experienced an increase in liquid production rate, a steep rise in water cut, and a continuous decrease in the producing GOR. A further batch of waterflood infill wells were drilled in 2001 to provide more information on waterflood performance. It has been found out that there are usually one or more layers with good rock properties in all wells that act as thief zones. These zones are the cause of early water breakthrough. At that time, the recovery factor was only 15% of original oil in place, suggesting that there was still a good potential to improve the oil recovery from the area.

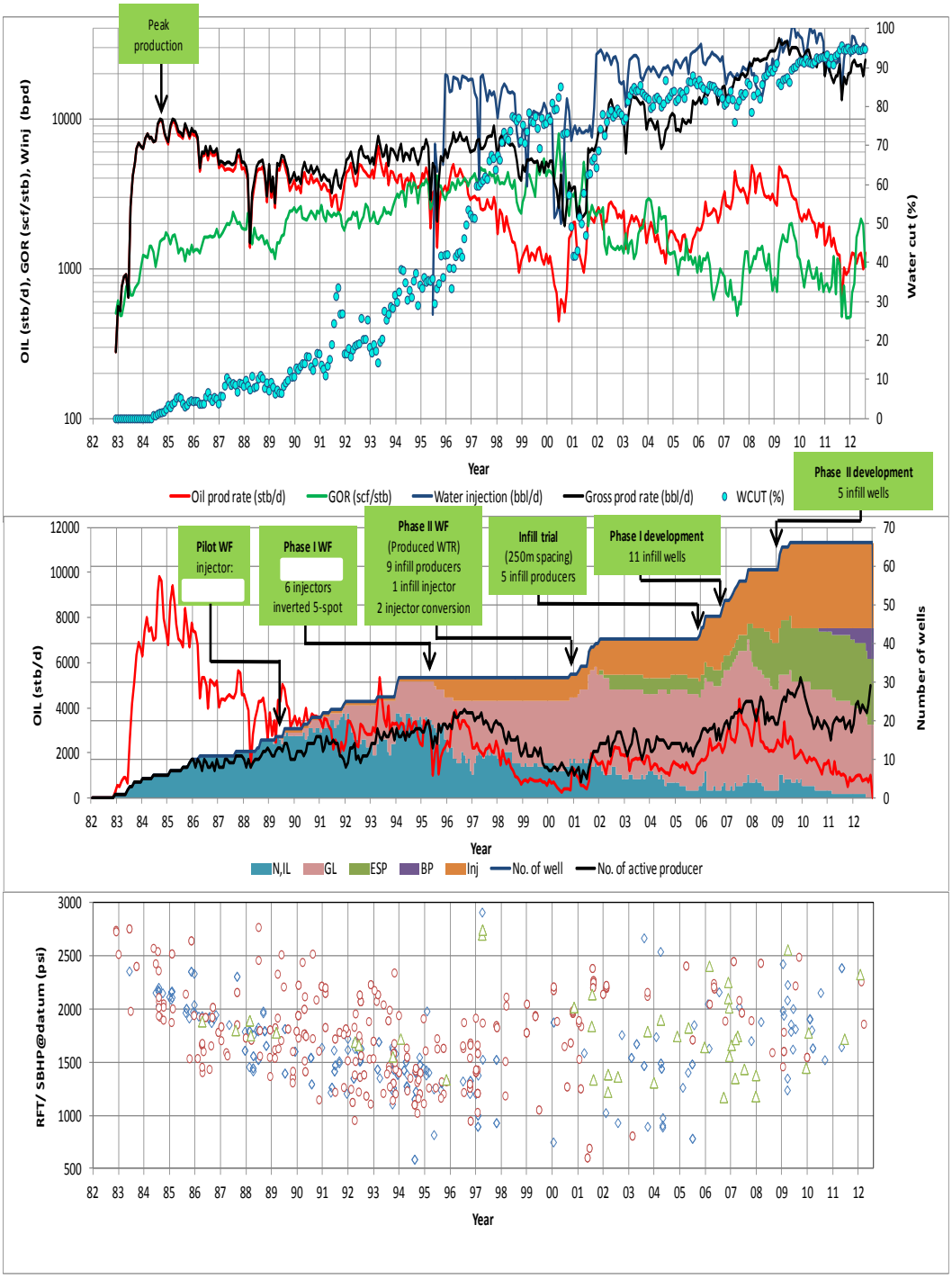

Figure 3.2 Production and development history of the field

The main strategy was to reduce the well spacing to 200 m by drilling more than 20 20-50 degree-deviated wells from 2006-2014. Apart from the inverted 5-spot, the flooding pattern has been extended to peripheral flooding with several injector-to-producer conversions of down-dip wells. Currently, at the recovery factor of 25%, the waterflood is considered to be mature with the production from each well exhibiting high water cut (90% on average) and high liquid production rate. There are in total 53 wells with 31 producers, mainly producing under gas-lift (GL) and electrical submersible pump (ESP) as shown in the pink and green areas in the middle plot of Figure 3.2, and 22 injectors. A few wells are producing via beam pump (BP) or even natural flow (the violet and light blue areas). The reservoir pressure has been built up remarkably from as low as below 1,000 psi to almost at the original bubble point, which is 2,300 psi, meaning that there is now a much smaller free gas or gas cap than originally and the reservoir oil can be considered as a slightly compressible fluid and a two-phase flow of oil and water. Correspondingly, the producing GOR has declined to roughly the initial solution GOR representing in a saturated reservoir with negligible gas cap. These conditions make the reservoir favorable to the CRM application as they will satisfy the model's main assumptions.

Another interesting feature is the plot of RFT pressures versus depth (Figure 3.3). The pressures plotted here is the one that are collected at several depths from each well at the time they were drilled (i.e. the initial pressure of each well). Each color of the points plotted represents the data collected from each well. The data from the group of early wells apparently indicated the existence of both gas-oil and oil-water contacts as displayed by the negative-slope straight lines. Depletions from the initial gradients were always found at the wells drilled later on implying a proof of connectivity. However, most of the data from late wells reveal different degree of depletion because of primary

production or pressure build-up because of waterflood. Unlike the early wells, they can vary randomly and do not exhibit straight lines showing the fluid contacts. The key point here is that there is different degree of depletion in various layers which reflects a non-uniform sweep with possibility of bypassing significant oil volumes. This makes the reservoir to be an appropriate candidate for this research.

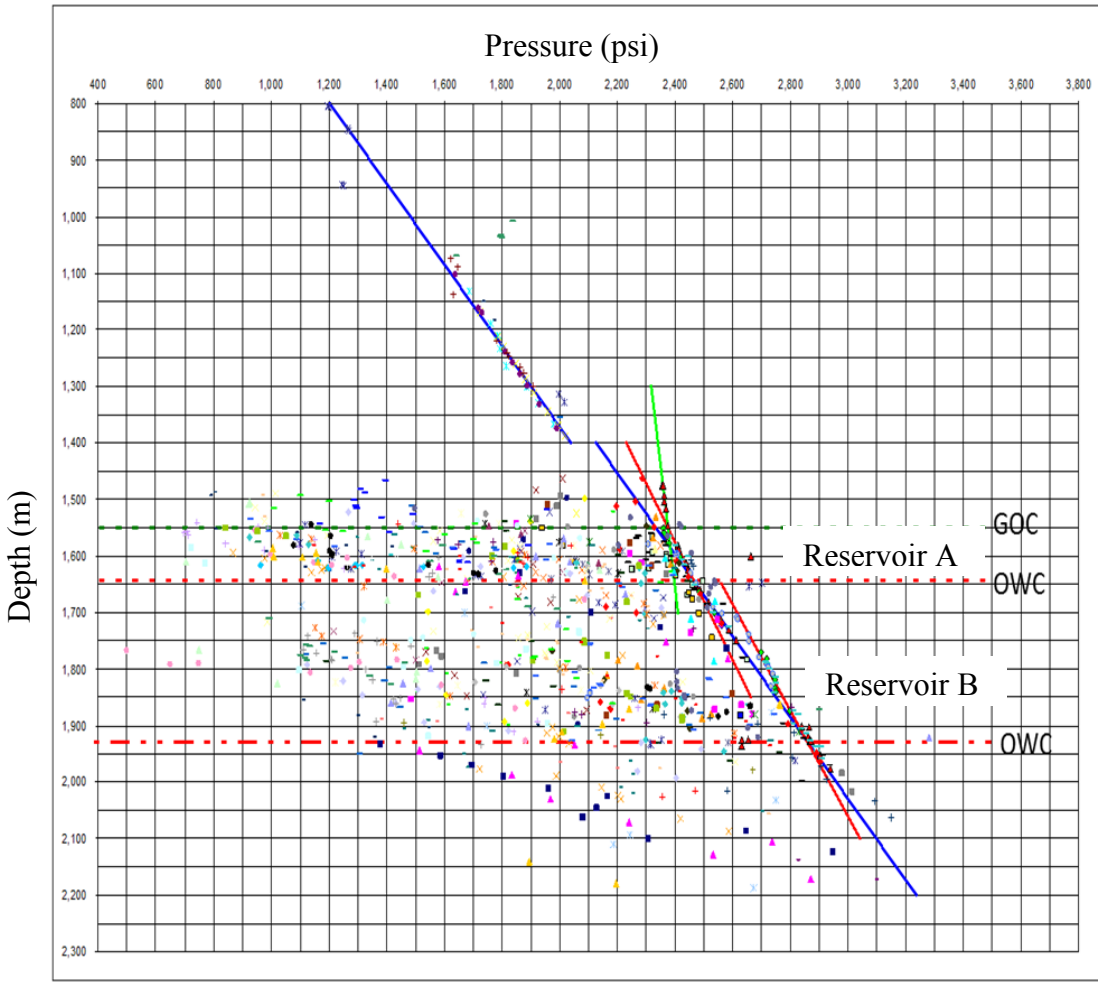

Figure 3.3 A plot of RFT pressures versus depth

3.2 INPUT DATA PREPARATION AND EXAMINATION

Fitting the CRM to field data has several challenges because of the model's assumptions and the data availability. This topic will provide discussions on analyzing the data, identifying key considerations and how the issues were being addressed.

3.2.1 The single-phase original CRM

The most essential inputs to the CRM are rates and pressure. The production data is reported monthly while, however, the injection data is available on a daily basis. Therefore, to make them consistent, the selection of data frequency must rely on the monthly data by simply averaging the daily injection rates to determine the monthly one. In addition, the well rates were allocated to reservoir levels by field personnel as illustrated in Figure 3.4. Generally, there are two reservoirs, which are completely sealed vertically by continuous shale layers, contributing mainly to the production of each well. In most cases, both reservoirs have been developed together as the deviated wells were able to penetrate them both. Available field data such as production tests, petrophysical information, production logging tool (PLT) and RFT pressure data, are used to allocate the well rates, which definitely involves some kinds of calculation, approximation and assumption violation. This makes the allocated data contain considerable uncertainties.

On the other hand, the CRM is a point-to-point model evaluating the inter-well relationships, which makes it a large-scale properties determination. It is more appropriate for not adding more uncertainties into the calculation, and thus, the analysis is performed on a well level, not a reservoir level.

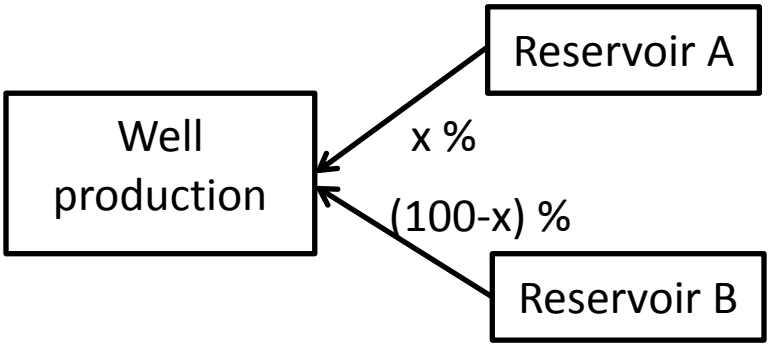

Figure 3.4 Two reservoirs contributing to the production

Unlike synthetic data, there are frequent well activities that interfere with the continuity of the production or injection that are happening in the real field and cause the CRM assumptions to be violated. Commonly, the objectives are to improve well performance and collect data for reservoir characterization. Examples of the results of those wireline and workover activities are additional perforation, zone change, recompletion, pressure gradient survey, PLT measurement, water shut-off and artificial lift conversion.

The principle of the CRM is that the production responds to either the injection rate or to the FBHP change. Recalling Eq. 2.16 which defines the productivity index (PI):

$$J = \frac{2\pi kh}{\left[\frac{1}{2}\ln\left[\frac{4A}{\gamma C_A r_w^2}\right]\right]}\left[\frac{k_{ro}}{\mu_o} + \frac{k_{rw}}{\mu_w}\right] \tag{2.16}$$

It is obviously seen that the PI depends on reservoir thickness and permeability. The main assumption of the CRM is that the productivity index must be steady for the whole fitting window. However, these field activities such as zone change, perforation and recompletion alter these parameters leading to the violation of this assumption. To obtain the accurate results, the production history of each well must be examined to identify these key events that can affect production rates. Examples are presented below.

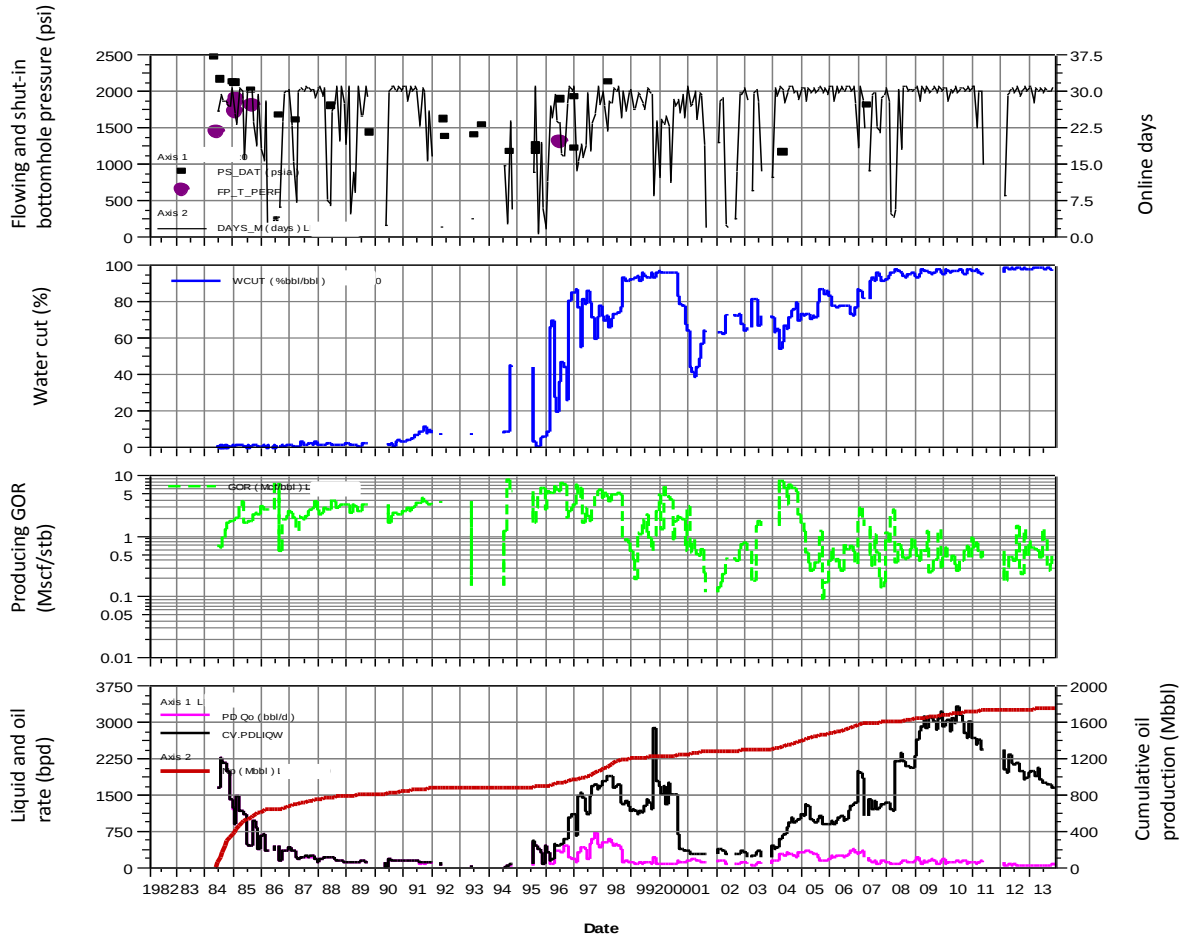

Figure 3.5 Production history of well X

These plots are the template used for analysis in this work. The combination of the parameters on the plot helps understand the well performance. The key activities related to the CRM application were summarized in the table below.

Date	Key activities
Jul-95	The production exhibited waterflood (WF) response right at the beginning of injection. The liquid production rates went up together with the water cut and reservoir pressure. Likewise, the GOR declined gradually to the initial solution GOR at around 800 SCF/STB.
Date	**Key activities**
	During this period, there were multiple zone change activities which are undesirable for the CRM as discussed.
Aug-00	The well was producing from zone 1 until ESP conversion. GOR kept decreasing implying the reservoir was approached a liquid phrase.
Dec-03	There was a 6-metre additional perforation leading to a small sudden jump in gross rate. However, the well has also been shut-in for half a year and the rates kept increasing and stabilized. This is the injection respond, not the effect from perforation.
Apr-08	The artificial lift of the well was converted from gas-lift (GL) to ESP resulting in an immediate and huge increase in gross rates.
Dec-08	Liquid rates jumped again before decreasing gradually.
Jan-12	The pump was broken down and replaced with a new one. After replacement, the rates still kept declining at the same trend reflecting the effect from wateflood.

Table 3.1 Key activities of well X

Regarding the analysis, the data quality of this well is good in the aspect of the CRM application. Before implementing the waterflood in 1995, the well was produced under a solution gas drive, which was obviously reflected in its production

characteristics. The gross and oil rates exponentially declined together with reservoir pressure while the water cut remained small and the GOR kept increasing because of higher amounts of free gas. Right after the first injection, the well apparently has been gotten a good pressure support from injection. While producing via gas lift, there were some outside operations that significantly affect the production such as one zone being changed and additional perforation. Nevertheless, the field was already under secondary recovery meaning that the primary depletion has been mostly completed; thus, most of the production came from the injection. The sudden jump or drop because of primary recovery generally does not last long for the data. For this well, a sudden jump in December 2003 because of perforation was actually small and last for only a month before the well began receiving a strong pressure support. This kind of issue was addressed by manually removing these anomalous data from fitting, which will result in an improvement in the accuracy of the output parameters. The appropriate CRM fitting window is the period that the well exhibited WF response, few interruptions from field operations and no violation in constant productivity index. For this well, it is from 2003 onwards.

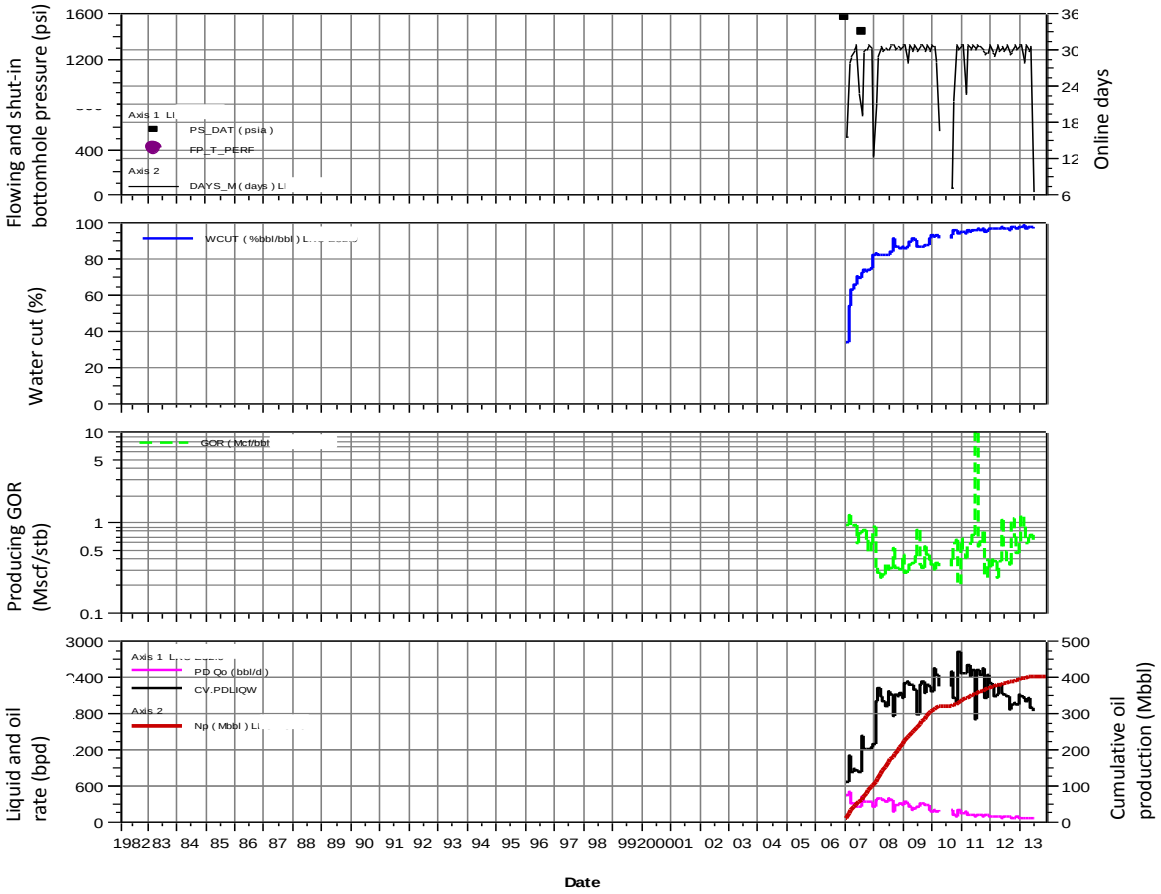

Figure 3.6 Production history of well Y

Date	Key activities
Jan-07	The well was firstly put on production via GL.
Jul-07	Gross production rate jumped due to additional perforation but declined rapidly within a month due to low reservoir pressure because of already depleted reservoir.
Jan-08	The lifting mechanism was converted to ESP.
Aug-10	The ESP was being replaced.

Table 3.2 Key activities of well Y

Most of the time, the well has been producing stably and continuously via electrical submersible pump (ESP) despite one replacement, which did not change the production trend. The well was subjected to little operational interference. The production history exhibited a considerable fluctuation in liquid rate which should be attributed to fluctuations in water injection rates. Hence, this well is a very good candidate for CRM fitting.

Wells in a real field are shut-in frequently because of several reasons such as well interventions, safety and limitation on surface facilities. For each month, each well was produced or injected for different amount of times indicating by number of online days plotted as the black lines in the upper chart of Fig 3.6. This partial month production issue was addressed by converting the calendar-day (CD) rate to the producing-day (PD) rate using the equations below:

$$CD\ rate = \frac{Total\ volume\ of\ production\ or\ injection\ in\ that\ month}{total\ number\ of\ days\ in\ that\ month} \quad (3.1)$$

$$PD\ rate = CD\ rate \times \frac{total\ number\ of\ days\ in\ that\ month}{number\ of\ days\ the\ well\ is\ active\ in\ that\ month} \quad (3.2)$$

If the well was inactive for the whole month, the rates will be set to zero. According to Weber (2009), periods with zero data are excluded in the sum in the objective function (Eq. 2.10), which means that in these periods, the total production rate is not computed from the Eq. 2.08.

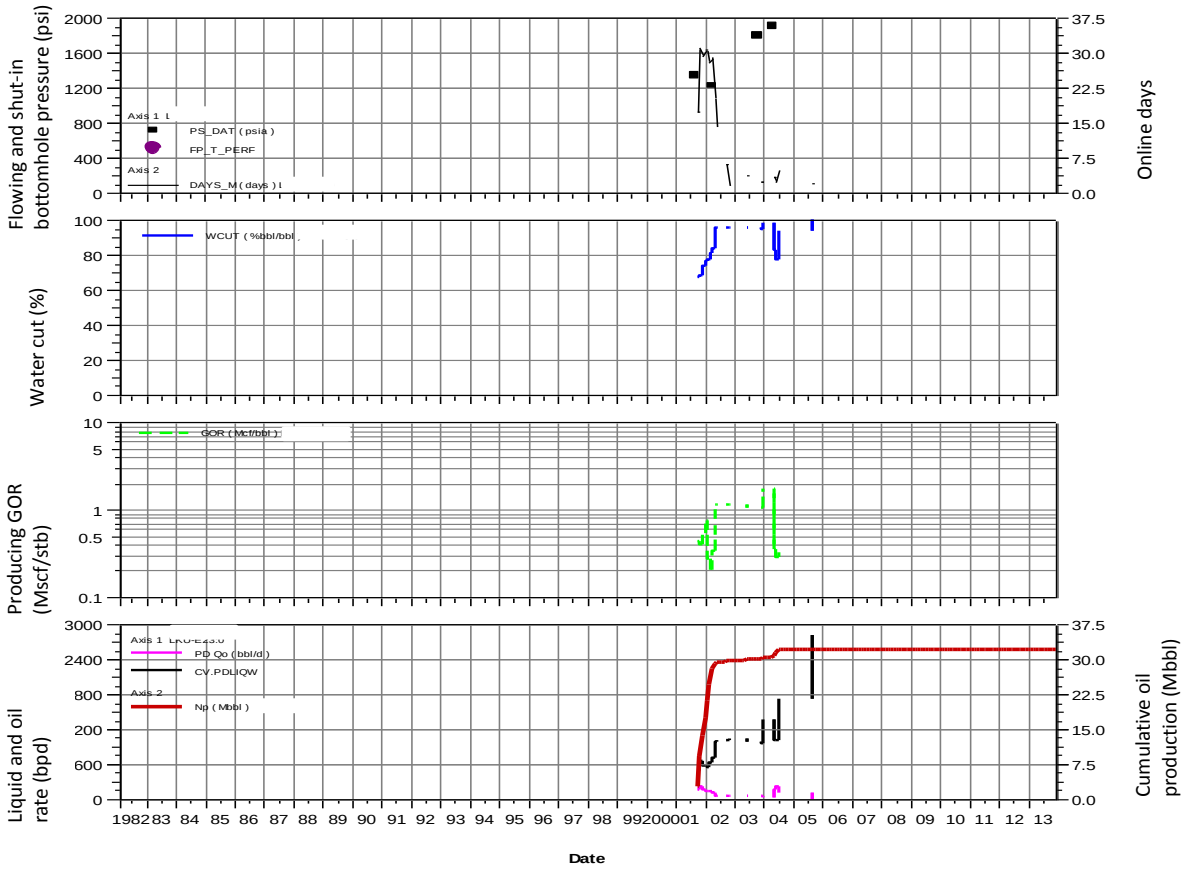

Figure 3.7 Production history of well Z

Figure 3.7 displays an example of production data that is poor for CRM fitting. The well has been shut-in most of the time because of extremely high water cut at the early stage. The reason is that at the time the well was drilled, that area has already been water-broke through. The sudden increase in liquid rate in May 2002 is because of the perforation change, not the response from injection. As expected, the jump lasted only a month because of the highly depleted reservoir. Afterwards in 2008, the well was converted to an injector. Therefore, this well was excluded in the analysis as a producer but will be treated as an injector. In this work, there will be no dual-role wells. The role of each well, either producer or injector, is assigned based on the appropriateness of the

data. Three examples above demonstrated how the data was examined and the issue of violating the model's assumption of constant productivity index was handled.

Another assumption of the CRM is that the compressibility of the system is constant. The total reservoir compressibility is given by:

$$c_t = c_g S_g + c_o S_o + c_w S_w + c_f \tag{3.3}$$

where c is the compressibility, S is the saturation and the subscripts g, o, w, f denote gas, oil, water and rock respectively. While the compressibility values of oil, water and rock are in the same range, the value of gas is much higher than all of those. Hence, if free gas presents in the reservoir, the total compressibility of the reservoir will be dominated by the gas compressibility, which is a strong function of pressure. Furthermore, in this case, changes in fluid saturations also largely affect the total compressibility. This violates the constant-compressibility assumption and may yield a serious error in the calculation. On the other hand, in the absence of gas, changes in saturation cause a negligible effect on the total compressibility as the compressibility of those substances is small and constant. This implies that it is favorable to have only oil and water in the reservoir with minimal amount of free gas. For a system with large compressibility, the gain cannot be determined for a distant pair because the injection signal tends to be fully dissipated before being seen in a producer.

The presence of free gas is indicated by the large producing GOR (R_p), especially when it is larger than the initial solution GOR (R_{si}), which is around 800 scf/stb for this field. According to the upper plot of Figure 3.2, in 1995 when the injection was first implemented, the field R_p was as high as 3,000-4,000 scf/stb corresponding to 50%-lower than the bubble point reservoir pressure because of 12-year pure primary depletion. As expected, R_p has gradually dropped as the reservoir voidage was being filled by water. From 2002 onwards, the producing GOR has become more stable and approached the R_{si},

which signifies that the reservoir fluids are approximately liquid. Therefore, in the aspect of fluid compressibility, this period is suitable for CRM application.

Despite the selection of the appropriate fitting period, to further improve the accuracy of the model, free gas production is determined and converted to equivalent liquid rate using this equation:

$$q_{fg} = q_o \times (R_p - R_s) \times B_g \tag{3.4}$$

where q_{fg} is the free gas production rate in reservoir barrel per day and can be added directly to the liquid rate:

$$q_t = q_o + q_w + q_{fg} \tag{3.5}$$

where q_t is the total production rate used in the model. This conversion is substantially useful when the reservoir is highly saturated, in which there is significant amount of free gas production. R_s and B_g data are available from PVT analysis and they depend on pressure as shown in the Figures below.

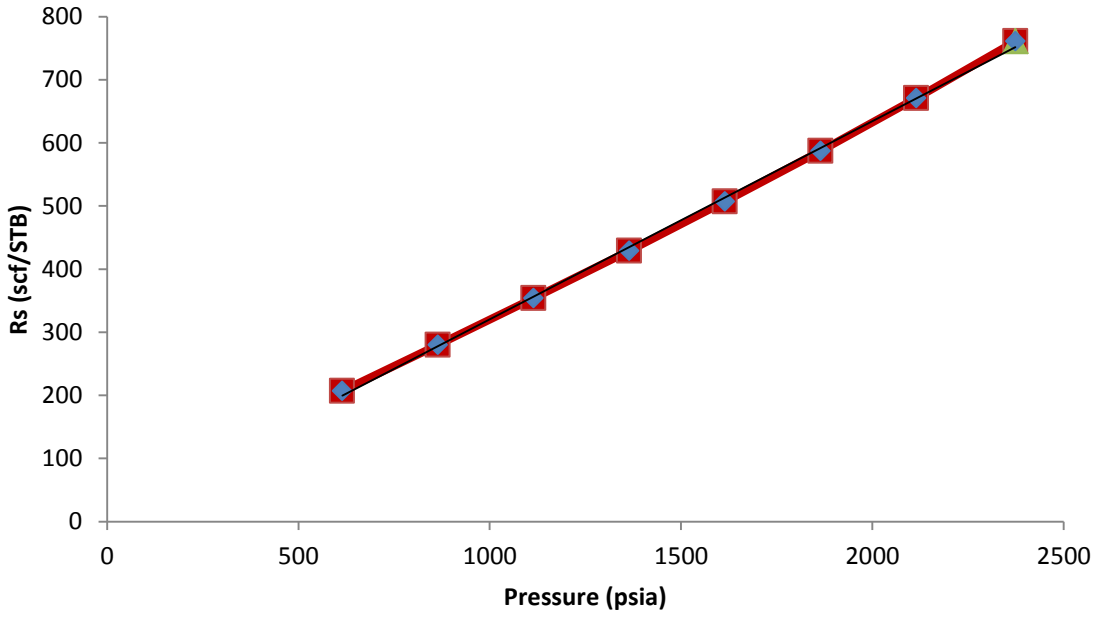

Figure 3.8 Saturated solution gas-oil ratio (R_s) versus pressure of the oil in this field

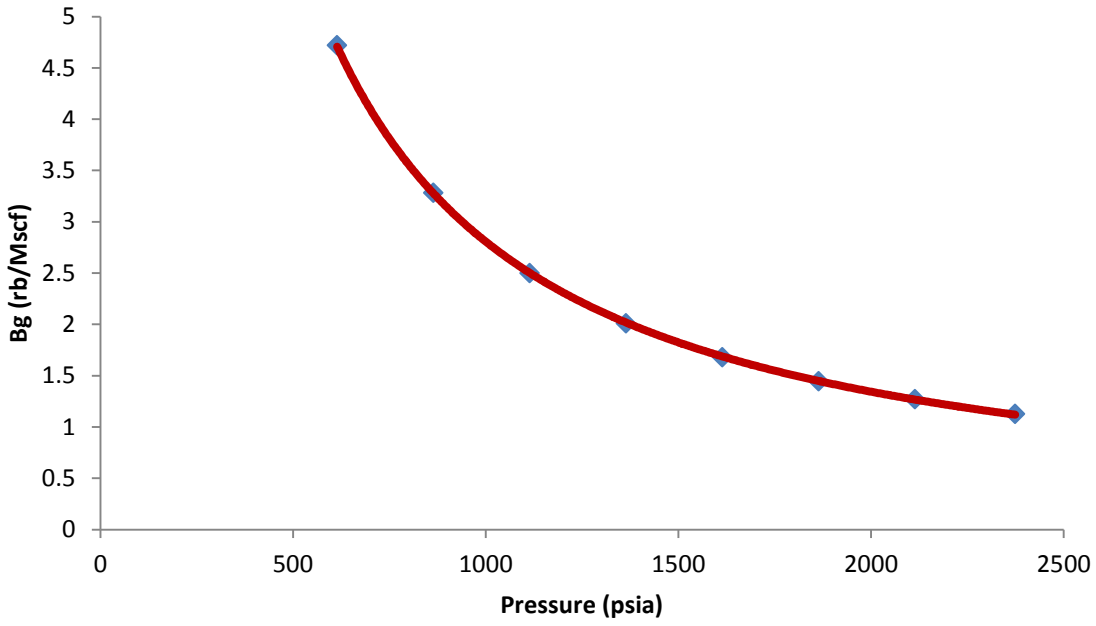

Figure 3.9 Gas formation volume factor (B_g) versus pressure for the fluids in this field

As both parameters vary with pressure, it is essential to establish the plot of average reservoir pressure versus time using pressure survey data from all wells across the field as shown below.

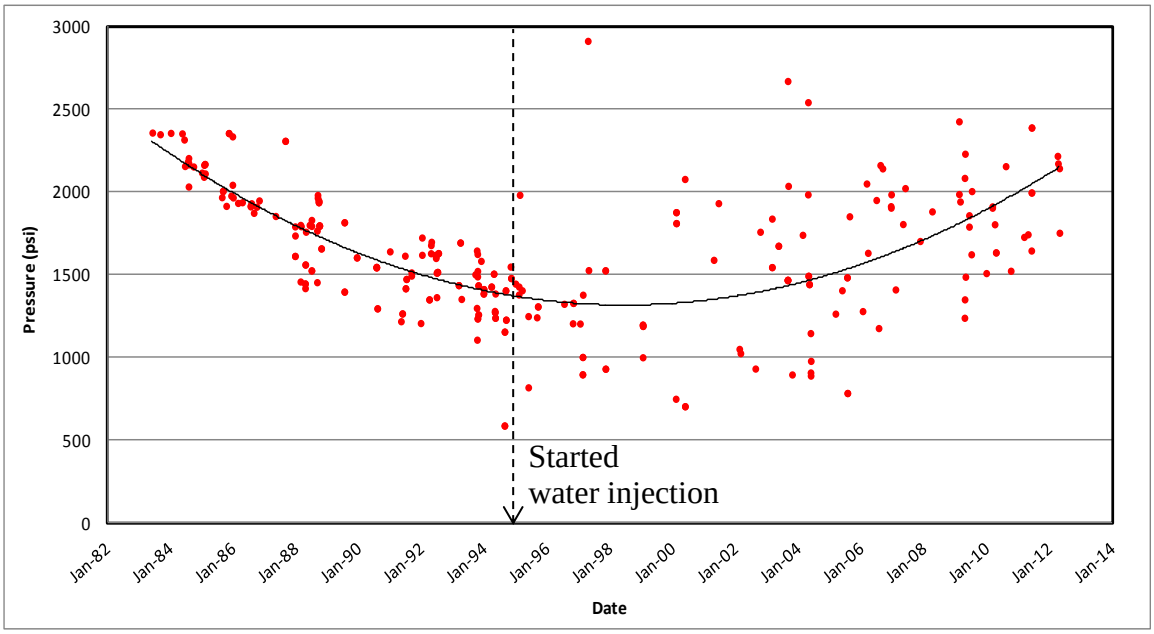

Figure 3.10 Average reservoir pressure versus time

Based on this information, free gas production of each well in each month can be calculated. To demonstrate how much the field production is free gas compared to liquid; the fraction of free gas to total production for the whole field was determined by summing the production of each well and shown in Figure 3.11. The higher the fraction, the more errors in the output calculated from the CRM as the reservoir significantly become more compressible.

The result looks reasonable as the values increased continuously during the primary production's period and began to drop after injection. Corresponding to the stabilized and low producing GOR from 2002 onwards, as previously discussed, during this period, the fractions were mostly negligible as the values become negative. This implied that the unfavorable effect of the presence of the compressible fluid in the reservoir is minimized. In addition, the issue was addressed by adding the free gas production into the liquid production. All of these handlings satisfy the assumption of

slightly compressible fluid and assure the good quality of the estimated gains and time constants. On the other hand, the fraction of liquid to total production on the lower plot is inversely related to that of the free gas. Theoretically, they should sum to unity. At the late time when waterflood has matured, the fraction has become stable at almost 1.

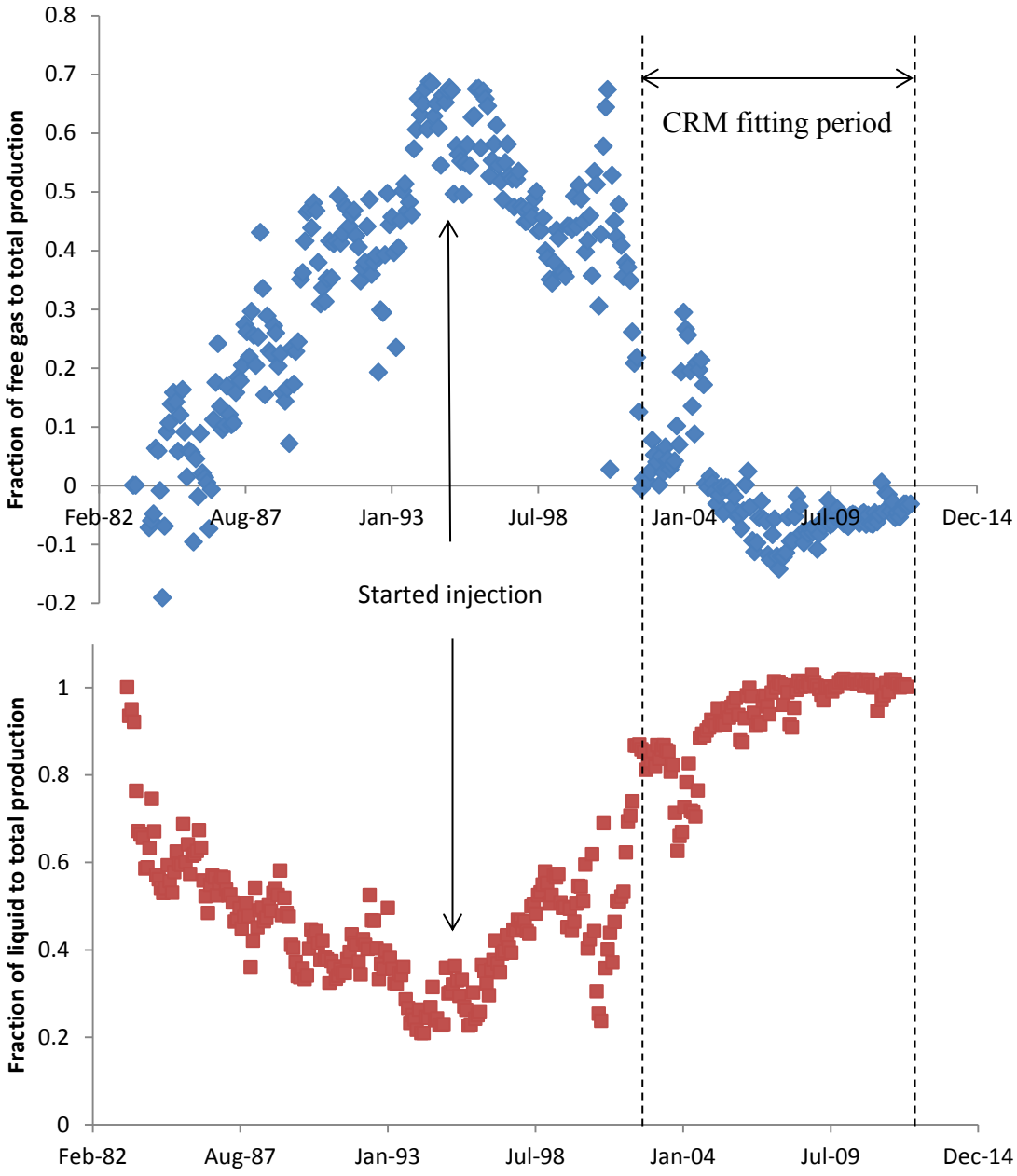

Figure 3.11 Amount of free gas and liquid production compared to the total production

Well bottom-hole flowing pressure (FBHP) is another CRM input parameter. Elements contributing to well production rates can be divided into 2 groups, reservoir and non-reservoir elements. The reservoir elements include geology, reservoir properties, fluid characteristic and rock-fluid interaction. This is the one that is of main interest as the objective of the CRM is to quantitatively define it. On the other hand, the non-reservoir elements consist of all factors that are not related to the reservoir, such as near wellbore effects, artificial lift, well mechanical problems, surface facilities, manifold pressure, choke size and etc. All of them can substantially affect the production rate. The CRM treats this issue by using the FBHP data to capture the changes in these conditions from bottom-hole to separator. For instance, when the manifold pressure increases, the decrease in production rate is accounted by the rise in the FBHP; thus, the fitting will not suffer.

Nevertheless, installing down-hole pressure gauges to measure real-time FBHP is generally not practical because of cost concerns. Although the FBHP is measured periodically by a wireline unit, it is still not measured at every time interval. This makes the data unavailable; most of the previous CRM field case studies solved the problem by assuming them constant all over the considered periods so that the FBHP term can be dropped out of the equation (Eq. 2.8). To satisfy the elimination of FBHP, it should be inferred that the non-reservoir elements are steady during the fitting period for the gain and time constant to represent the true reservoir characteristics. For a real field, it is almost inevitable to select the CRM fitting period that each well produces via the same artificial lift for the whole period as the reservoir condition is dynamic so that producers are worked-over to improve the performance. For example, when an artificial lift method is converted from gas-lift to electrical submersible pump (ESP), the pump will produce the well at a much higher flow rate because of input power, which definitely causes a

huge change in FBHP. Obviously, the immediate increase in flow rates cannot be attributed to the injection response; thus, the rate data alone is insufficient to characterize the inter-well properties in the case of varying FBHP, which is usually unavoidable in every oil field.

Therefore, assuming the FBHP constant because of its unavailability can lead to significant errors on the output. Although the surface well-head pressure (WHP) is generally available for any field, calculating the FBHP from WHP is troublesome as the estimation of pressure drop in case of multiphase flow is complicated. It requires approximations of fluid properties and each correlation (i.e. Hagedorn and Brown (1965), Beggs and Brill (1973) can provide different output. Moreover, the flow condition in wellbore is dynamic; it always changes from time to time. Hence, it is considered to be unpractical to estimate the FBHP from the WHP for all wells in the field for a period of more than 10 years.

It is essential to look for a method to compensate the absence of FBHP. Actually, the surface well-head pressure (WHP) itself can be substituted straightforwardly because they are physically related and fluctuate up and down almost together. Figure 3.12 is a generic plot of measured FBHP and measured WHP versus time. The purpose is to illustrate their trends that run together. Even though they are not on the exact same trend, because the pressure drops in wellbore change with time depending on flow conditions and fluid properties, at least it is better for the CRM to have the WHP instead of having nothing about the pressure data. Hence, to capture changes from non-reservoir elements, the WHP will do the task acceptably instead of the FBHP. As for most fields, this data is usually access available. Thus, the WHP data, treated exactly as the FBHP of each well is gathered and input into the model.

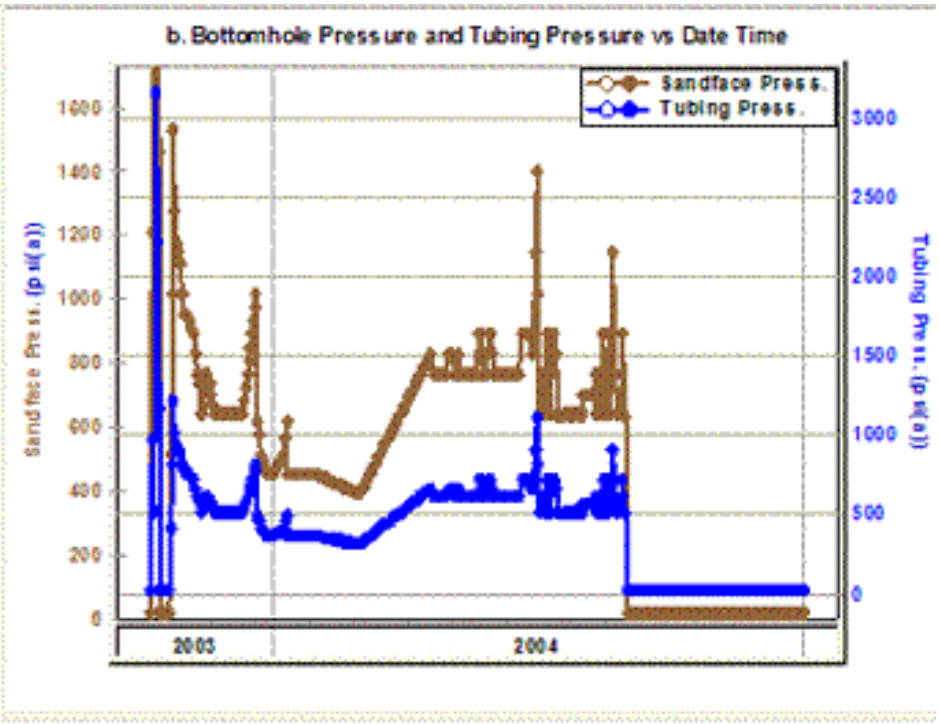

Figure 3.12 The FBHP and the WHP have similar trends (IHS Inc., 2014)

Preparing the well injection data is not as complicated as the production data. The simplicity is because it is an input signal and there is no necessity to identify when and why the rates jumped or dropped. This is unlike a producer, which the changes in rates can be attributed to the non-reservoir elements; thus, they can mislead the CRM's interpretation. As exemplified in Figure 3.13, the data quality for the injectors in this field is good for the CRM analysis as there were considerable fluctuations.

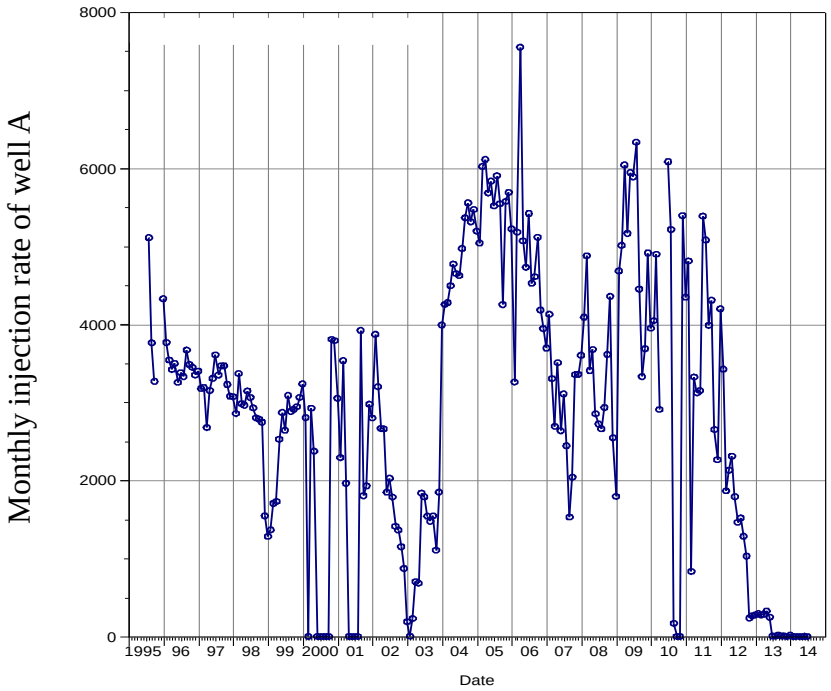

Figure 3.13 Example of well injection data of this field

The dynamic conditions of a real field that can change individual sand connectivity of an injector with surrounding producers, such as sand and scale accumulation, zone change and additional perforation, can introduce uncertainty in CRM's output. This is because these modifications are not relevant to reservoir properties. For example, an injector used to distribute water into both reservoir A and B for 2 years before sands that are gradually accumulated completely plugged the perforation into reservoir B, the bottom one. After that, this injector will not be able to inject any water into this reservoir and thus, can connect to the nearby wells only through reservoir A. The connectivity change here definitely affects the estimations of the gain and the time constant. Therefore, it should be conscious that any injector that had a very dynamic down-hole condition might result in high uncertainty of CRM parameters associated with it.

3.2.2 The two-phase coupled CRM

As previously discussed in the literature survey section, there are additional inputs required for the two-phase flow coupled CRM. Firstly, the reservoir pore volume associated with each producer must be determined from matching each well's historical water cut with Koval's equation. The procedures are explained in chapter 2. Theoretically, the water cut increases smoothly with time either concave or convex upward (Figure 3.14). This makes matching with synthetic data simple. An example of a well that has a good water cut trend is shown in Figure 3.15. In this case, the matching is straightforward.

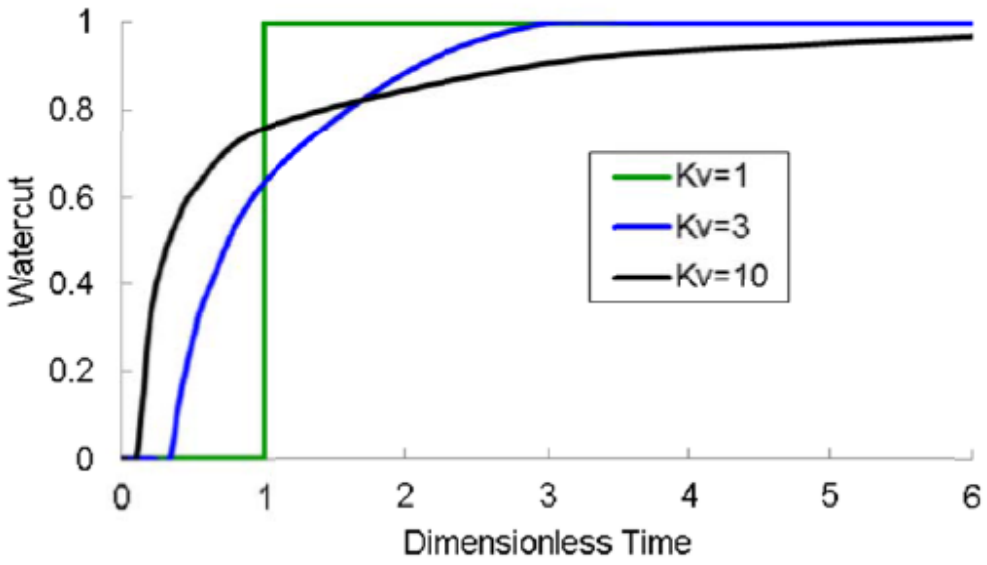

Figure 3.14 Synthetic water cut matched with Koval's model

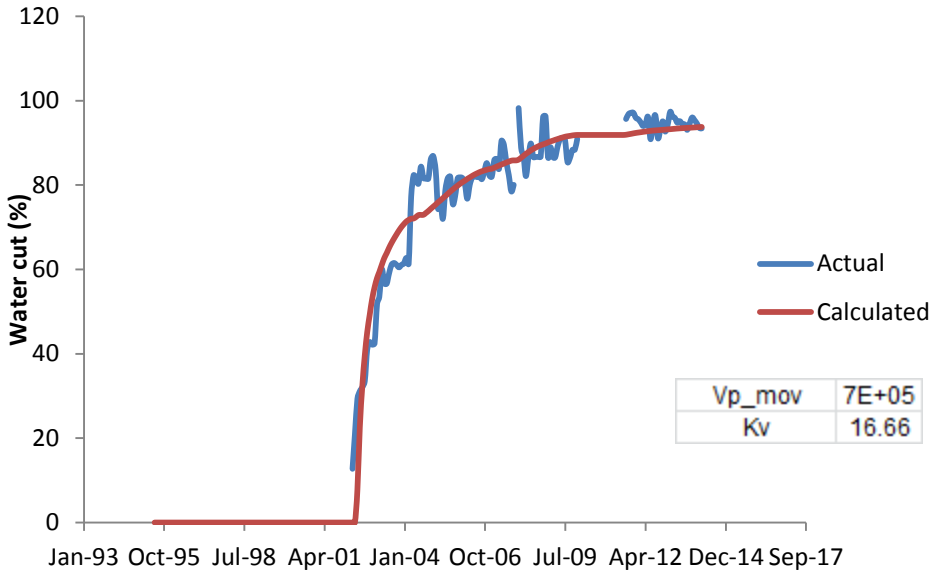

Figure 3.15 Example of a good water cut data fit

Nonetheless, matching the model with field data is more complicated for many producers as the trend might not follow the theory because of field operations and constraints. Sometimes, the water cut increased very rapidly as exemplified in Figure 3.16. This might be because of an early water breakthrough in a thief zone or poorly managed waterflood. After that, the well was shut-in permanently as it might not be able to be worked-over because of operational constraints; thus, there is no late trend of high and more stabilized data. Another similar example is shown in Figure 3.17. For this well, however, there is only a late trend. This is because the well was drilled later at a mature stage of field waterflood in which there were many water breakthroughs throughout the field. As a result, the well has been producing with a high water cut from the first day on stream. If the results, the Koval factor and the pore volume, look infeasible, they will not be used and will be obtained from nearby-well performance.

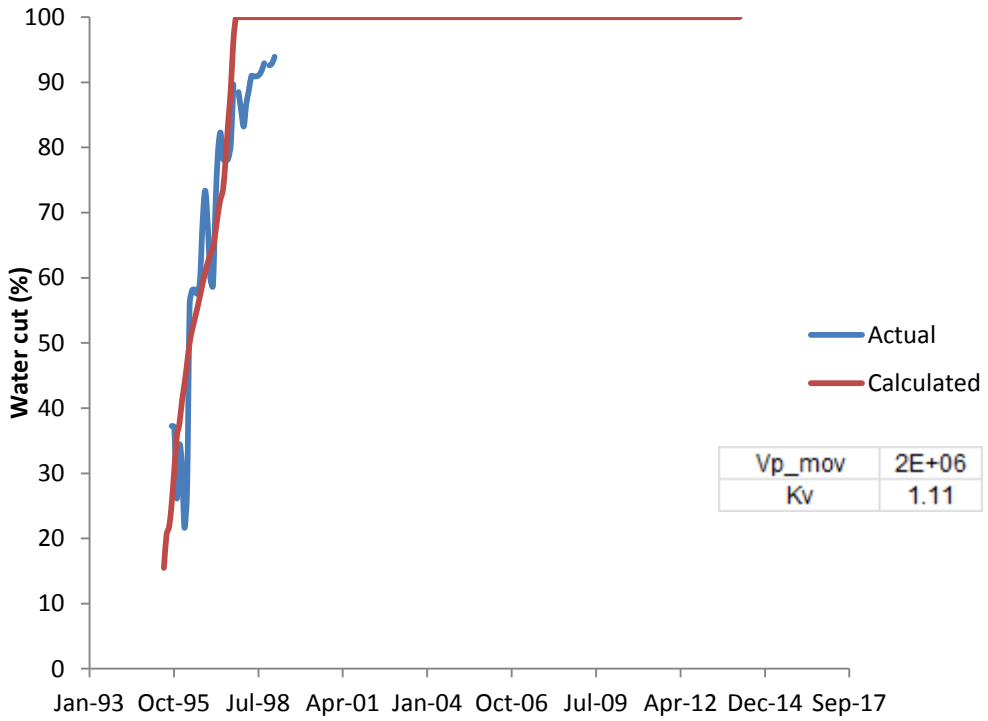

Figure 3.16 Example of a poor quality water cut data with only the steep increase interval

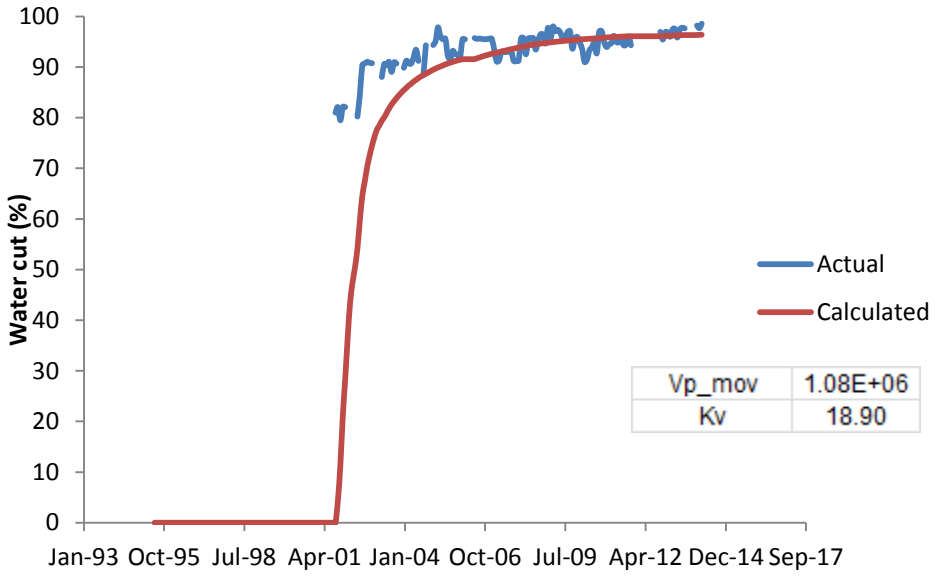

Figure 3.17 Example of a poor quality water cut data with only the late stabilized interval

As shown in Figure 3.18 the well's water cut exhibited two separate trends. The first trend is subjected to the primary production while the second one can be classified as the waterflood response. In this case, it is essential to clearly distinguish the data and identify the one that is result of the injection.

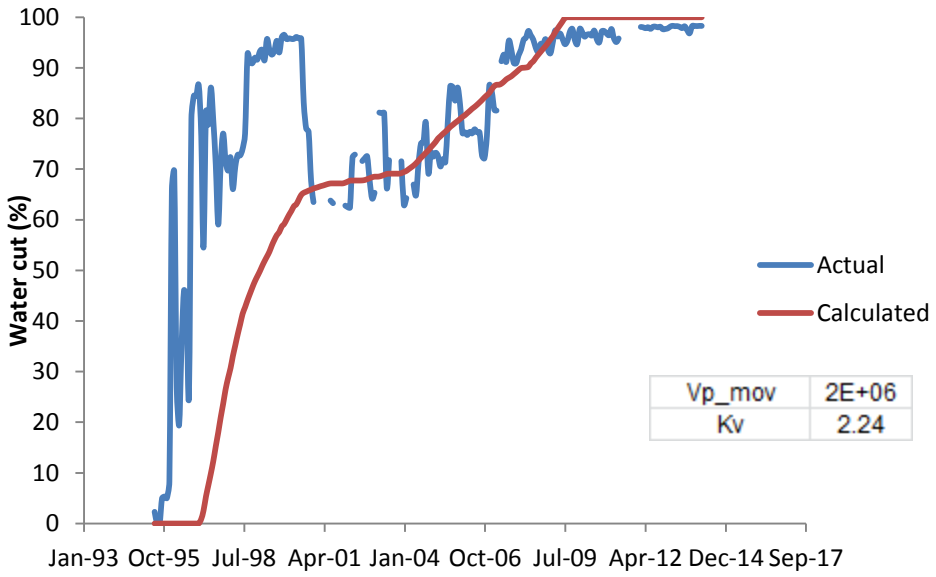

Figure 3.18 Example of a poor quality water cut data with 2 separate trends

The pore volume obtained from this matching is the movable pore volume. The Eq. 3.6 is used to convert this to the dynamic pore volume, which is more useful in the analysis of bypassed area.

$$V_{p,dynamic} = \frac{V_{p,movable}}{movable\ saturaions} = \frac{V_{p,movable}}{1 - S_{wc} - S_{or}} \qquad (3.6)$$

where S_{wc} is the connate water saturation and S_{or} is the residual oil saturation. Both of them are determined from special core analysis (SCAL) data. The acquired dynamic pore volume of each producer is displayed in Figure 3.19, together with well cumulative liquid and oil production for comparison. The dynamic pore volume is the estimated ultimate

drainage volume of a producer. The wells in Figure 3.19 are shown in a chronological order from left to right, the first drilled wells on the left. The general downward trend of the dynamic pore volume (the blue line) is reasonable as the early wells tend to have larger drainage area than the late wells because of the larger production time. Using these values to estimate the volume drained by the group of injectors, the combination of the associated pore volume of all wells in the well adds up to 70% of the total static volume. This is understandable as many wells are still producing and there are some down-dip and remote areas having small well density.

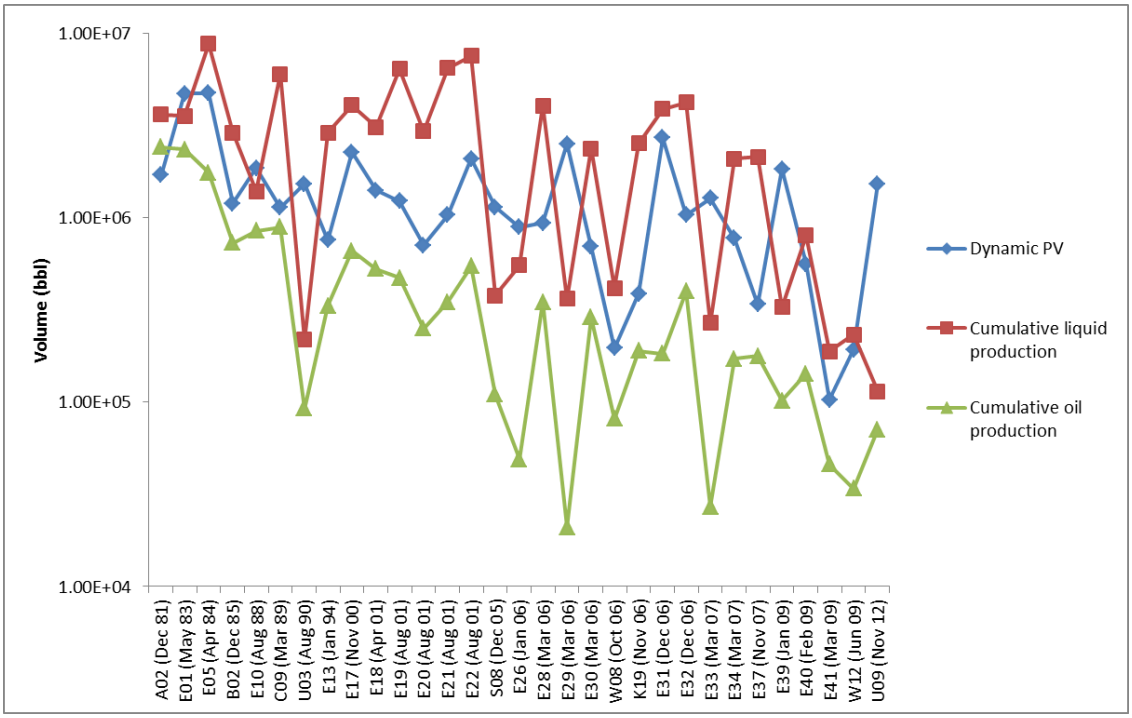

Figure 3.19 Dynamic pore volume, cumulative liquid and oil production associated to each producer, to date

Compared to the total amount of liquid produced (the red line), many wells have their dynamic pore volume less than their actual production. This finding is explainable as the reservoir is not a closed system because significant amount of water has been injected into it for 20 years. The producers here were producing both the reservoir and injected fluids. Currently, the reservoir is in the mature stage of waterflood and there is ineffective cycling of water occurring in several injector-producer pairs that are highly connected through high permeability streaks. This phenomenon is an evidence of inefficient waterflood that is to some extent inevitable, especially in the late stage of a reservoir. On the other hand, the cumulative oil production (the green line) should definitely less than the dynamic pore volume because the oil has been solely produced from the reservoir. The comparison between the green and blue lines satisfies this condition.

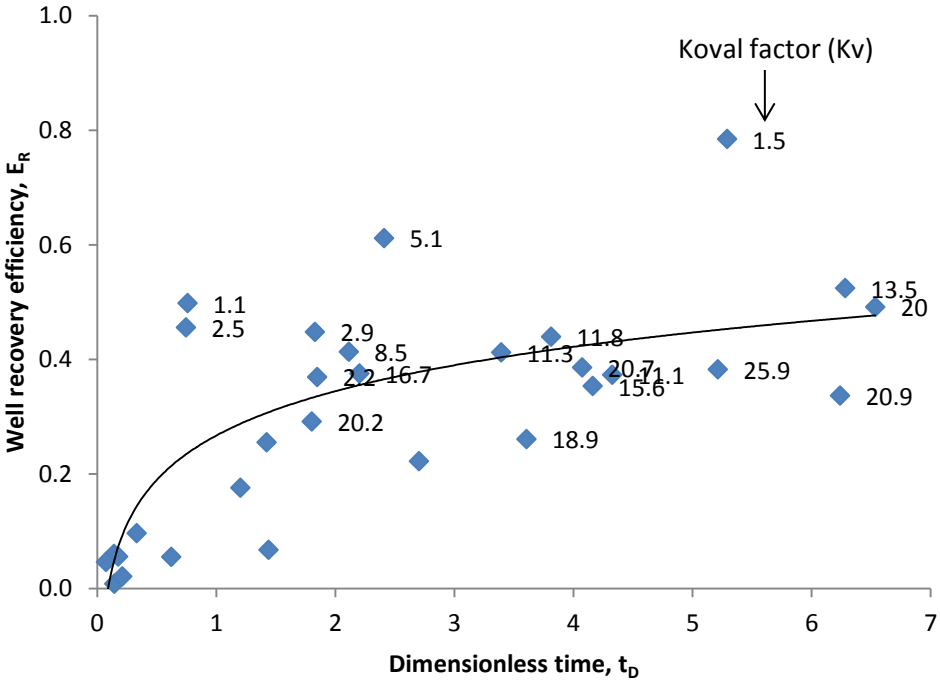

Figure 3.20 Estimated well recovery efficiency versus pore volume injected

To validate the estimated dynamic pore volumes, the data on Figure 3.19 was used to calculate the recovery efficiency of each well and their pore volumes injected using the following equations:

$$E_R = \frac{Cumulative\ oil\ production}{Dynamic\ pore\ volume} \tag{3.7}$$

$$t_D = \frac{Cumulative\ water\ injection}{Dynamic\ pore\ volume} \approx \frac{Cumulative\ liquid\ production}{Dynamic\ pore\ volume} \tag{3.8}$$

where E_R is the well recovery efficiency and t_D is the dimensionless time. The result is displayed in Figure 3.20. Each data point, labeled with the Koval heterogeneity factor (Kv), represents a single producer. The theoretical relationship between E_R and t_D is shown in Figure 3.21. In the early stage of waterflood, the recovery efficiency steeply increases with pore volume injected. However, the rate of increase, i.e. the slope, decreases as injection proceeds because some areas or layers have already been water-broke through. In the late time, considerable amount of water injected only causes small incremental oil production as displayed by the decrease in slope.

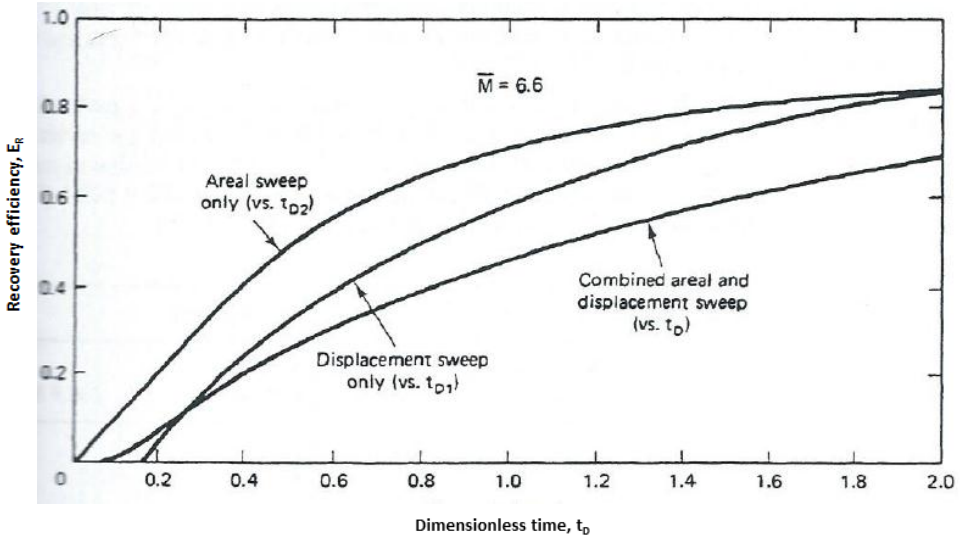

Figure 3.21 Theoretical relationship between recovery efficiency and dimensionless time (Lake, 1989)

Unlike the simulated data, the field data contain many uncertainties including the production allocation, the measurement accuracy, the reservoir heterogeneity and the operational disruption. Moreover, the Koval equation (Eq. 2.21) used to match historical water cuts to determine the dynamic pore volume and the Koval factor, is based on several assumptions. According to these influences, the obtained result (Figure 3.20) is considered to be satisfactory compared to the theoretical one (Figure 3.21). In addition, overall, the good-performance wells, which are the one that has higher recovery efficiency at the same amount of water injected, tend to have lower Koval factors. In other word, at the close positions on the x-axis, the lower points seem to have higher Koval factors than those of the upper points. This observation is as expected because the high Koval factor means high heterogeneity leading to poor waterflood recovery.

Another input is the average initial saturation around each producer. It can be estimated from well logging data, which are generally available for the wells in this field. As the reservoir is a combination of multilayer stacked sands, the average initial saturation is determined from the saturations of each layer weighed by the porosity and the thickness of that layer:

$$\bar{S}_{o,i} = \frac{\sum_{n=1}^{n=N}(S_{o,n} \times \emptyset_n \times h_n)}{\sum_{n=1}^{n=N}(\emptyset_n \times h_n)} \tag{3.7}$$

where N is the total number of sand layers in that well. For this field, the data range from 0.36 to 0.69, with the average value of 0.51.

Other input parameters for the two-phase CRM are the oil and water viscosities and relative permeability. The oil viscosity is determined from PVT data of the reservoir fluid in this field as shown in Figure 3.22. Despite the property's dependency on pressure, the reservoir pressures during the CRM fitting period seemed stabilized at the values close to the bubble point pressure; thus, the single value of oil viscosity for this

range of pressure is reasonably estimated to be 0.8 cp. The water viscosity, a constant value of 0.37 cp., is determined from correlations of Chestnut (unpublished) and Bradley et al. (1987) with salinity and temperature.

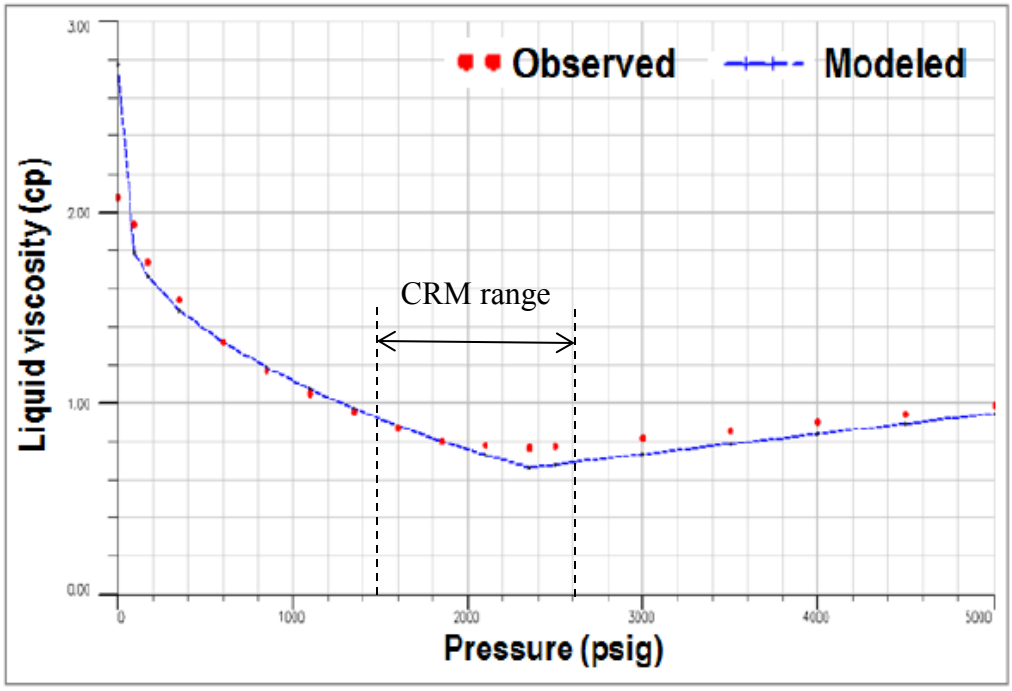

Figure 3.22 Oil viscosity versus pressure obtained from fluid sampling analysis

Lastly, core analysis reports were analyzed to select the proper set of oil-water relative permeability that represents the whole field. The data used is displayed in Figure 3.23. All of these data consisting of the dynamic pore volume, the initial saturation, the viscosity and the relative permeability are used by the two-phase coupled CRM as previously explained in section 2.1.2.2.

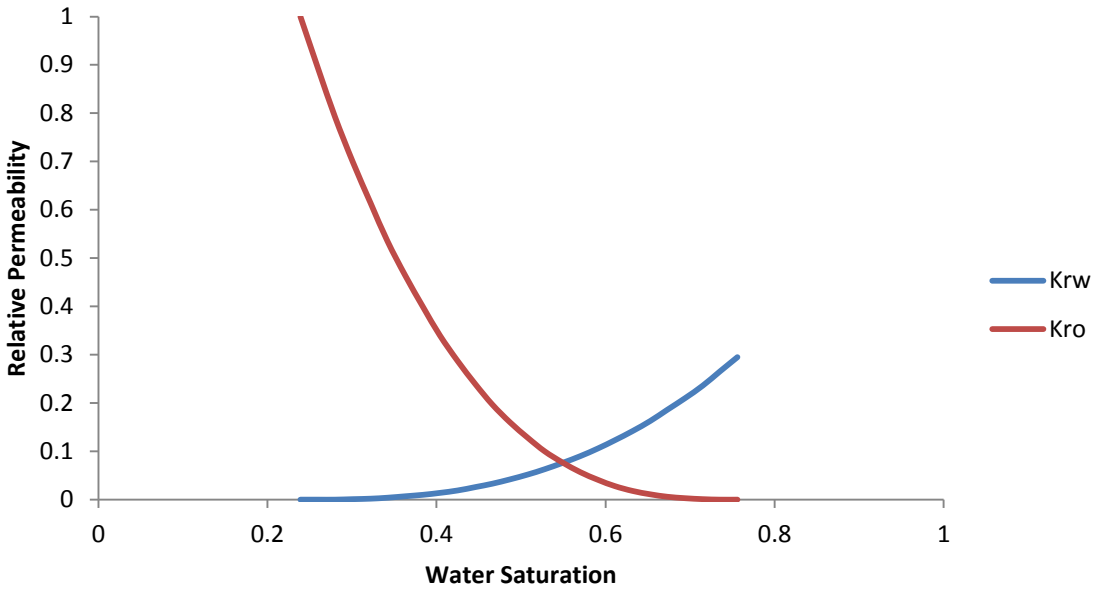

Figure 3.23 Oil-water relative permeability

3.3 MODEL SETTINGS

The selection of fitting interval is one of the most critical steps as the CRM is based on several assumptions. The more deviation from the assumptions, the less accuracy there is in the obtained output. On the other hand, if the interval is restricted to a very short time period to satisfy all conditions, the number of data points might not be sufficient compared to the number of unknowns. In this scenario, the fitting quality will deteriorate. This matter should be addressed as a compromise.

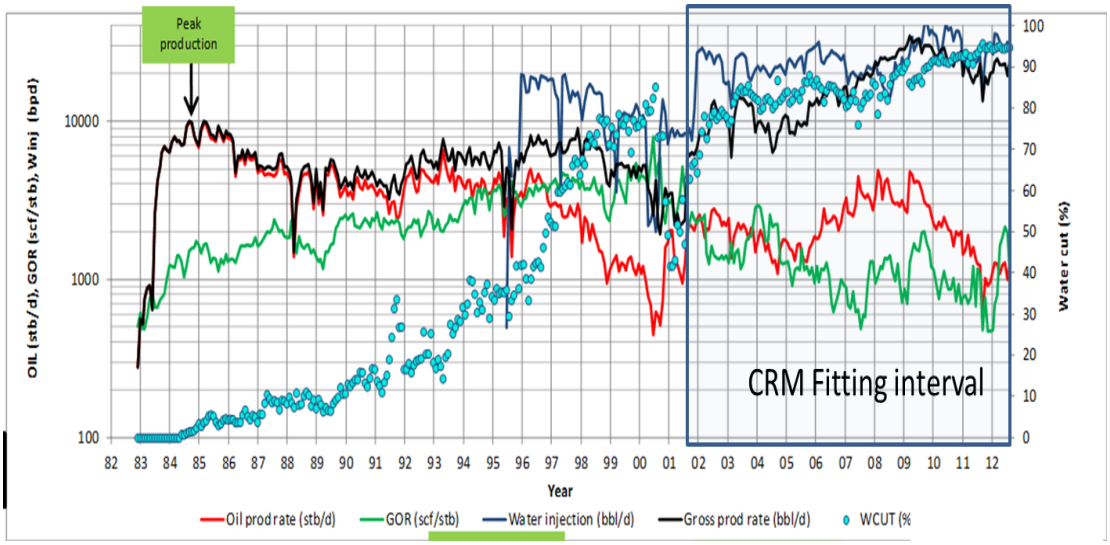

Figure 3.24 Field production history

The field production history, Figure 3.24, was examined. Because the reservoir has been continuously depleted for the first 13 years, during the early period of the waterflood, in which there were large amount of free gas in the pore space, water was injected faster than fluids that were produced. In the other word, the voidage replacement ratios were much greater than 1 during this period. While the injected water was displacing and compressing the free gas back to be dissolved in the oil, the gross production rates were still not responsive to the injection. Additionally, the producing GOR was another indicator informing that the fluid in the reservoir was compressible as the values were two to three times more than the solution GOR. This made the early period of waterflood, 1995 to 2002, not suitable for applying the CRM.

From 2002 onwards, the gross production rates began to increase gradually and within 4 years, they are approximately equal to the injection. The producing GOR became stabilized at the value of initial solution GOR. Therefore, the fitting period from 2002 to 2014 is selected for CRM's analysis.

Considering the adequacy of data points, the number of CRMP unknowns is:

$$No.of\ CRMP's\ unknown = N_p \times (N_i + 1) \tag{3.8}$$

where N_p is the number of producers and N_i is the number of injectors. This field has 31 producers and 22 injectors; thus, there will be totally 713 unknowns to be solved. According to Sayarpour (2008), although this is the minimum number of data points required, as a rule of thumb, the recommended number of data points is four times the number of unknowns in order to obtain a very good fit. Likewise, for the selected fitting period of 2002 to 2014, there are 1,982 data points available for fitting. Regarding the suggestion, this is almost three times the number of unknowns here so that the good fitting quality can be expected.

Another important model parameter is the radial limit, which is defined as the maximum separation distance that any well pair can connect to each other. If the distance between any injector and producer is more than the radial limit, the gain between them is automatically set to zero without any calculation. This leads to the reduction of the number of unknown from 713 to 682. Hence, the fitting quality increases unquestionably with the radial limit. This number, however, should be determined based on the depositional environment of the reservoir, the well spacing and the depletion caused by the existing wells observed from RFT pressure of the new wells. The reasonable range for this field is from 600 to 900 meters.

The upper and lower bounds of the time constant is set to ensure that the weight of the injection and BHP terms in Eq. 2.8 satisfies the condition:

$$0.001 \leq \left(1 - e^{-\frac{\Delta t_k}{\tau_j}}\right) \leq 0.999 \tag{3.9}$$

where Δt_k is the frequency of the rate and pressure data. For this data set in which sampling is on monthly basis, Δt_k is 30 days. Solving the equation, the time constants are allowed to range from 4.4 to 30148.2 days. In addition, if the calculated gain for any pair is less than 0.02, it will be set to zero. Wells with fewer data points than 10% of the total

number of fitting periods are also considered to be inactive and removed from the calculation.

3.4 RESULTS AND DISCUSSIONS

All the well-prepared data discussed in the previous section are subsequently input into the CRMP's and the coupled CRM's models, which were constructed on a platform called GAMS. GAMS is a powerful optimization software used to solve for the output parameters. For the size of this data set, the computation times are short compared to a finite-difference numerical simulation, ranging from 1 to 2 minutes. The word CRM used below will be specifically referred to the CRMP. The results obtained from these two models can be categorized for discussion into 4 groups consisting of fitting quality, gain, time constant and saturation.

3.4.1 Fitting quality

The final fit of total production rate for the entire field is illustrated in Figure3.25. Overall, the CRM is able to give an excellent fit as expected because of sufficient amount of data points, the appropriate selection of the fitting period as well as the quality control of the input data. The model slightly underestimates the measured data during some early and late periods. The system-wide R^2 value of the matching is 0.928.

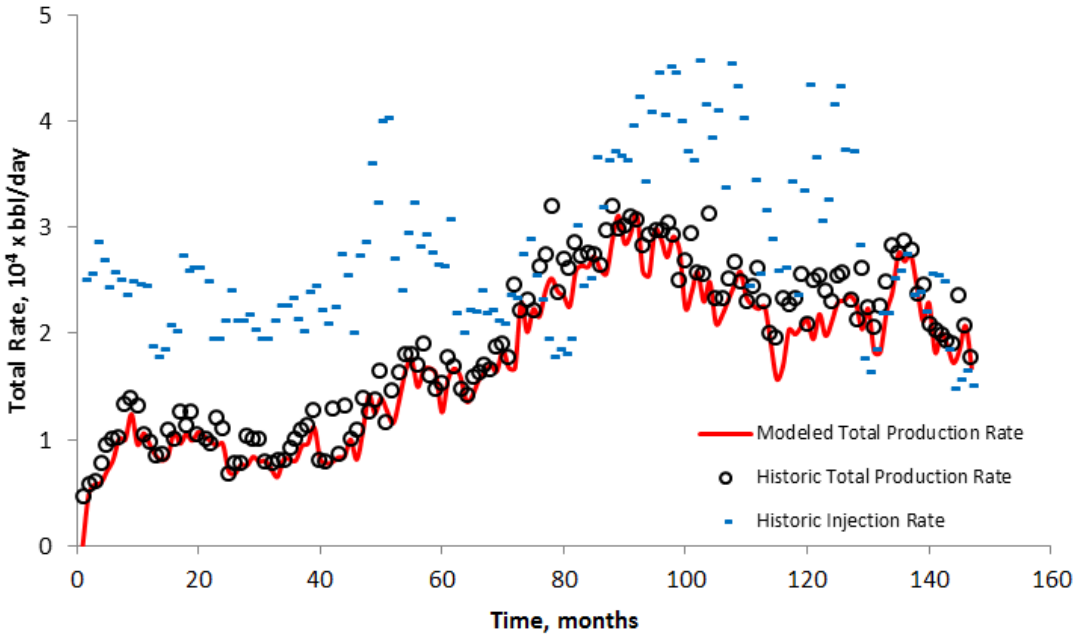

Figure 3.25 Total Liquid production match over the entire field

The goodness of fit was also examined well by well. The R^2 values for each producer's CRM fit are displayed in Figure 3.26. Despite the wide range of the R^2 values, from as low as 0.19 to 0.98, the history matching on a well basis behaves quite well as the average and the median of these data are 0.756 and 0.839, respectively, without any negative value. Examples of wells with excellent, good and poor quality matches are shown in Figs. 3.27- 3.29, respectively.

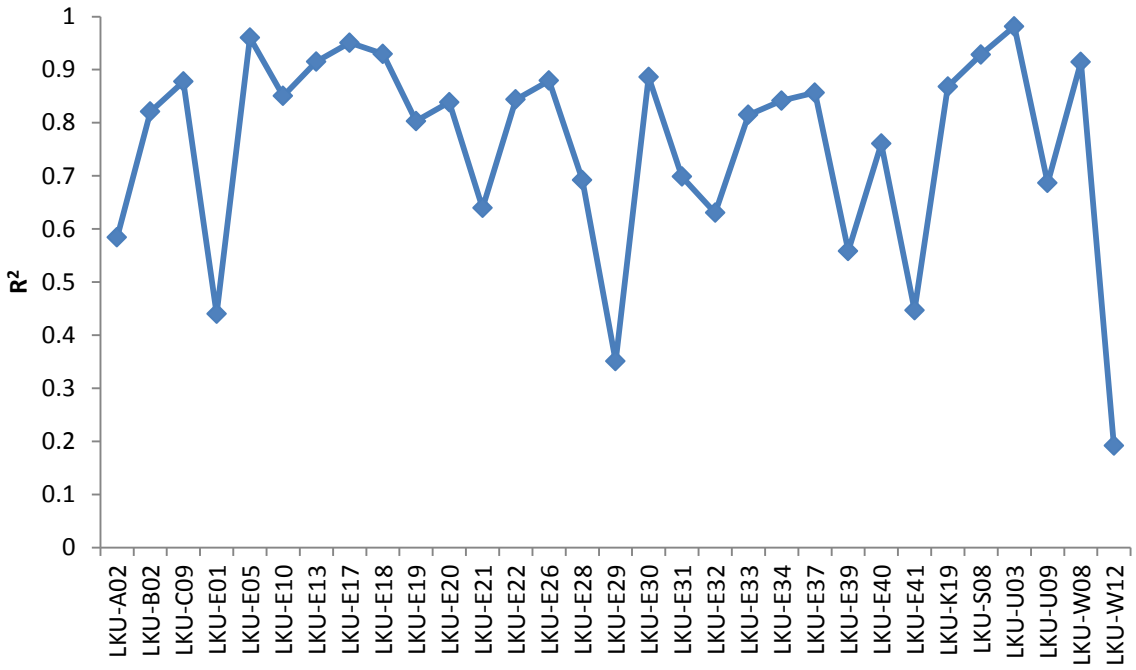

Figure 3.26 R^2 values of the CRM fits by producer for the field

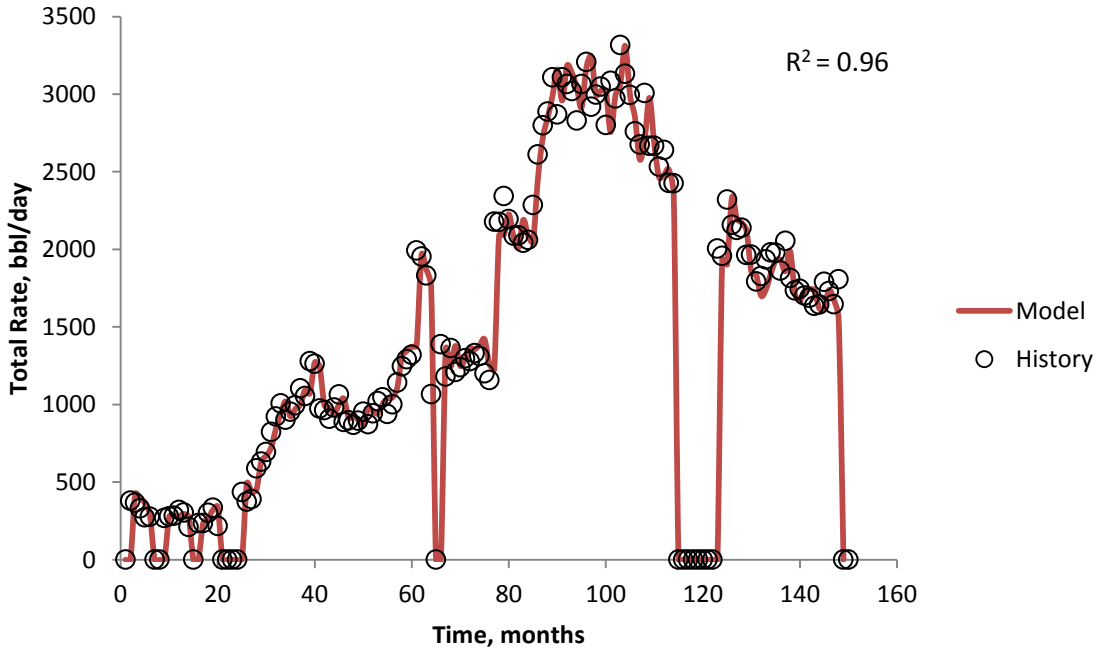

Figure 3.27 Example of an excellent total liquid production match

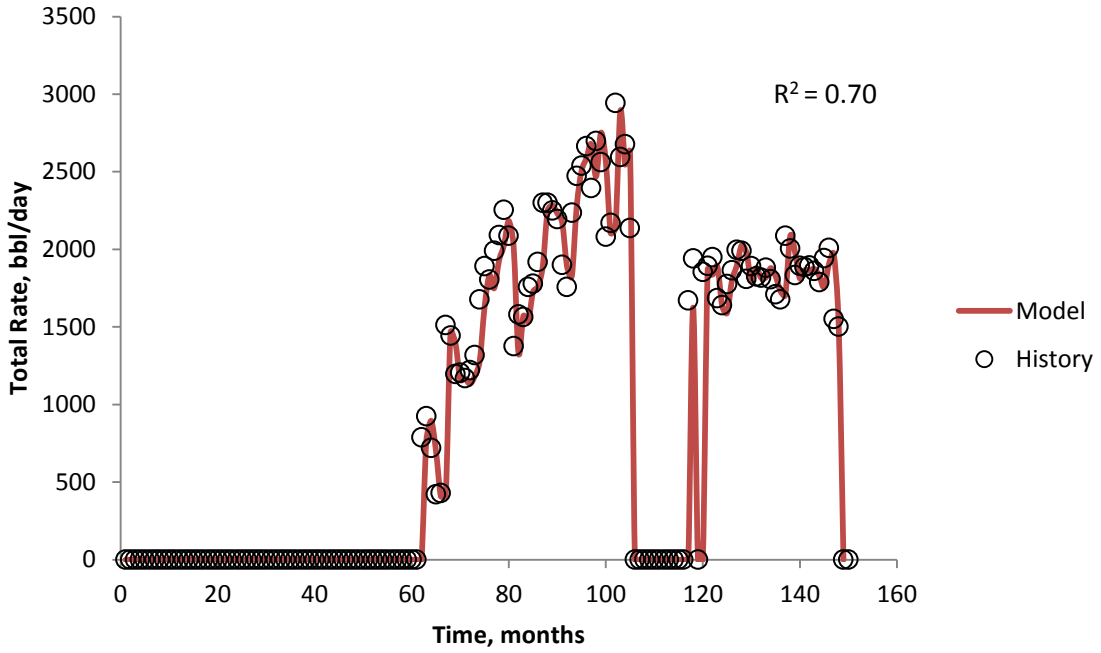

Figure 3.28 Example of a good total liquid production match

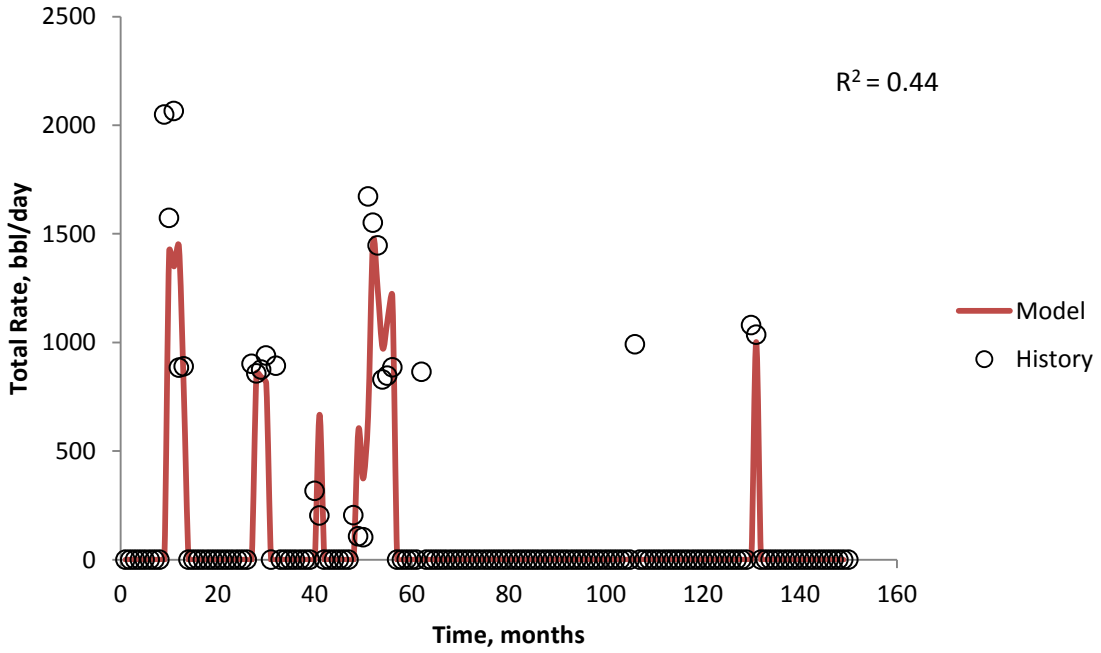

Figure 3.29 Example of a poor total liquid production match

The quality of matching seems to depend on the available number of data points of each well as shown in the Figure 3.30. Each producer is represented by a single point in the plot. It is obvious that 6 wells with low R^2 values (circled) have very limited available data for matching. There are several possible reasons for this. For example, the well was drilled in a water breakthrough area resulting in a poor performance; thus, it was shut-in for most of the time. On the other hand, the well was drilled lately relative to the fitting window so that it has been put on production for only a short period of time. The frequent or long shut-in of wells is also attributed to the mechanical problem of the artificial lift or the completion, the surface facility's constraints.

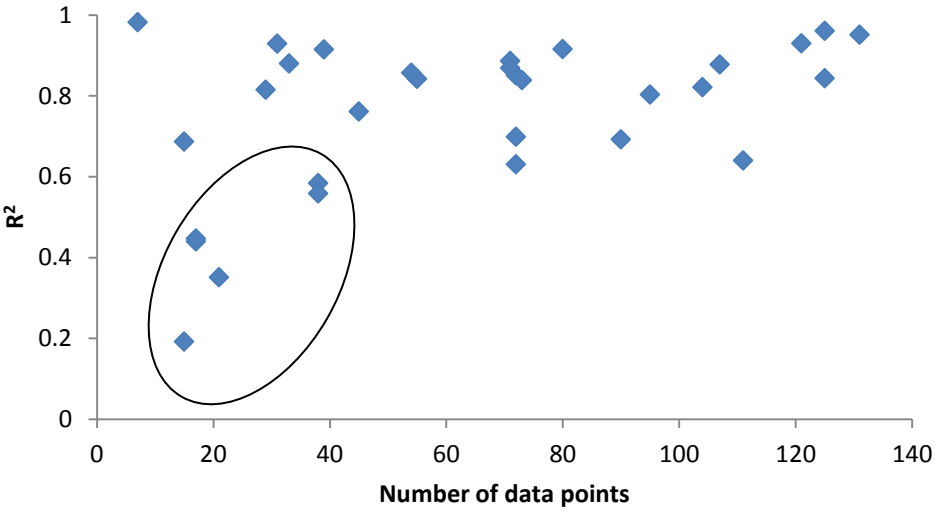

Figure 3.30 R^2 values of each producer versus its number of data points

3.4.2. Gain

The gain, or the interwell connectivity, is the key information for this research. It provides insights into the reservoir characterization and waterflood performance leading to the identification of bypassed areas. A connectivity map showing all calculated gains is

shown in Figure 3.31. The gain is denoted by a colored line joining an injector (the blue triangle) and a producer (the green circle). The color of the line is proportional to the magnitude of the gain as shown at the scale on the upper right of the figure. Because there are too many small gains, only the values that higher than 0.1 are shown to make the map clear for the analysis.

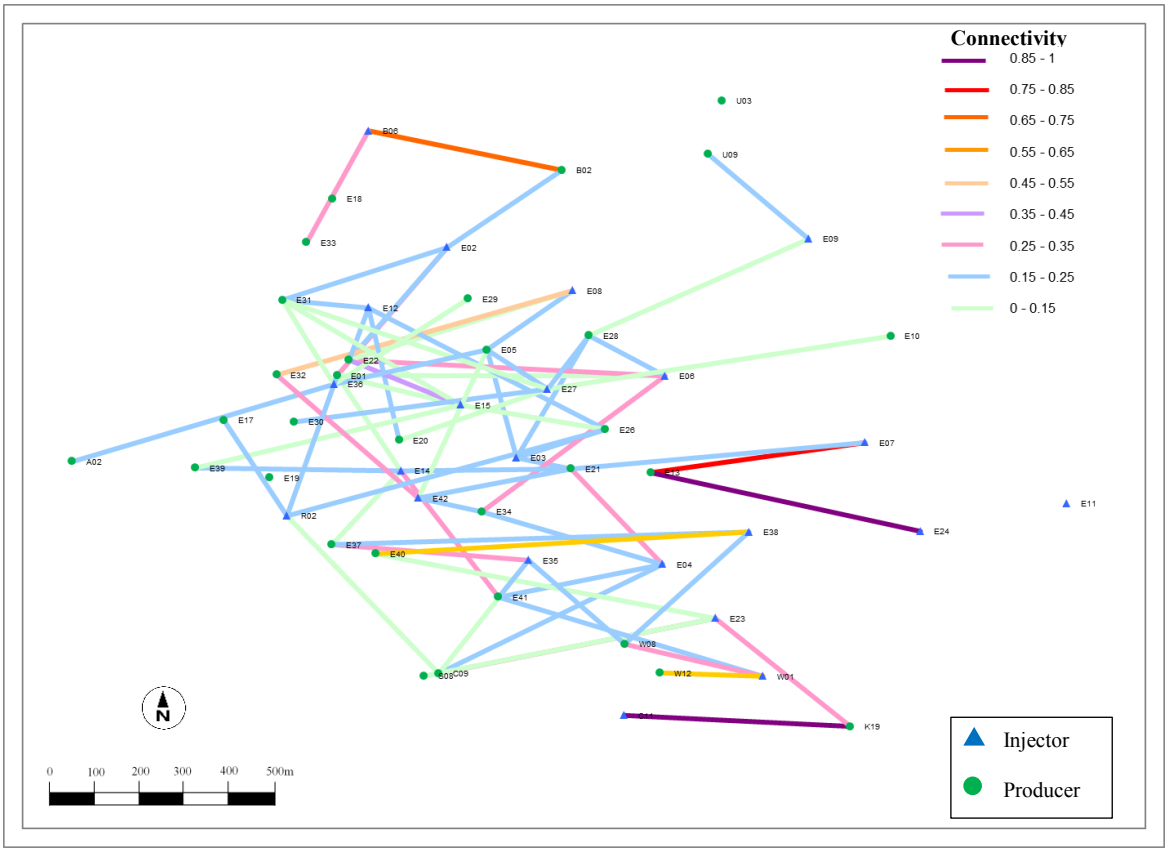

Figure 3.31 Interwell connectivity map of the field

The total number of possible gain for 22 injectors and 31 producers is 682. It is found that 83% of them are extremely small, i.e. less than 0.02; thus, they are forced to be zero. Only 118 values are allowed to be positive. A histogram of the gains is shown in Figure 3.32. It is immediately apparent that majority of the gain values are less than 0.3

as the distribution is positively skewed. This means that unless there is an injection loss, one injector generally provides support to several surrounding producers.

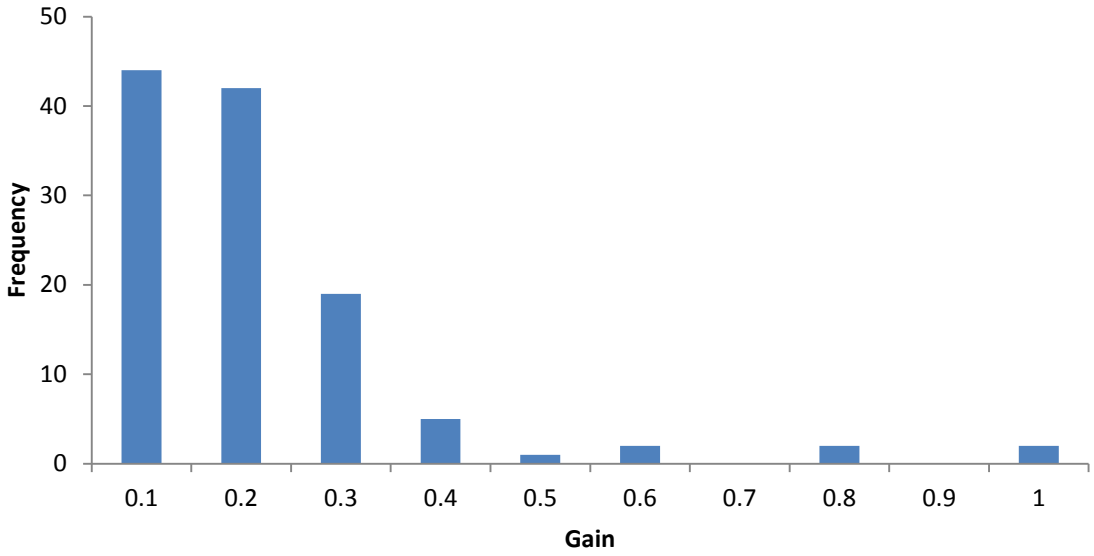

Figure 3.32 Histogram of the gain

A rose diagram showing orientation of observed interwell connectivities is presented in Figure 3.33 below. The orientation is measured relative to an injector. For example, the gain between E09 and U09 (the upper right corner of Figure 3.31) is aligned in the NW direction. According the results, the gains are oriented equally in all directions except the E and NE directions. Because the reservoir is dipped toward the east, the up-dip side where there are oil and gas accumulation is situated on the west while the down-dip side where there is water is located on the east. The main flooding patterns of this field are five-spot and peripheral. The peripheral flood was performed by down-dip injectors directing the injected water toward the up-dip producer which is the reason why the flows toward the east directions are less than that of the west directions.

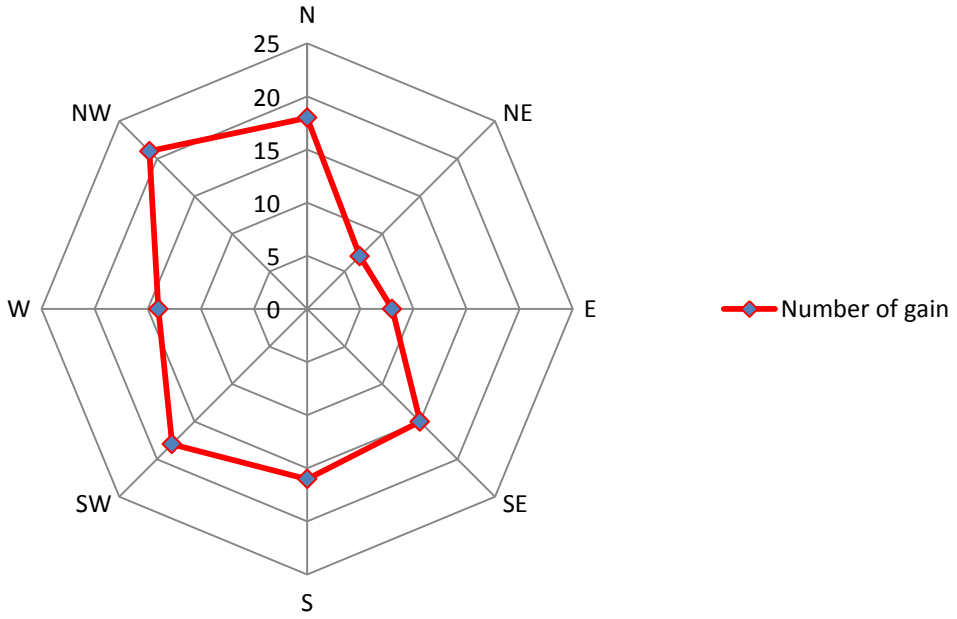

Figure 3.33 Rose diagram showing orientation of the gains in this field

According to the histogram and the rose diagram, it can be inferred geologically that the field is weakly anisotropic. There is no obvious preferential flow path in any specific direction. Most of the injectors distribute water into all directions while very few of them connect to favored flow paths. The strong connections, reflected on the gain values higher than 0.5, through these paths are attributed to high permeability channels which were infrequently penetrated by some wells. Actually some of them occur with pairs that are not geographically close, agreeing with the nature of the channel deposition which is elongated. Corresponding to geological background of the field, the CRM demonstrates that there is no obvious favored flow direction of the fluids in this reservoir.

The determined interwell connectivities also reveal the efficiency of the waterflood strategy by quantifying the fraction of lost injected water using the equation below:

$$f_{i,lost} = 1 - \sum_{j=1}^{j=n_p} f_{ij} \tag{3.10}$$

where n_p is the number of producers that injector i supports. The CRM allows the summation of gains in each injector to be less than or equal to 1 because of the fact that there are usually some injection loss into aquifer or other permeable paths that do not connect to the reservoir. One goal of the waterflood management is to minimize this loss and optimize the use of all injected water. For this field, there are only 2 injectors indicating loss. This might be because of the high well density such that one injector can support up to 10 producers within the specified radial limit. The inefficient injectors are E09 and E23 with the loss of 71% and 11%, respectively. The reason for the severe loss of E09 is that it is located at the remote down-dip location where there are only few producers surrounding it. Most water injected into this well is appears to be lost into the aquifer. Also, the slight injection loss of E23 is caused by its down-dip location that makes it unable to reach many up-dip producers. The amount of injected water into these 2 wells should be diverted to other injectors as it does not contribute to the production.

There are several field evidences and measurements supporting the CRM results. Firstly, considering No. 1 in Figure 3.34, the determined gains suggest that the northern part of the field (the green dashed rectangular) was well swept as indicated by the high density of the gains. The gain density is analogous to the streamline density, which is the number of streamlines passing through a unit area. The dark colors of the gains, like red and purple, represent the strong interwell connectivity, which can be inferred directly to the high number of streamlines. Therefore, as illustrated in Figure 3.34, the area with high gain density is the area that has many dark lines passing through. On the other hand, the southern part (the red dash-dot rectangular) has less gain density implying that the area has poorer sweep efficiency compared to the northern one. This is verified by the

repeat formation tester (RFT) pressures of the wells recently drilled in these areas as illustrated in Figure 3.35.

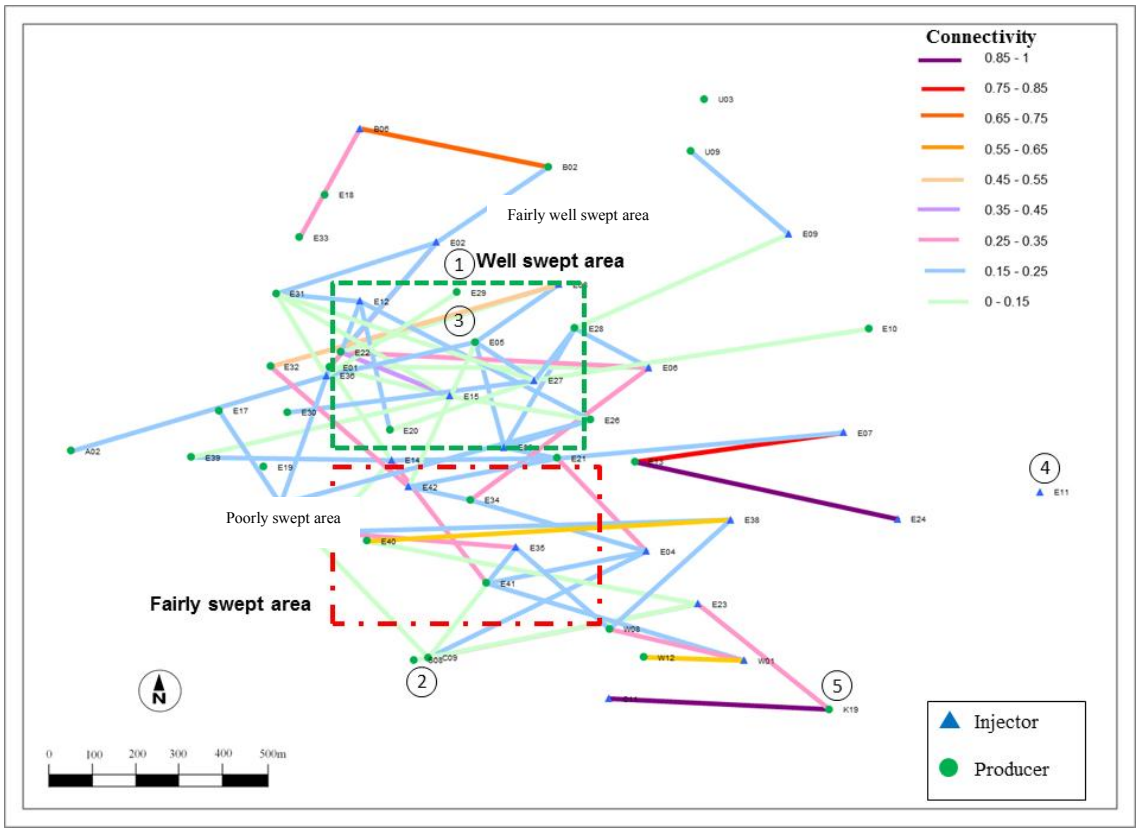

Figure 3.34 Interwell connectivity map with some highlighted wells labeled

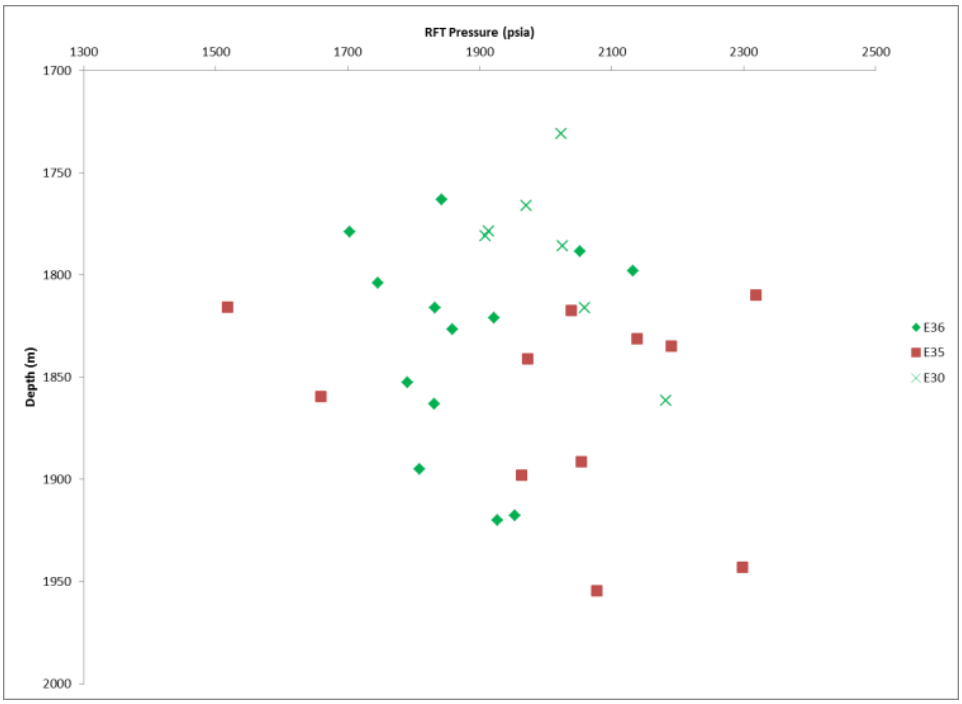

Figure 3.35 Comparison of RFT pressures of the wells in well and fairly swept areas

The green points are from the wells drilled in the well swept area while the red ones are from the well drilled in the poorly swept area. Each single point represents the pressure of each layer encountered by that well. A wide range of pressures signifies a significant difference in the degree of depletion. As expected, the wells in the green area had more uniform degree of depletion, supporting the fact that the area was efficiently swept. On the other hand, the well in the poorly swept area had larger range of pressure among various layers indicating poorer sweep efficiency.

Next, looking at No. 2 in Figure 3.34, there are 2 wells, S08 and C09, situated close to each other. However, as suggested by the CRM, both wells have penetrated into different reservoir layers since only C09 got pressure support from nearby injectors while none of the injectors contributing to the production of S08. This corresponds to their production history as shown in Figure 3.36 and 3.37 below.

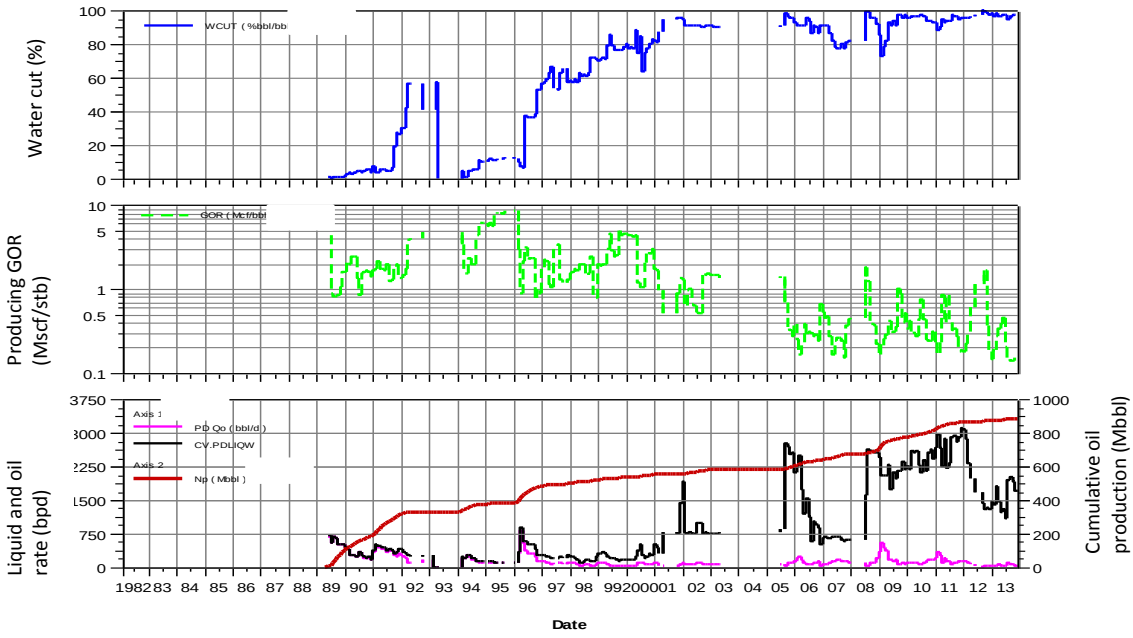

Figure 3.36 Production history of C09

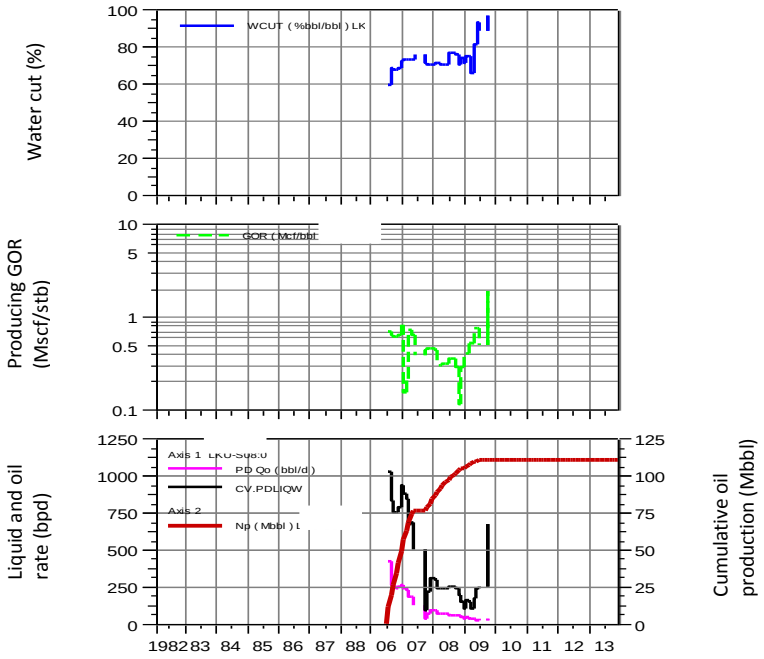

Figure 3.37 Production history of S08

C09 has been exhibiting the secondary-recovery characteristic as the liquid rates were not declining, but they fluctuated according to the injection while the GOR was lowered and stabilized at the value of the initial solution GOR. Additionally, it is immediately apparent that S08 has been producing under depletion-drive mechanism. Its gross and oil rates have been exponentially declined together with negligible amount of water production.

Number 3 in Fig 3.34 shows the high connectivity of the pair located far apart. The distance between E32 and E08 is approximately 700 m. while the average well spacing of the field is 300 m. Surprisingly, this pair is well connected with 50% of injected water from E08 allocating to E32 while the average gains of the nearby wells are only around 0.1 to 0.2. The field reported that there was a tracer test conducted at E08 to evaluate the degree of connectivity of the reservoir and predict waterflood performance. The results of the test validate this high CRM gain as there was a tracer from E08 presented in the collected sample of E32.

E11 (number 4) is an injector located down-dip and far away from current flooding pattern. The CRM indicates that the well did not support any producer, which corresponds to the field classification of it to be a water disposal well. Moreover, K19 (No. 5) is a successful down-dip infill producer lately drilled. Its performance, however, was even better than some up-dip producers drilled simultaneously. This is because the well had exceptionally good connectivities with surrounded injectors as displayed by the dark violet and the pink lines in Figure 3.34.

3.4.3. Time constant

The time constant, or tau, of each producer is displayed in the bar chart in Figure 3.38. Most of the tau range from 100 to 1,000 days. The average and median of the data are 1,780 and 223 days, respectively. According to the lower and upper bounds of 4.4 and 30148.2 days, there is only 1 producer, E19 that has tau reaching the maximum allowable value. With the exception of E19, tau values are in a good range, pointing out that during the fitting period, the reservoir behaved approximately as slightly compressible fluids satisfying the model's assumption.

E19 is an up-dip producer with 6 surrounding injectors. None of them provided support to E19 based on the gain results. However, its production history (Figure 3.39) proved that the well was actually a good waterflood producer with higher-than-average reserves per well. It is also observed from the plot that the well has been producing at an abnormally high liquid rate. While the average liquid rate of the waterflood producers in this field is around 1,500 bpd, E19 has produced at 3000 bpd, twice the average value, for many years. In term of fitting quality, it is optimal to allocate the injection to several producers rather than the only high-rate one. This is the reason why there is no contribution from the injectors toward this well. In other word, the model can determine the optimal solution for the well by setting its time constant to the maximum value such that all injected signals coming to this well are fully dissipated. This is an issue that should be aware of when the model is dealing with some producers that had much higher liquid rates than others.

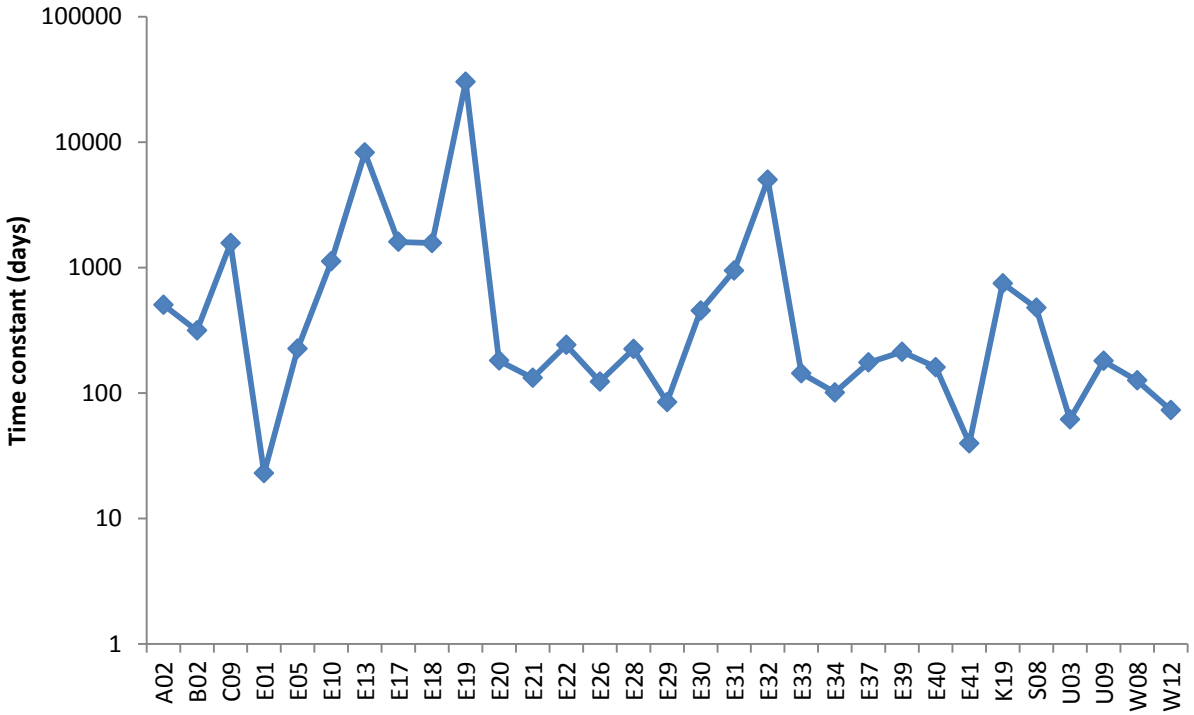

Figure 3.38 Time constants of each producer

Another observation is that most of the wells with large time constants, such as E17, E18 and E32, are situated at up-dip. This area is actually a gas zone and some layers even have a gas cap; thus, it is reasonable that the control volume of these wells is highly compressible and the effect of injection is significantly attenuated before arriving at the wells.

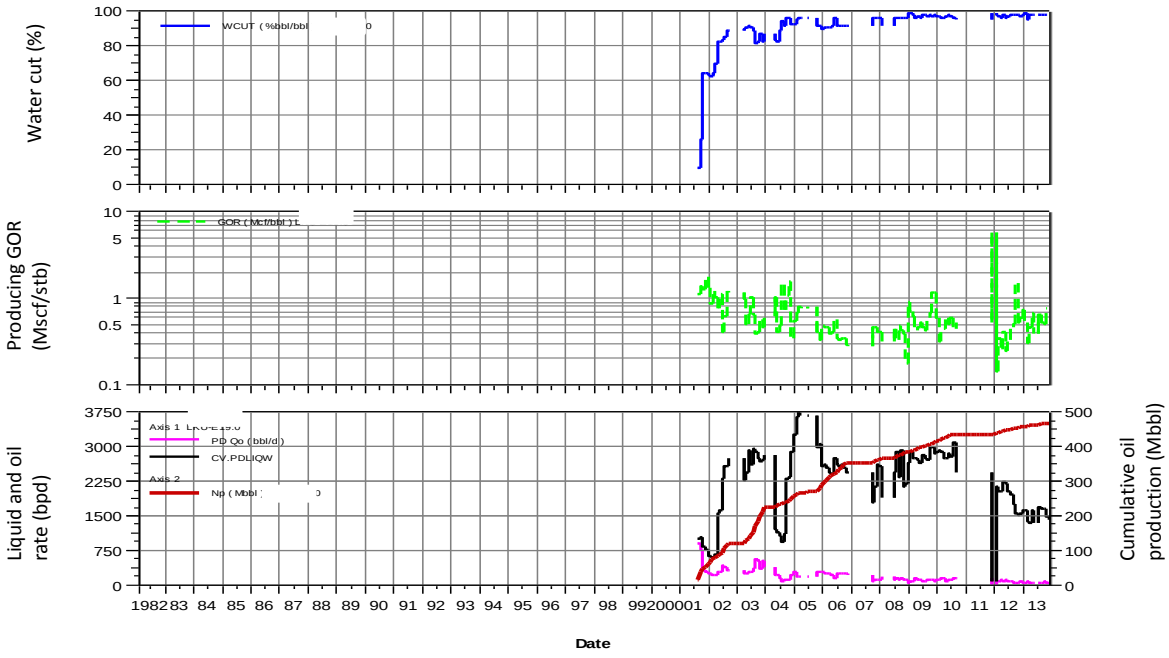

Figure 3.39 Production history of E19

3.4.4. Saturation

The saturation is an additional output parameter obtained from the coupled CRM aside from the gain and time constant from the original CRM. The coupled CRM is able to capture the average saturation change per time step. At the last time step, it represents the remaining oil saturation of the reservoir, which will provide insight on the analysis of location of infill drilling. Therefore, the average oil saturation within each producer drainage volume at the final time step is selected to be presented here as shown in Figure 3.40. The color scale was used to display the saturation and ranges from the lightest green for the lowest oil saturation to the darkest green for the highest one. The scale was normalized to the range of the data which is from 0.24 to 0.43. The average and the median of the remaining oil saturations were close, at values of 0.3 and 0.29, respectively. The drainage radius of each producer was already determined from the matching of water cut data to the Koval equation.

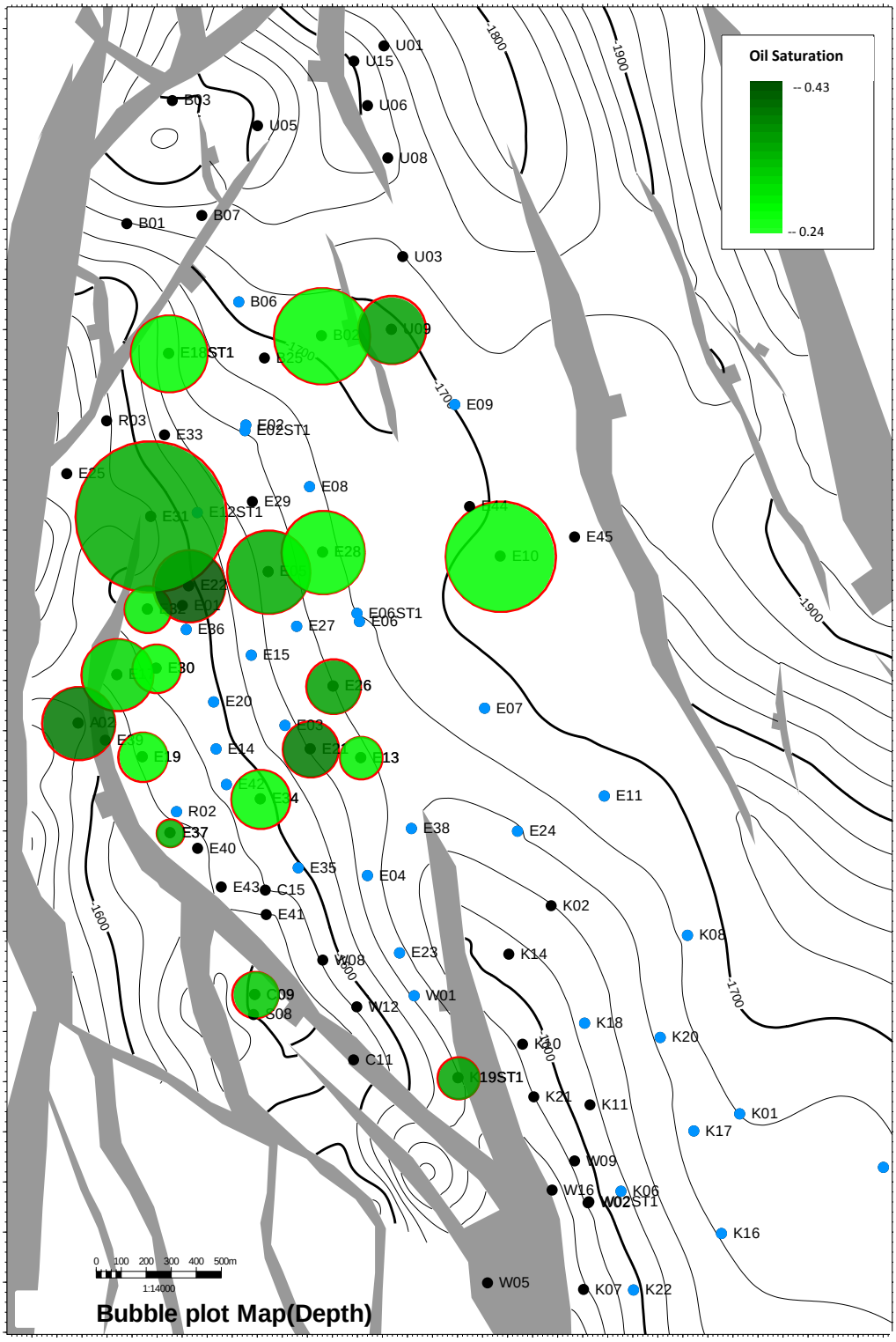

Figure 3.40 The remaining oil saturation map from the coupled CRM

According to the map, areas with high remaining oil saturation are mostly located in an up-dip or middle parts of the reservoir. The down-dip part has low oil saturation which is reasonable as the reservoir has also been peripherally flooded. Some producers, despite being situated closely, can have considerable difference in the final saturation, according to the CRM.

Another way to demonstrate the saturation map is to incorporate the Kriging (or Gaussian process regression) method. The map is presented in Figure 3.41. The drainage volume of each producer is not being used here as the method treats the well as a point with single value of saturation. In other word, it assumes that the drainage radius of each well is equal.

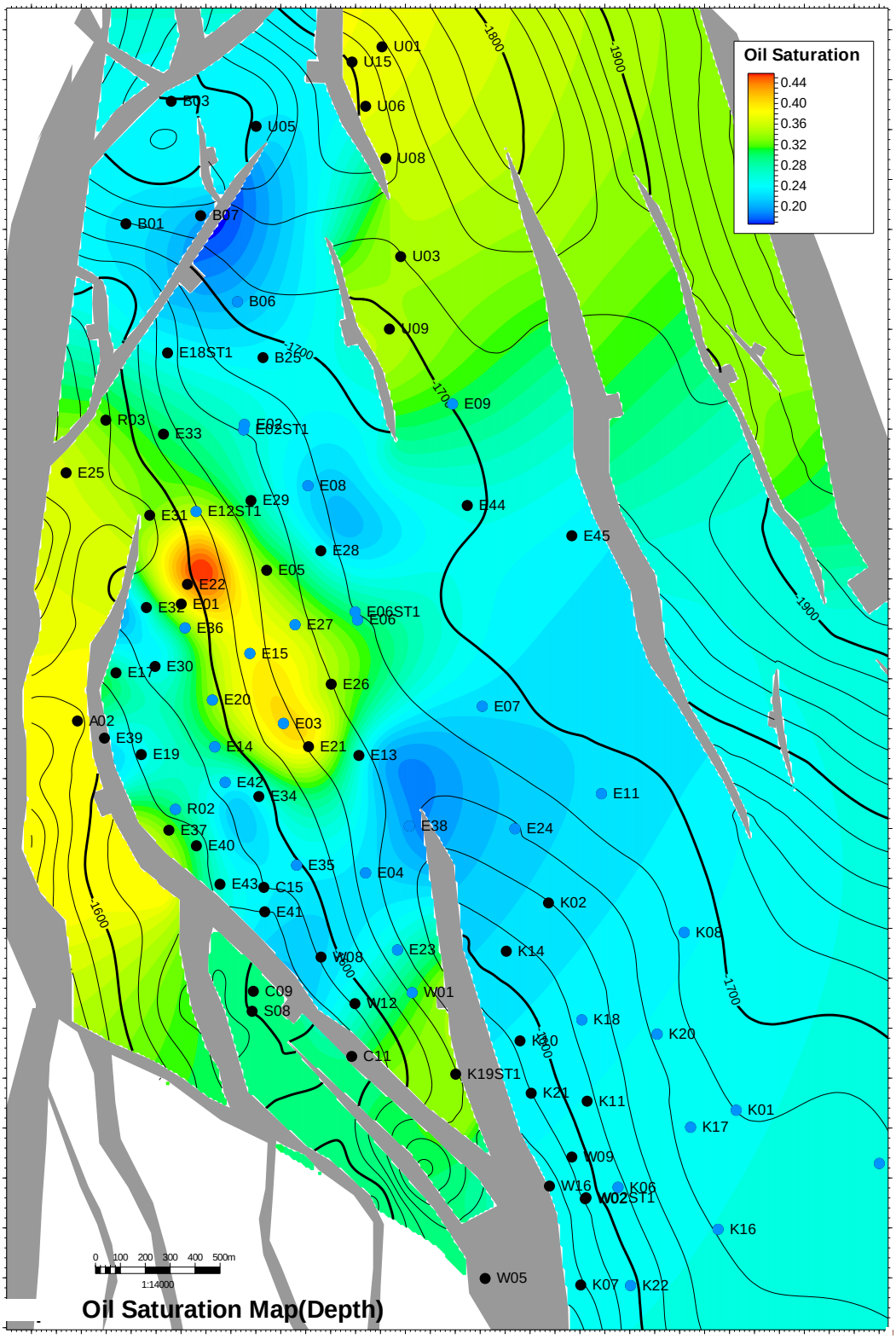

Figure 3.41 The alternative remaining oil saturation map obtained from kriging method

Chapter 4: Identification of infill locations

This chapter concentrates on the identification of potential infill locations. Firstly, numerical experiment will be performed with synthetic reservoirs. The CRM's results are compared with the remaining oil saturation obtained from the simulation. The following section will discuss the estimation of interwell permeability from the CRM's time constant. An analytical formulation is proposed and validated with synthetic case studies. Next, the obtained CRM's results from its application to the field data previously explained in chapter 3 will be combined with other reservoir characteristic maps including porosity, thickness and permeability, to analyze for potential location for infill wells, which will be validated with actual infill wells' performance of this field.

4.1 SYNTHETIC RESERVOIR STUDIES

4.1.1 Locating the bypassed oils

Synthetic case studies were designed to examine the relationship between the CRM gains and the distribution of the remaining oil in a mature waterflood reservoir. For this research, a commercial reservoir simulator, namely CMG, was used. For this purpose, it is necessary to construct the synthetic reservoir that traps oil at the end of simulation and one simple way to achieve this is to make it anisotropic. When waterflooding a homogenous, anisotropic reservoir, it can obviously be anticipated that the sweep efficiency will be better in the direction of high permeability rather than the direction of low one. Poorly swept area, which is usually associated with poor connectivity or low gain, directly results in high remaining oil.

The first case study is a three-dimensional homogeneous reservoir (Figure 4.1) with anisotropic ratio of 200. In other word, horizontal permeabilities in x and y

directions were assigned to be 1,000 and 5 md, respectively. Key reservoir and fluid parameters of this reservoir are summarized in Table 4.1. The synthetic field consists of 2 producers and 2 injectors (Figure 4.1). All wells are vertical and completed over the entire thickness of the reservoir. The producers are operating under a constant FBHP of 250 psi. The injection rates are fluctuating monthly as shown in Figure 4.2. The total simulation time is 284 months and all the calculations were done on a monthly basis.

Parameters	Value
Number of grid blocks	33 × 33 × 5
Grid block sizes (ft)	77.5 × 77.5 × 77.5
Porosity	0.2
Permeability in x, y, z directions (md)	1000, 5, 60
Fluid types	Oil and water
Oil compressibility (psi^{-1})	3×10^{-5}
Water compressibility (psi^{-1})	1×10^{-6}
Rock compressibility (psi^{-1})	1×10^{-6}
Initial oil saturation	0.7
Irreducible water saturation	0.3
Residual oil saturation	0.4
Oil viscosity (cp)	0.96
Water viscosity (cp)	0.72
Initial reservoir pressure (psi)	1,250

Table 4.1 Key reservoir and fluid parameters of the synthetic reservoir

Figure 4.3 shows the simulated production rates of both producers with regard to the injection rates input. It is observed that the fluctuation of production rates of PROD2 mainly corresponds to the injection of INJ2. This is justifiable as both of them are aligned in the direction of high permeability; thus, they are well connected.

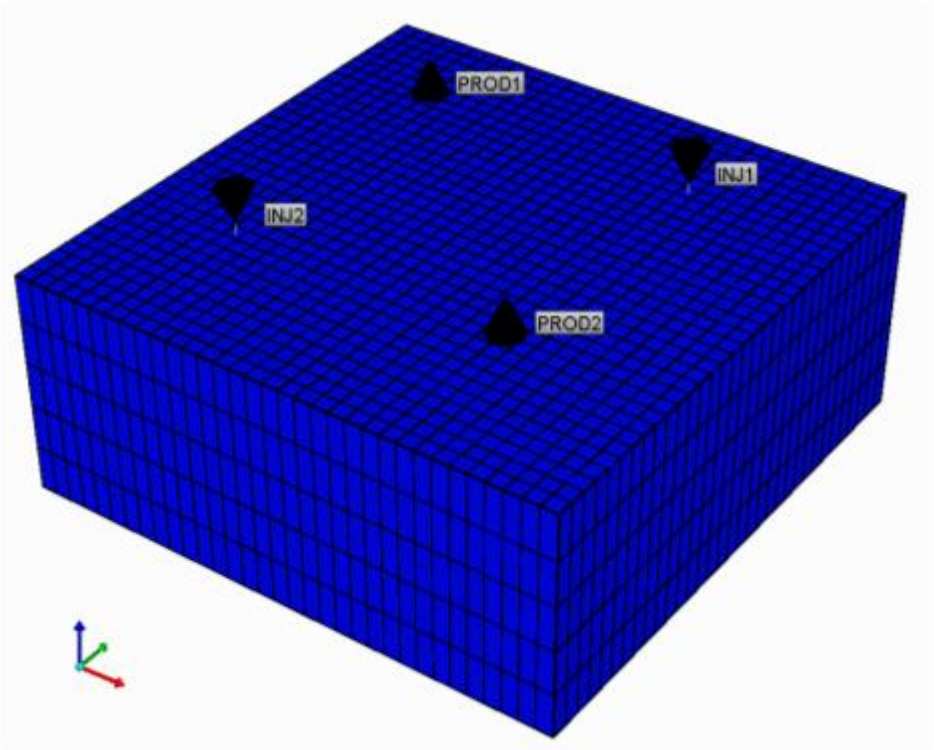

Figure 4.1 The synthetic field to test effect of anisotropy

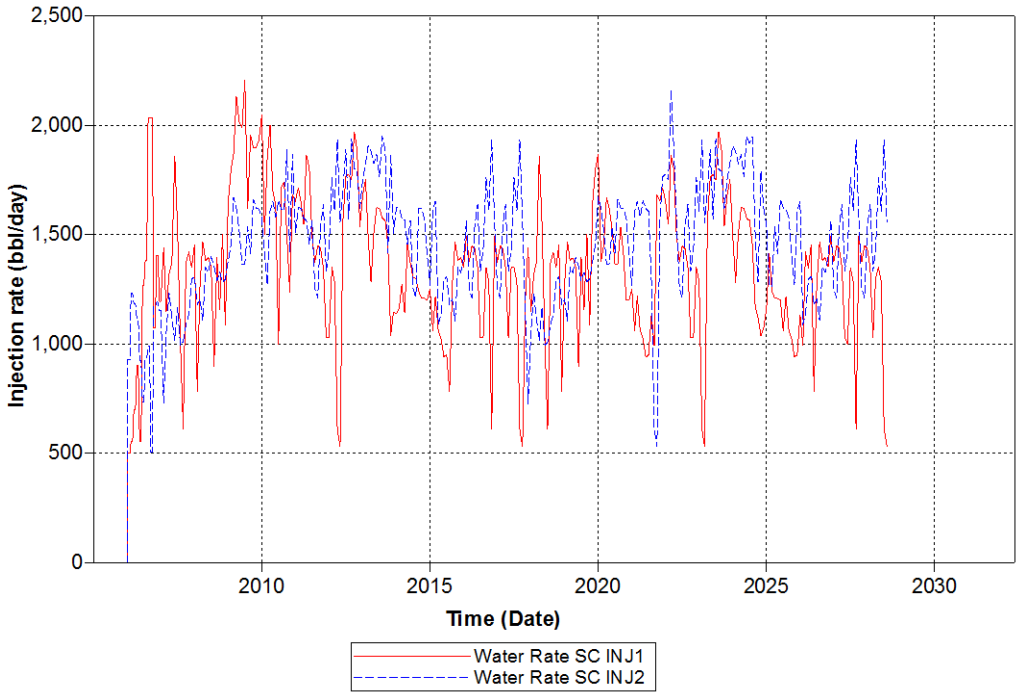

Figure 4.2 Injection rates of the two injectors in the synthetic case study

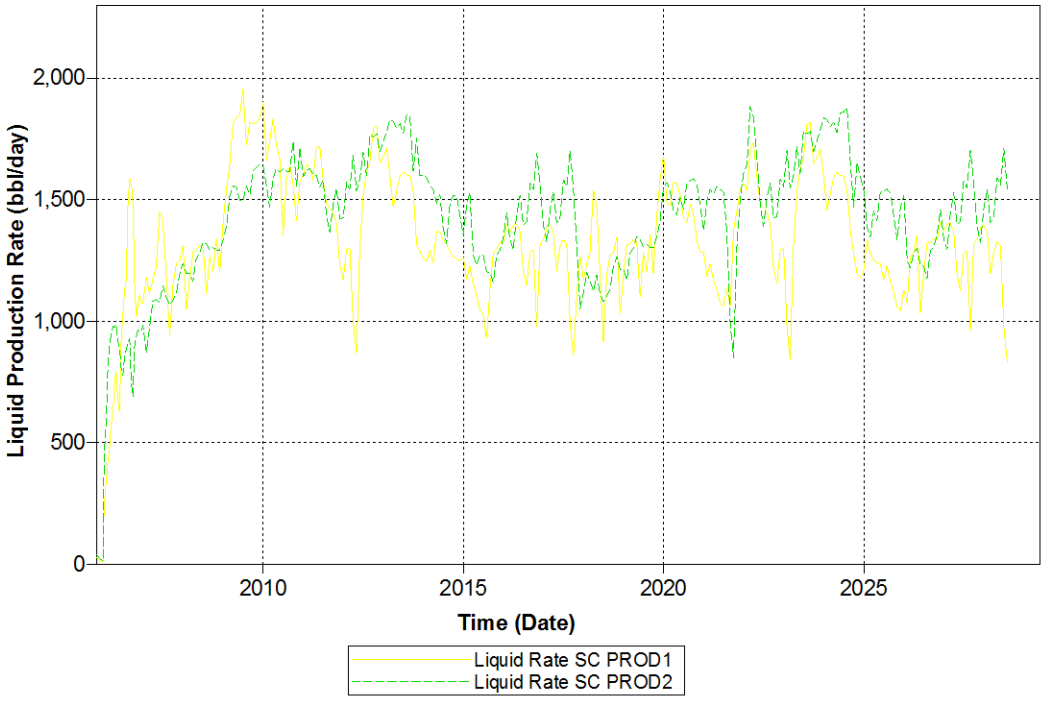

Figure 4.3 The simulated total production rates of the two producers

The remaining oil potential at the end of simulation was presented by the oil per unit area map (Figure 4.4) rather than the oil saturation alone because it takes into account the total volume by including the porosity and the thickness. Oil per unit area is defined as:

$$Oil/area = S_o \emptyset h \tag{4.1}$$

where the bypassed oil is located in the area of high oil per unit area. As anticipated, the areas with a large amount of bypassed oil are located between the producer and the injector in the direction of low permeability (the y-direction in this case). This is because the flooding is highly efficient in the direction of good connectivity such that most of the oils in those areas were swept toward the producer. Therefore, in this case, a good infill target will be between PROD1 and INJ2 rather than between PROD1 and INJ1.

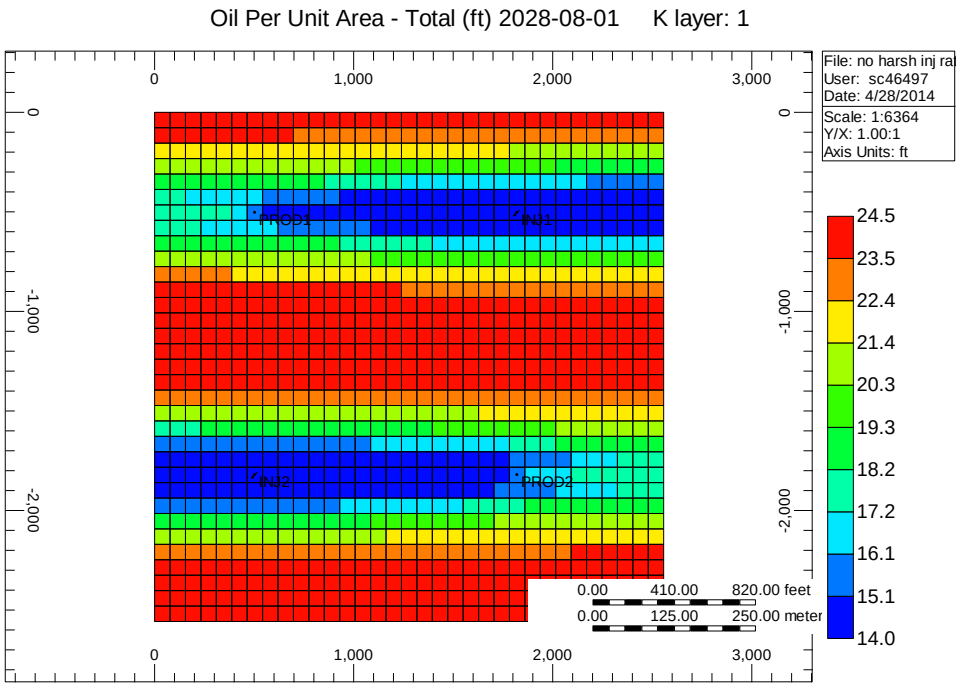

Figure 4.4 Oil per unit area at the end of simulation

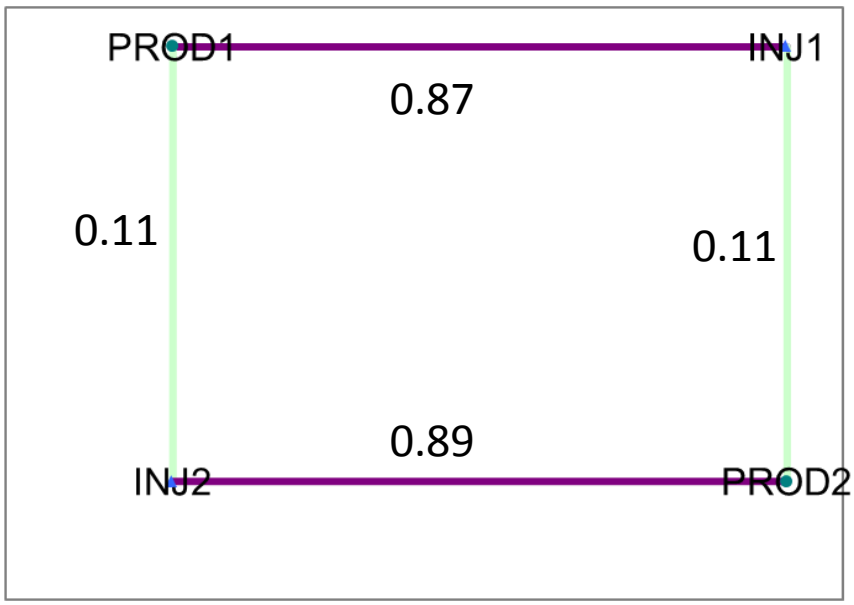

Figure 4.5 Connectivity map of the first synthetic case study

The injection rates used and the production rates obtained from the CMG were then input into the CRM to determine the interwell connectivity (Figure 4.5). It is as expected that the gain is large in the direction of high permeability and vice versa. Based on the results of both the CMG and the CRM, it is observed that the good-performance infill well is the one located between a pair that has poorer connectivity.

Next, there are some modifications needed for the first case study. Heterogeneity was added to the horizontal permeabilities. The permeability is log-normally distributed with Dykstra-Parson coefficient of 0.75 (Figure 4.6). The degree of anisotropy was reduced to 10, in which the permeability in x and y directions are 200 and 20 md, respectively. There is only one layer for this reservoir so that it is a two-dimensional model. In addition, the field consists of 4 producers and 5 injectors and all of them are arranged in the five-spot waterflood pattern. The other reservoir and fluid properties are similar to the first case study (Table 4.1). The proportion of the second synthetic field is illustrated in Figure 4.7.

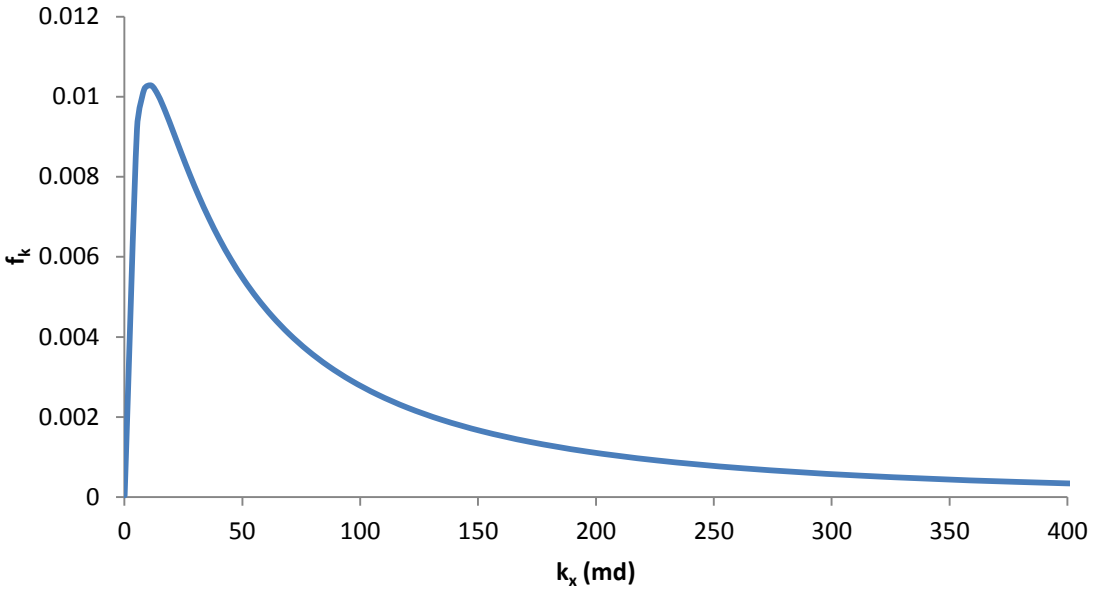

Figure 4.6 Probability density function (pdf) of permeability in x direction

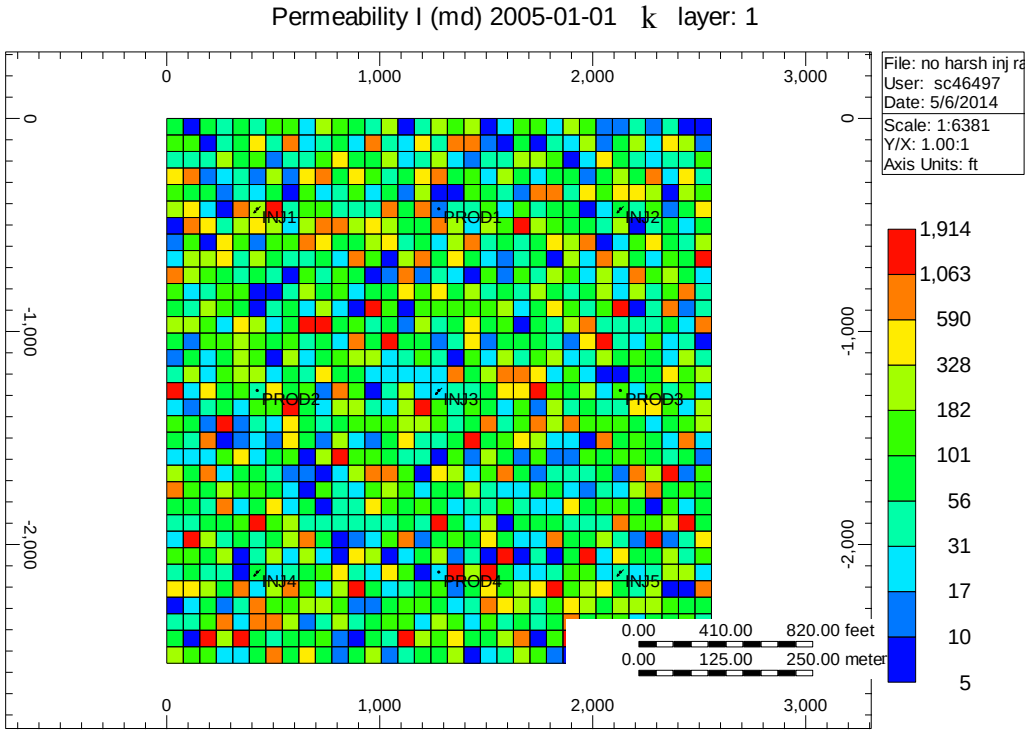

Figure 4.7 k_x distribution for the second synthetic case study

The oil saturation map at the end of the simulation is in Figure 4.8. For the single-layer reservoir, the oil saturation is equivalent to the oil per unit area. Similar to the first case study, oil saturations seem to be low in x-direction between producers and injectors. On the other hand, the CRM's connectivity map (Figure 4.9) shows that the interwell connectivity correspond to the assigned reservoir properties. In other word, the gains tend to be high in the x-direction which is the direction of higher permeability while they tend to be low, or even zero, in the y-direction which has lower permeability.

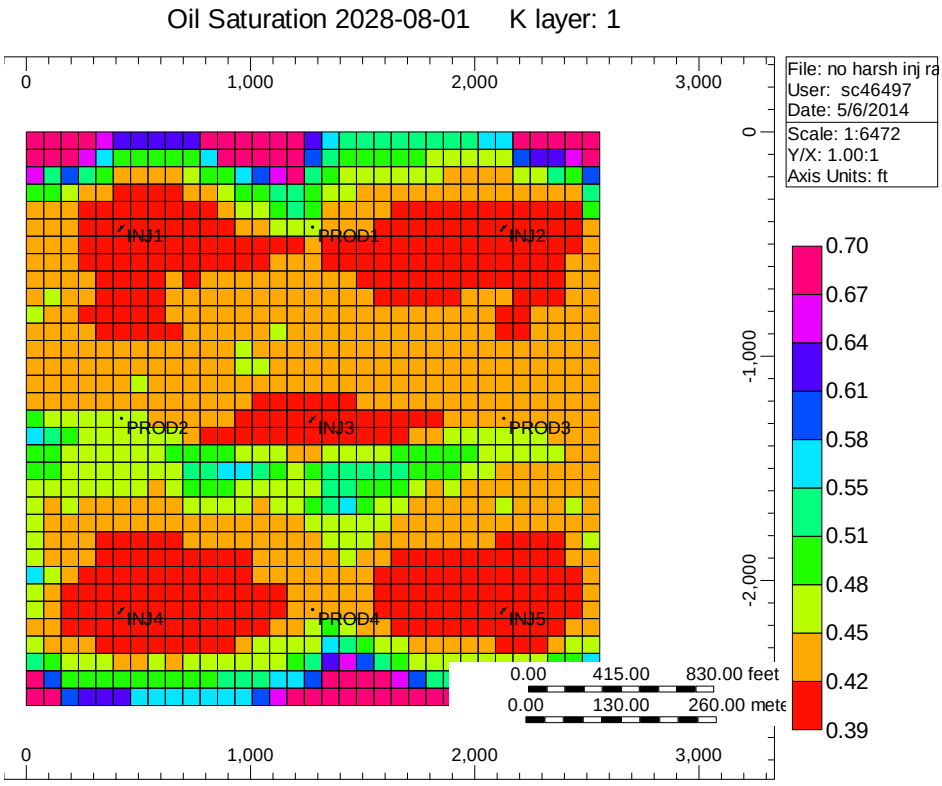

Figure 4.8 Oil saturation map at the end of simulation of the second case study

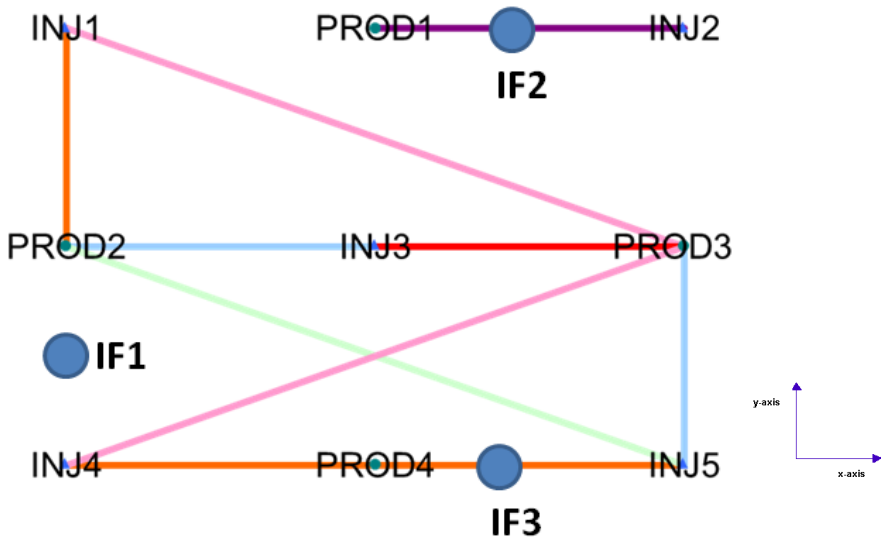

Figure 4.9 Connectivity map of the second case study with locations of infill well

Then, an infill well was added to the reservoir to validate the premise that the area of low gain has the most potential for infilling. Each infill well, IF1, IF2 and IF3, was added and run separately on different cases. Their performances were measured by the total field incremental oil recovery, which is plotted on Fig 4.10. This incremental recovery was determined by subtracting the total oil production of the case with an infill well with that of the base case, i.e. without an infill well. IF1 which was placed in the area of zero connectivity between INJ4 and PROD2 yields the highest incremental recovery to the field. IF3 is better than IF2 because it was located in the area of lower connectivity (between INJ5 and PROD4) compared to IF2 which was placed between INJ2 and PROD1 which is the pair with the highest connectivity.

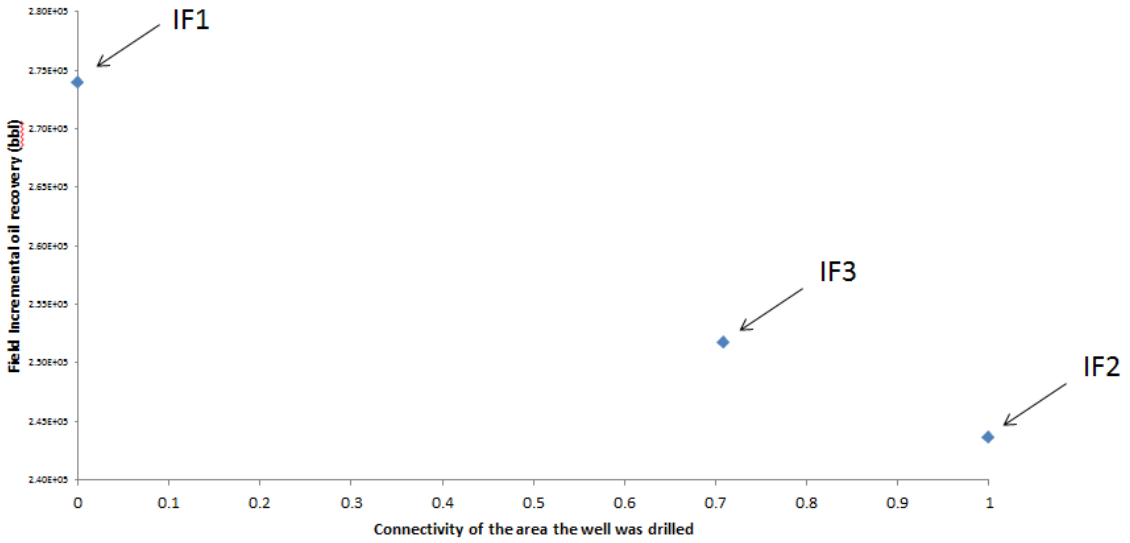

Figure 4.10 Field incremental oil recovery obtained from 3 infill wells vs. gain

4.1.2 Estimation of permeability from time constant

This topic will discuss a preliminary study on extracting the interwell permeability value of a well pair from their CRM time constant. The idea evolved from the possibility that the time constant is likely related to a so-called diffusivity, a reservoir engineering parameter. The diffusivity (η) controls the speed with which pressure signals generated from perturbations travel through the reservoir. A reservoir with higher diffusivity will have more rapid communication of an imposed effect. It is defined as:

$$\eta = \frac{k}{\phi \mu c_t} \tag{4.2}$$

where the unit of η is length squared divided by time. According to the equation, it also can be viewed as the division of the mobility (k/μ) by the storativity (ϕc_t). High mobility causes fast signal transmission while high storativity leads to slow signal transmission.

On the other hand, the time constant or τ (Eq. 2.4 below), by definition, physically contains information of reservoir mobility (J) and storativity ($c_t V_p$). Higher values of τ mean large dissipation and more delay of the pressure signal.

$$\tau = \frac{c_t V_p}{J} \tag{2.4}$$

Based on the definition of both the time constant and the diffusivity, these two parameters seem to be inversely related. In other words, a reservoir with high diffusivity should exhibit a small time constant. The derivation to relate them is simple and shown below. Recalling the well-known Darcy's law:

$$q = \frac{kA\Delta P}{\mu L} \tag{4.3}$$

and the productivity index is defined as:

$$J = \frac{q}{\Delta P} \tag{4.4}$$

Substituting Eq. 4.3 into Eq. 4.4 obtains:

$$J = \frac{kA}{\mu L} \tag{4.5}$$

and the pore volume is simply defined as:

$$V_p = \phi AL \tag{4.6}$$

Because the interwell properties are the main focus in this section, it makes more sense that the time constant referred here is the one obtained from CRMIP, in which a control volume is defined to be an arbitrary drainage volume between an injector-producer pair (Figure 2.7). Finally, substituting Eq. 4.5 and 4.6 into Eq. 2.4 and have the cross-sectional areas cancelled out yields:

$$\tau_{CRMIP} = \frac{\phi \mu c_t L^2}{k} \tag{4.7}$$

and the diffusivity can be related to the τ as:

$$\eta = \frac{L^2}{\tau} \tag{4.8}$$

Because the diffusivity provides insight into the permeability, it seems feasible to determine the permeability from the time constant using Eq. 4.7, which can be re-written in field units as:

$$k = 158\frac{\phi\mu c_t L^2}{\tau_{CRMIP}} \tag{4.9}$$

where k (md) is the interwell permeability between an injector and a producer pair, μ (cp) is the viscosity of reservoir fluids, c_t (psi^{-1}) is the reservoir total compressibility, L (ft) is preliminarily expected to be the distance between the well pair and τ (days) is the time constant associated with that pair.

Synthetic case studies were designed to evaluate the validity of the proposed relationship (Eq. 4.9). The reservoir fluid is only water and all properties are uniform. Most of the parameters are similar to the one used in the previous section (Table 4.1) with the exception of only water and isotropy.

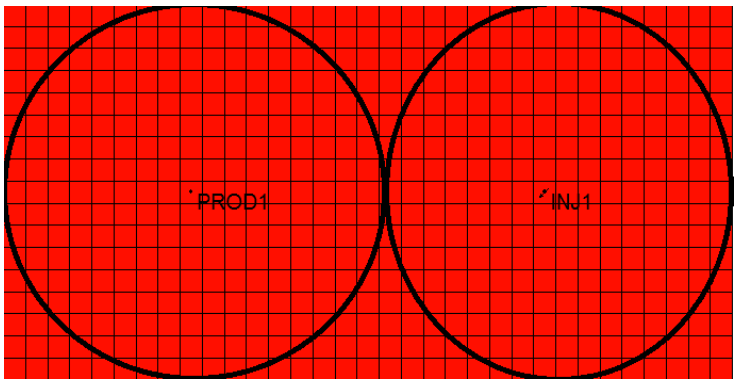

Figure 4.11 The first case with a single well pair symmetrically arranged

The first case consists of a single well pair arranged such that they have symmetric drainage areas (Figure 4.11). The distance between them is 1,319 ft. The input injection rate, which is identical to the one used in the previous section (Figure 4.2), and

the simulated production rate were put into the CRMIP model to obtain the time constant. Then, the CRM permeability (k_{CRM}) can be calculated using Eq. 4.9 and compared to the known actual permeability of the reservoir (k_{CMG}). The permeabilities of the synthetic reservoir are varied from 20 to 200 md. The results are shown below (Figure 4.12) where k_{ratio} is defined as the ratio of k_{CMG} to k_{CRM}.

The CRM significantly underestimates the permeability as the ratios range from 3.8 to 5.7. However, there is a correlation; as the reservoir becomes more permeable, the discrepancy increases linearly. Examination through Eq. 4.9 found that the error should be attributed to the distance L because uncertainties in other parameters have been eliminated. All the porosity, compressibility and viscosity are constant and independent of pressure. The corrected L that makes the agreement between k_{CMG} and k_{CRM} is calculated and plotted in Figure 4.13. The corrected distances begin with almost twice the actual distance of the pair and increase linearly with increasing k_{CMG}.

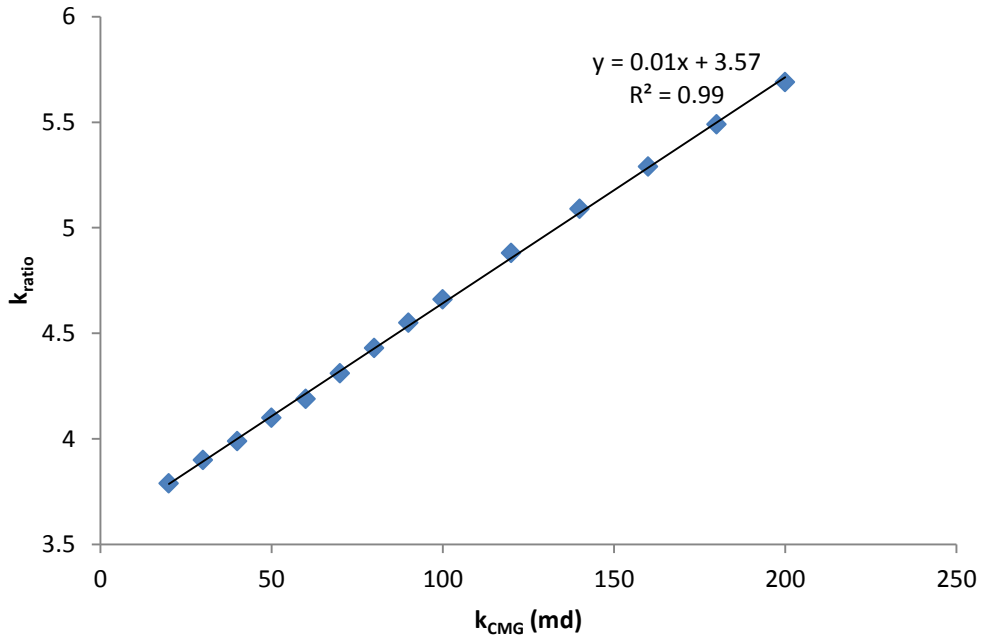

Figure 4.12 Relationship between k_{CMG} and k_{CRM} for the first case study

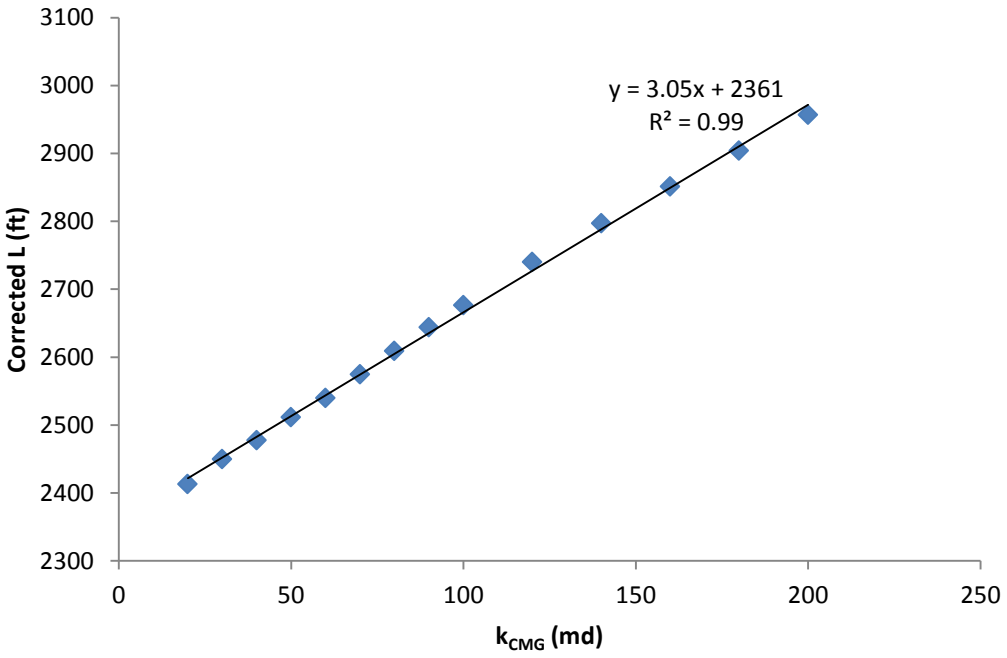

Figure 4.13 The corrected length vs. k_{CMG} (L_{actual} is 1,319 ft.)

The second case study was modified from the first one by increasing the number of wells and changing the flooding pattern into a five-spot as shown in Figure 4.14. Other properties are identical. The k_{ratio} of all pairs for the case with k_{CMG} of 20 md are shown in Table 4.2.

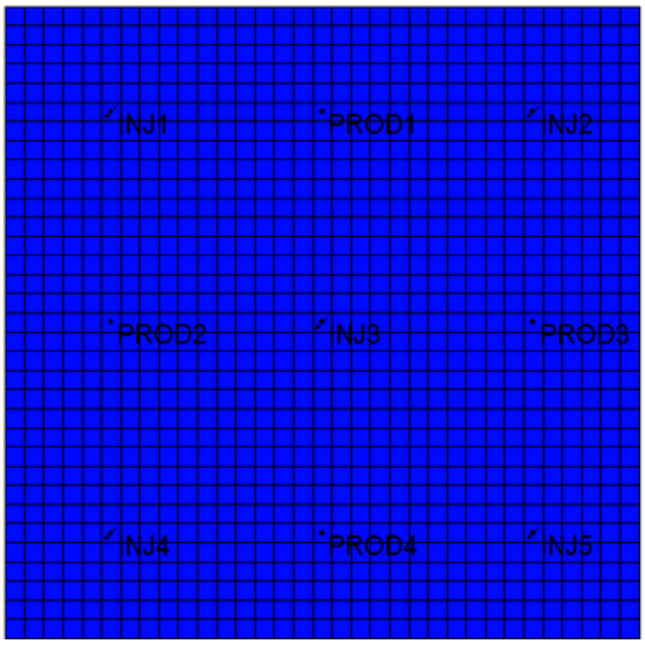

Figure 4.14 The synthetic reservoir of the second case study

k_{ratio}	PROD1	PROD2	PROD3	PROD4
INJ1	2.82	2.89	1.07	1.07
INJ2	2.95	1.01	2.93	0.89
INJ3	3.09	3.12	2.98	2.94
INJ4	0.83	2.70	0.83	2.83
INJ5	0.93	0.92	2.66	2.72

Table 4.2 The ratio of k_{CMG} to k_{CRM} of each pair for the 20-md case and five spot pattern

The ratios roughly range from 1 to 3 with the average value of 2.1 meaning that the CRM-calculated permeability is twice the actual one on average. The ratios of the most distance, like PROD1 and INJ4 are actually close to unity meaning that the permeabilities perfectly agree, while those of the closer pairs, like PROD1 and INJ1, are about three times more deviated from the expectation. Similar to the first case, the permeabilities of the reservoir are varied and the average values of k_{ratio} of each case were

plotted against the true permeability (Figure 4.15). As in the first case study, the CRM always underestimates the permeability compared to the actual one (k_{CMG}) and the errors increase linearly with the true permeability.

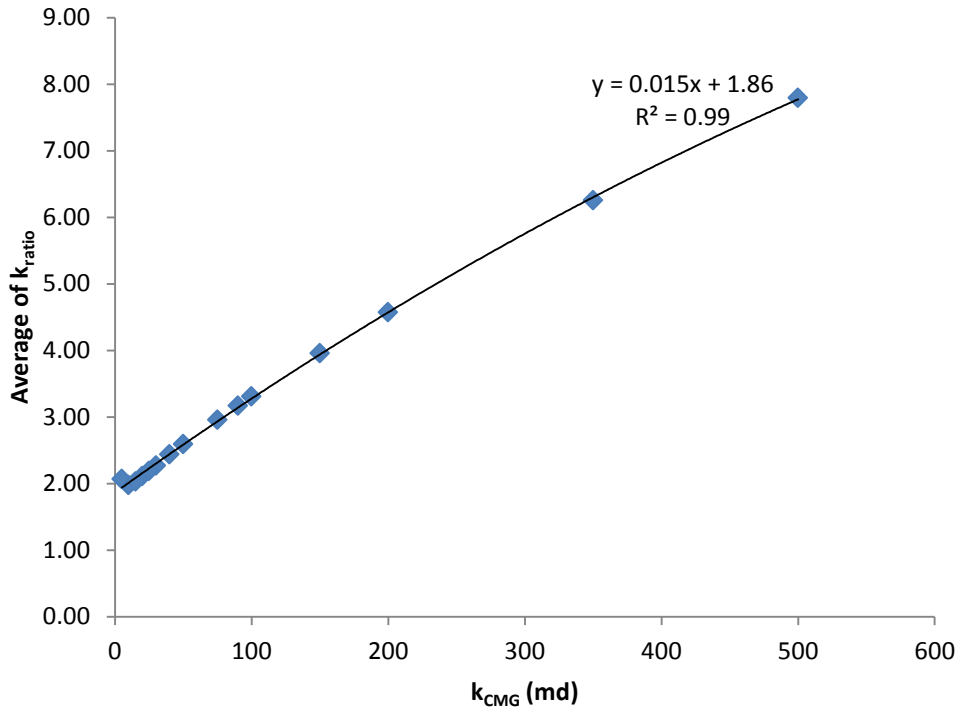

Figure 4.15 Relationship between k_{CMG} and k_{CRM} for the second case study

All in all, the underestimation of the CRM is likely to be attributed to the wrong specification of distance L which was preliminarily defined as the distance between injector-producer pairs. This probably can be explained as the flow path of water from an injector to a producer is actually tortuous, not along single straight line. The tortuosity may be simply defined as the ratio of the length of the curve to the distance between the ends of it. According to Carman-Kozeny (1956), permeability is inversely related to the tortuosity. In other word, the higher the tortuosity of the medium, the lower the

permeability will be. This supports the obtained results that because the proposed method treated the medium as it is not tortuous; the permeability will be overestimated as flow paths in the actual reservoir always has some tortuosity.

Hence, L should be re-defined as the average length of all flow paths of water. To apply Eq. 4.9, this L has to be properly determined. In addition, the tortuous flow path of water can also be used to elaborate the results that the discrepancy increases with the reservoir permeability. As the medium is more permeable, the drainage volume between a well pair becomes larger which makes the corrected L further higher than the displacement.

4.2 FIELD CASE STUDY

The field presented in chapter 3 is an appropriate candidate for the analysis of infill locations because it is suspected to have a significant amount of bypassed oil remaining in the reservoir, which is supported by several field indicators reflecting a non-uniform sweep. For instance, the repeat formation tester (RFT) pressures illustrated different reservoir pressure in various layers (Figure 3.3). In addition, a production logging tool (PLT) indicated poor vertical water distribution for some injectors, while static bottom-hole pressure (SBHP) surveys reflected significant variation in the distribution of areal reservoir pressures (Figure 3.2, lower plot). Measured chloride content of produced water revealed that some up-dip wells have been producing injected water while many of them have not received this support yet. All of these facts suggested the imperfect waterflood leading to opportunities for infill drilling.

4.2.1 Summary of infill wells' performances

A waterflood reaches a mature stage when the field water cut levels off at a high value. For this field, the mature period was roughly from 2003 onwards as shown by its water cut history (the blue dots in Figure 4.16). Most infill wells drilled after 2003 aimed to capture bypassed oil.

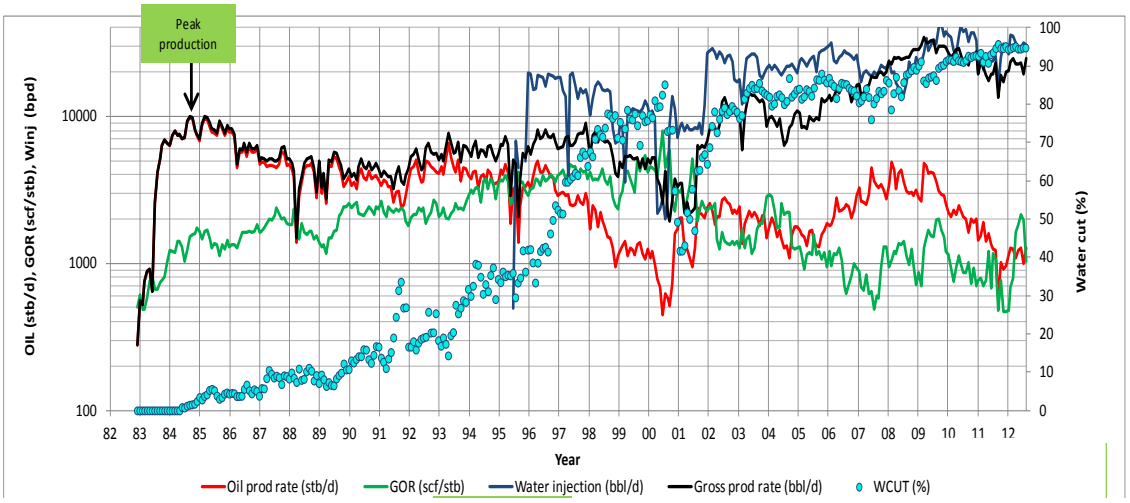

Figure 4.16 Field production history

The infill drilling programs were divided into 2 phases, 2007 and 2009 with 10 and 4 wells drilled, respectively. Their estimated reserves and actual cumulative oil productions (N_p) are summarized in Figure 4.17. The N_p is the sum of all oil that has ever been produced until a specific date. The pre-drilled reserves are the amount of oil expected to be recovered by that well before drilling. This value will be used to obtain economic values and thus propose the well for management's approval. However, because the well has not yet been drilled, none of the petro-physical and pressure data are available. A technique used by field personnel to estimate the pre-drilled reserves mostly relates to an analogue of the existing wells' performance, in which this chart reveals that

it is usually inaccurate compared to the wells' actual N_p. Moreover, it is immediately apparent that these pre-drilled reserves of each well are in a small range. In other word, the assumption that each well was expected to have similar performances is not entirely true because their cumulative oil productions (the green bar) differ considerably. The best one, E32, has already produced around 400 Mbbl of oil while some poor wells such as E33, E35, E36 and E38 have produced less than 30 Mbbl of oil. The amount of oil produced by the good wells, K19, E31, E34, E37 and E40, is still less than half of E32 despite being close to pre-drilled reserves. Thus, it can be inferred that the method used to predict future wells' performance can be improved. The analogous technique used here is actually performed empirically, in which the flooding performance is insignificantly involved. As a result, it comes to the main objective of this research that is to apply the CRM, along with other available data, to identify proper infill locations.

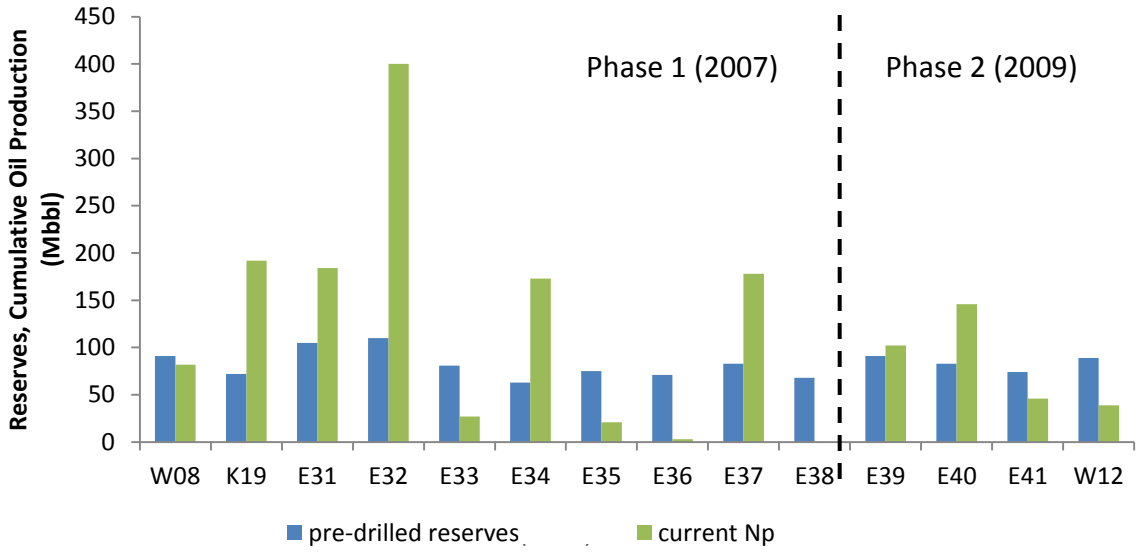

Figure 4.17 Summary of the performance of infill wells drilled in 2007 and 2009

Based on the actual performance which is solely reflected by the N_p, these wells can be categorized into 3 groups, namely, good, fair and poor ones as shown in Table 4.3.

Category (by actual performance)	Wells' name
Good	K19, E31, E32, E34, E37, E40
Fair	W08, E39
Poor	E33, E35, E36, E38, E41, W12

Table 4.3 Category by actual performance of infill wells

4.2.2 Method

From the literature review on the identification of infill locations (section 2.2), there are 2 main factors contributing to good infill performance: poor reservoir continuity and good rock quality. Firstly, an area with unusually poor continuity is generally poorly drained and poorly swept; this results in relatively high remaining oil saturation. Secondly, that area should have good permeability and large pore volume. The reservoir thickness, net-to-gross ratio and porosity constitute the pore volume. These 2 factors are mutually inclusive, i.e. they can both occur simultaneously and it is essential for the potential area to have both characteristics.

The systematic approach to determine how to use the CRM to identify the potential location is illustrated in Figure 4.18. Streamline simulation (SLS) is a traditional method as previously explained in chapter 2. Numerous authors have conducted the studies on the relationship between the key output of the CRM and the SLS and obtained equivalent results. Izgec and Kabir (2009) found near-perfect agreement of the SLS's well allocation factors (WAFs) and the CRM's gains. Because the WAFs are time-dependent while the gains are determined once for a selected fitting period, for consistency and direct comparison, the WAFs are time-averaged. Nguyen (2011) also concluded, based on her synthetic case studies that the CRM estimated gains should agree

with SLS's WAFs while the CRM's time constants are proportional to the average of the SLS's times of flight (TOF). Lately, Jahangiri et al. (2014) conducted a sensitivity analysis to analyze how the CRM and the SLS results change with different input setting, such as time interval and radial limit. They summarized that the CRM connectivity mostly agree with the SLS connectivity.

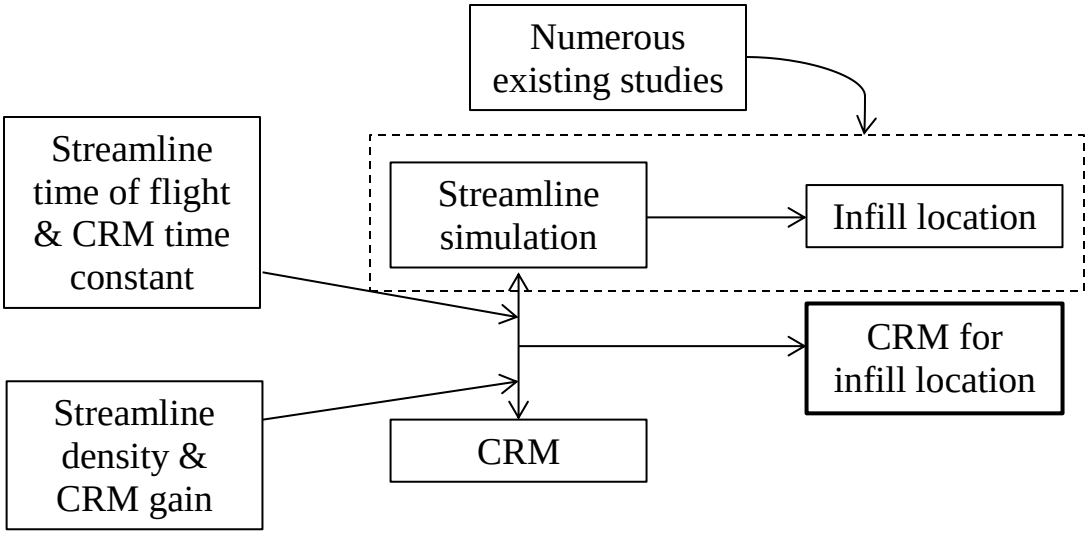

Figure 4.18 The systematic approach to determine how to use the CRM for infill locations

Based on these previous studies, the key output of the SLS and the CRM are identical. The application of the SLS to determine a potential infill location was described in chapter 2 and because these 2 methods are related, the way the SLS was used will be analogous to determine how the CRM will be used. Taking into account the 2 essential factors for good infill performances and the analogue of the SLS, the hypothesis can be made that areas with low gain, high oil saturation and high pore volume are attractive for new infill producers, as displayed in Figure 4.19.

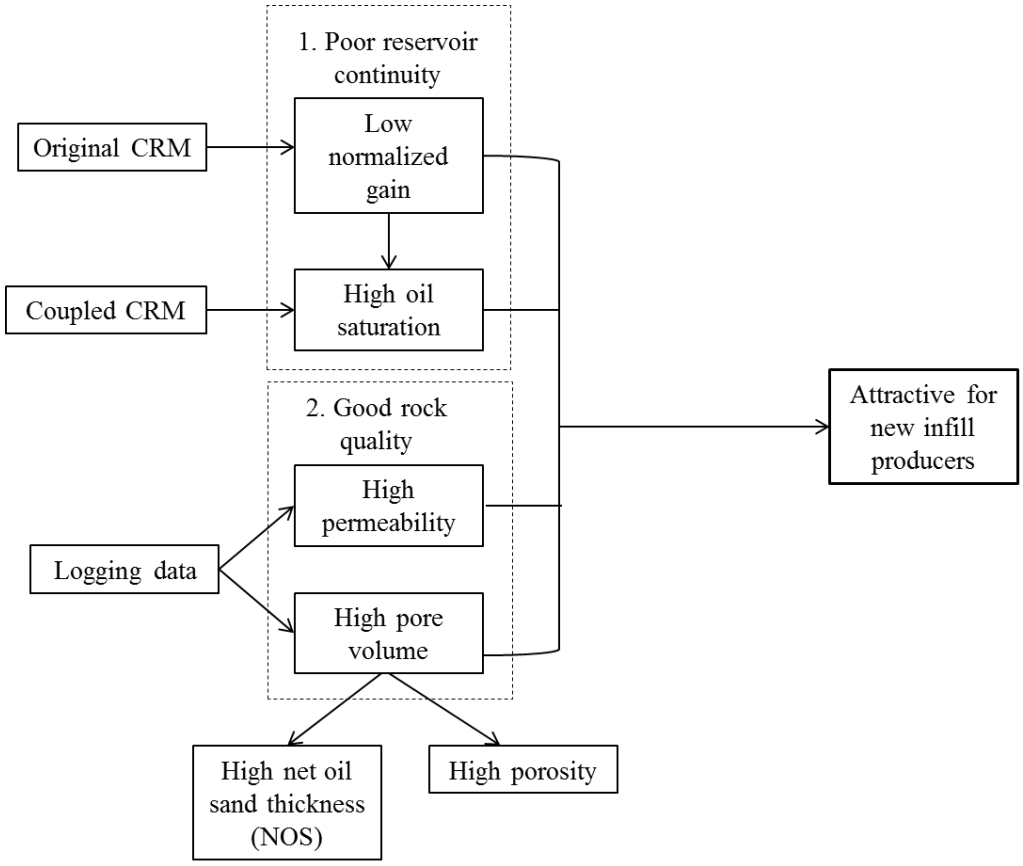

Figure 4.19 Procedures to determine infill locations

Some terminology from Figure 4.19 requires clarification. Firstly, the calculated interwell connectivity or gain is actually relative to each injector. Gains from different injectors are not comparable. By definition, it is the ratio of injected water from an injector contributing to the production of a producer to the total injection rate of that injector. For instance, a producer gets support from 2 injectors; INJ1 with a gain of 0.2 and INJ2 with a gain of 0.5, this does not mean INJ2 contributes to the production of this producer more than INJ1 because their average injection rates may be dissimilar. While the streamlines emanating from each injector in the SLS can be compared directly as each single line throughout the reservoir represents the same amount of flowing fluids, the

CRM's gains must be normalized so that they are comparable. The normalization simply follows the formulation below:

$$Normalized\ gain = \left[\frac{W_{inj,avg}}{W_{inj,avg,max}}\right] \times Gain \tag{4.10}$$

where $W_{inj,avg}$ is the average injection rate of an injector in the fitting period and $W_{inj,avg,max}$ is the $W_{inj,avg}$ of the injector injecting the maximum amount of water in the fitting period. For illustration purpose, the normalized gains should be rescaled so that they range from 0 to 1 using this equation:

$$Normalized\ gain\ (rescaled) = \frac{Normalized\ gain}{Max(Normalized\ gains)} \tag{4.11}$$

The connectivity maps presented later in this chapter will be represented by the normalized gain (rescaled), which will enable the comparison of the gain densities among each area, similar to the streamline map. Analogous to the SLS, an area with low gain density is poorly drained and poorly swept resulting in high remaining oil saturation. Therefore, the coupled CRM is expected to deliver a saturation distribution that is corresponds with the distribution of the gains.

In term of rock qualities, interpreted logging data of all wells were gathered to generate reservoir characteristic maps of permeability, net oil sand thickness (NOS) and porosity. The average permeability and porosity of each well are determined by weighting with the NOS as shown in these equations:

$$k_{avg} = \frac{\sum_{i=1}^{n} k_i\, h_i}{\sum_{i=1}^{n} h_i} \tag{4.12}$$

$$\emptyset_{avg} = \frac{\sum_{i=1}^{n} \emptyset_i\, h_i}{\sum_{i=1}^{n} h_i} \tag{4.13}$$

where h is the thickness of a sand layer and n is the total number of sand layers in that well. Hence, $\sum_{i=1}^{n} h_i$ is the NOS of that well. By inputting the data of each well, these maps were created using the kriging interpolation technique developed by Matheron

(1960). They represent the two-dimensional distribution of interested reservoir properties and can depict which area has good or poor properties. All of these reservoir characteristic maps will be presented together with the CRM's connectivity and saturation maps in the following section.

4.2.3 Validation

The method explained in section 4.2.2 will be validated with actual infill wells' performance previously presented in section 4.2.1. The combination of maps consisting of the connectivity, the saturation, the thickness, the porosity and the permeability maps, are analyzed simultaneously. The analysis is divided into 2 groups based on different timing of infill wells, which are 2007 and 2009. To make the realistic assessment, when considering the 2009 group, all data obtained after 2009 will be excluded from the analysis. For example, the CRM's fitting period of this group is from 2002 to 2008. Nevertheless, because of some limitations, the reservoir characteristic maps were generated using the same data input for both the 2007 and 2009 groups.

4.2.3.1 Validation with 4 infill wells drilled in 2009

Six maps including the connectivity, the saturation (both the bubble and the kriged one), the thickness, the porosity and the permeability maps, are presented in Figure 4.20 - 4.25. There were 2 maps of the oil saturation constructed based on different methods as explained in the previous chapter. The reservoir analyzed in this work is enclosed by the dashed line; the areas outside this line are ignored. These maps were generated to analyze if the potential areas identified by them correspond with the performance of these 4 infill wells. The fitting window for both the original and the

coupled CRMs is from 2002 to 2008. All the gains presented in the connectivity map are normalized. All maps are overlaid with the locations of these 4 infill wells, colored according to their performance. The green, blue and red ones are the good, fair and poor infill wells as categorized in Table 4.3. For the scope of this work, the analysis will be performed qualitatively by comparing among different areas.

As can be seen from the map, the poor ones, W12 and E41, were drilled in the area with higher gains compared to the area where E40, the good one, was drilled. On the other hand, E39, the fair one, seems to be in the area with the lowest gains. This is because there is no gain from any injector supporting E19, which is not realistic. As discussed in section 3.4.3, E19's production history has strong evidence that the well has good waterflood support; thus it should have many streamlines passed through, but the CRM allocates this injection to other producers, rather than this well.

Regarding the bubble saturation map (Figure 4.21), because there is no calculation for injectors, the areas around them have no data. Hence, in this case, this map is not useful for this analysis. On the other hand, the kriging saturation map (Figure 4.22) appears to be valuable. It is immediately apparent that E40, one of the good ones, is located in the area with the highest remaining oil saturation compared to the other, E39, E41 and W12.

For all the thickness (NOS), porosity and permeability maps (Figure 4.23, 4.24 and 4.25), the areas with the highest to the lowest properties are the areas around E41, E40, E39 and W12, respectively. The last three ones reasonably agree with their performances. The exception here is that E41, a poor one, was drilled in the area of better reservoir properties than E40, the good one. This can be explained using the gain map, in which the area around E41 was better swept than the area around E40, according to the

gain density. Overall, the qualitative analysis using the integration of these data is able to classify the potential infill locations.

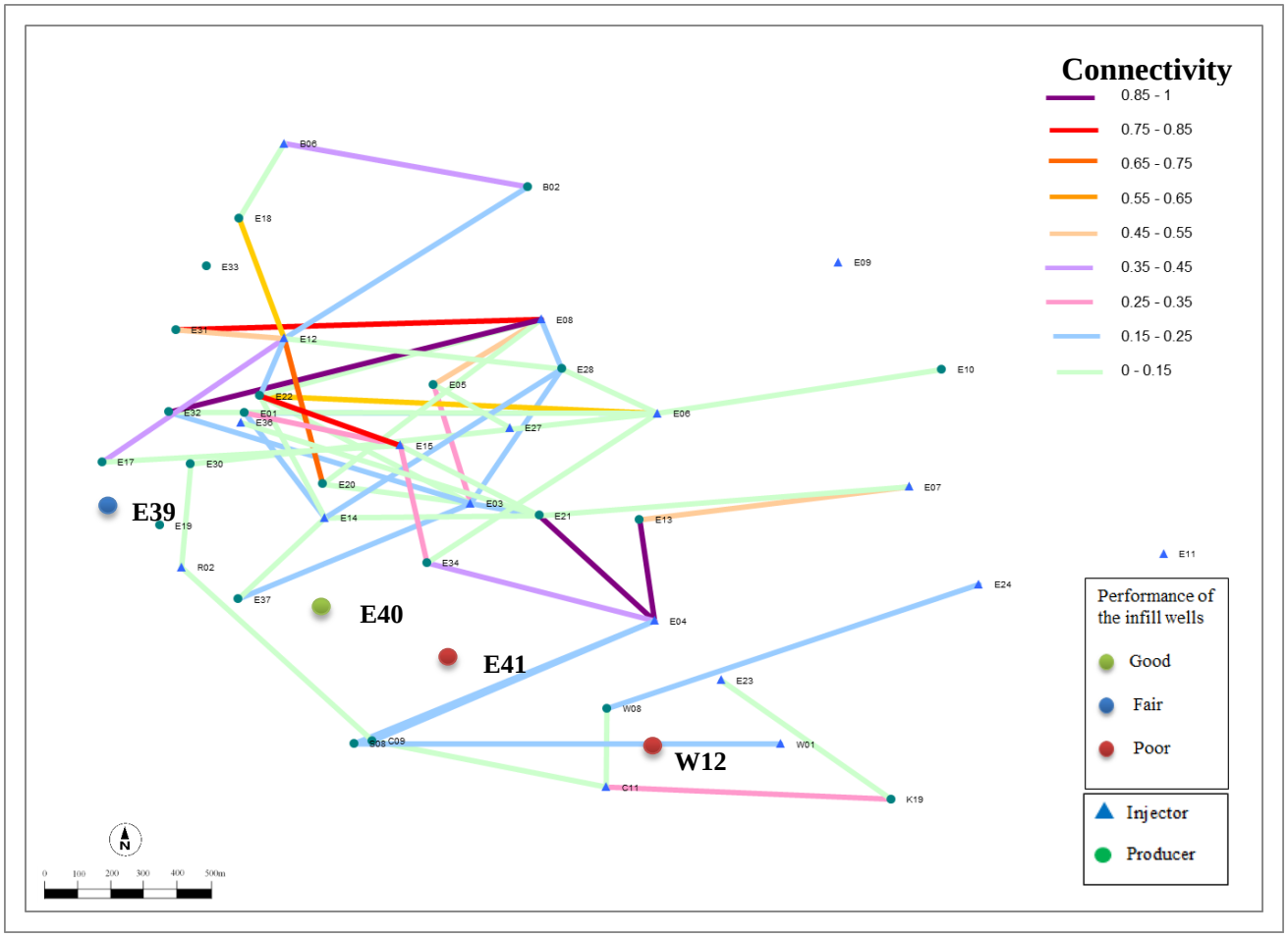

Figure 4.20 The normalized connectivity map overlaid with the locations of the 4 infill wells drilled in 2009

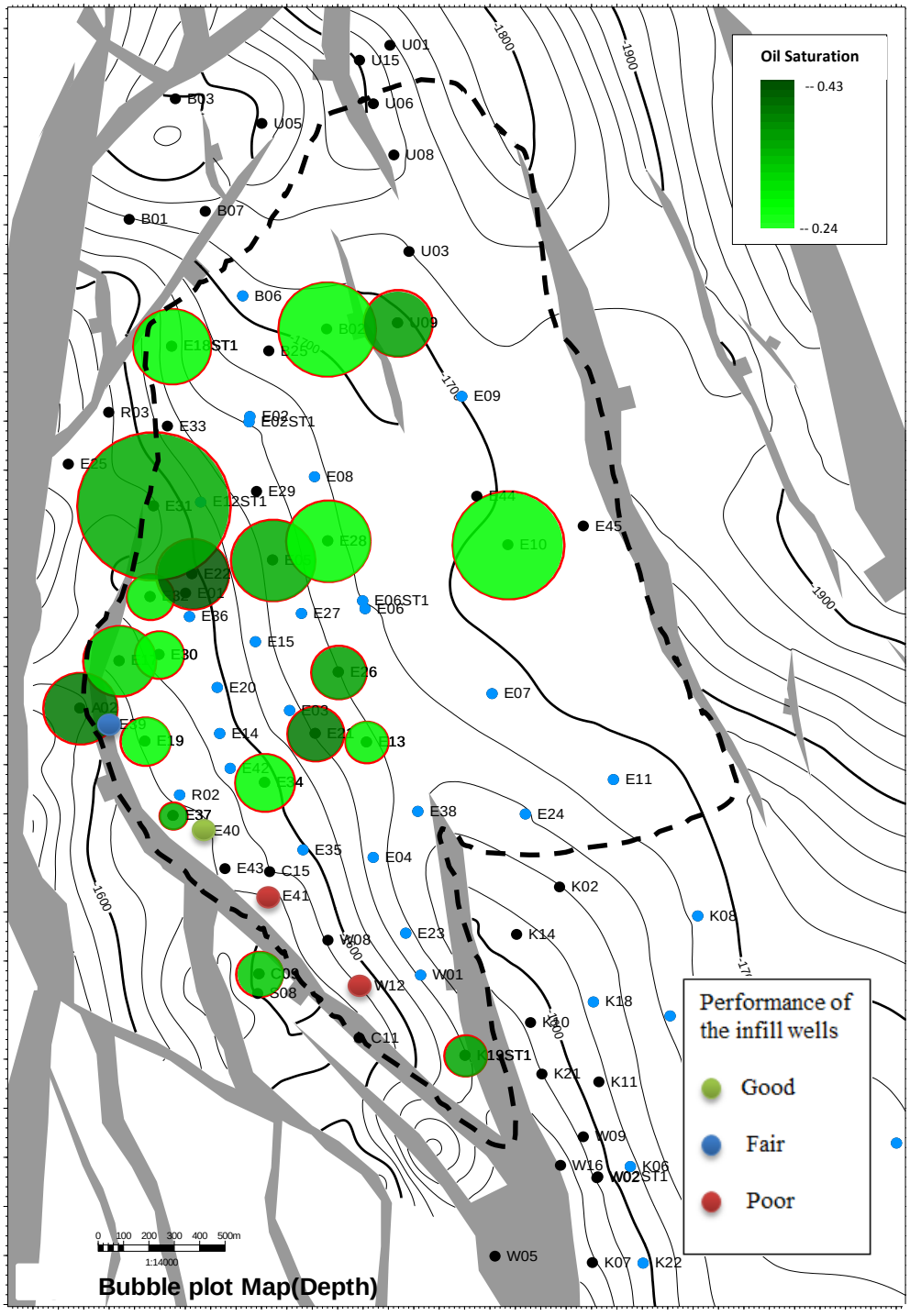

Figure 4.21 The bubble saturation map overlaid with the locations of the 4 infill wells drilled in 2009

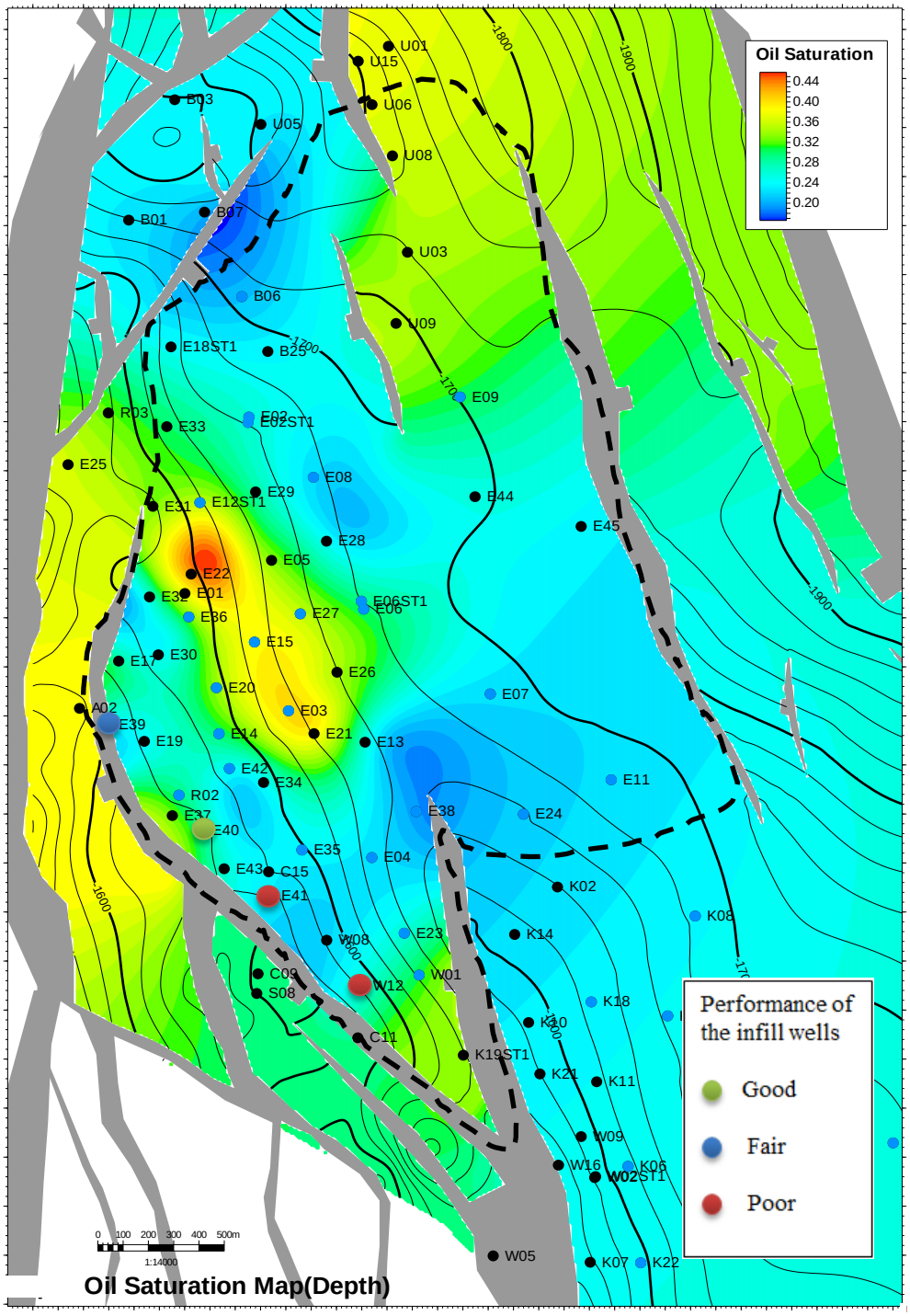

Figure 4.22 The kriging saturation map overlaid with the locations of the 4 infill wells drilled in 2009

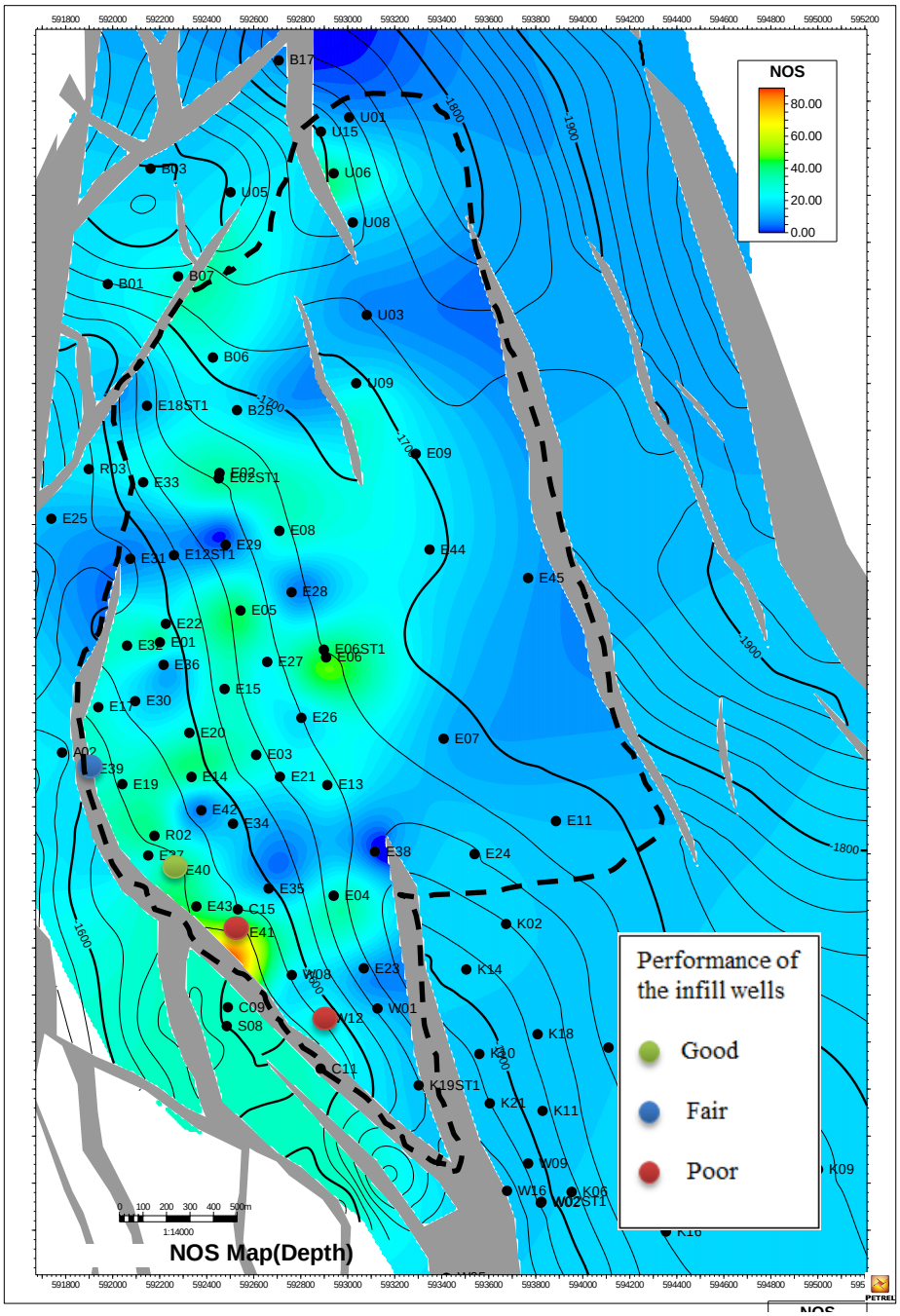

Figure 4.23 The thickness map overlaid with the locations of the 4 infill wells drilled in 2009

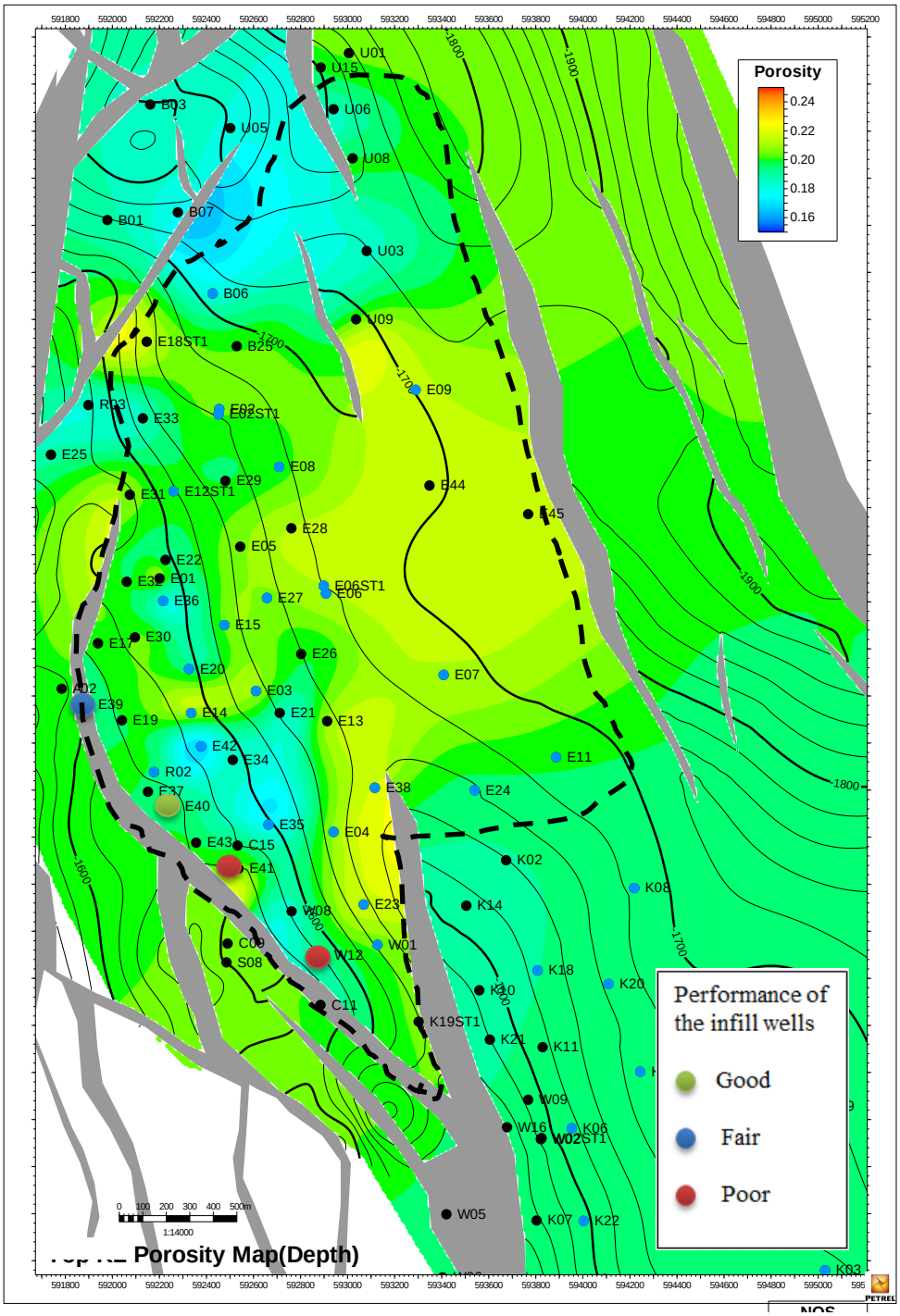

Figure 4.24 The porosity map overlaid with the locations of the 4 infill wells drilled in 2009

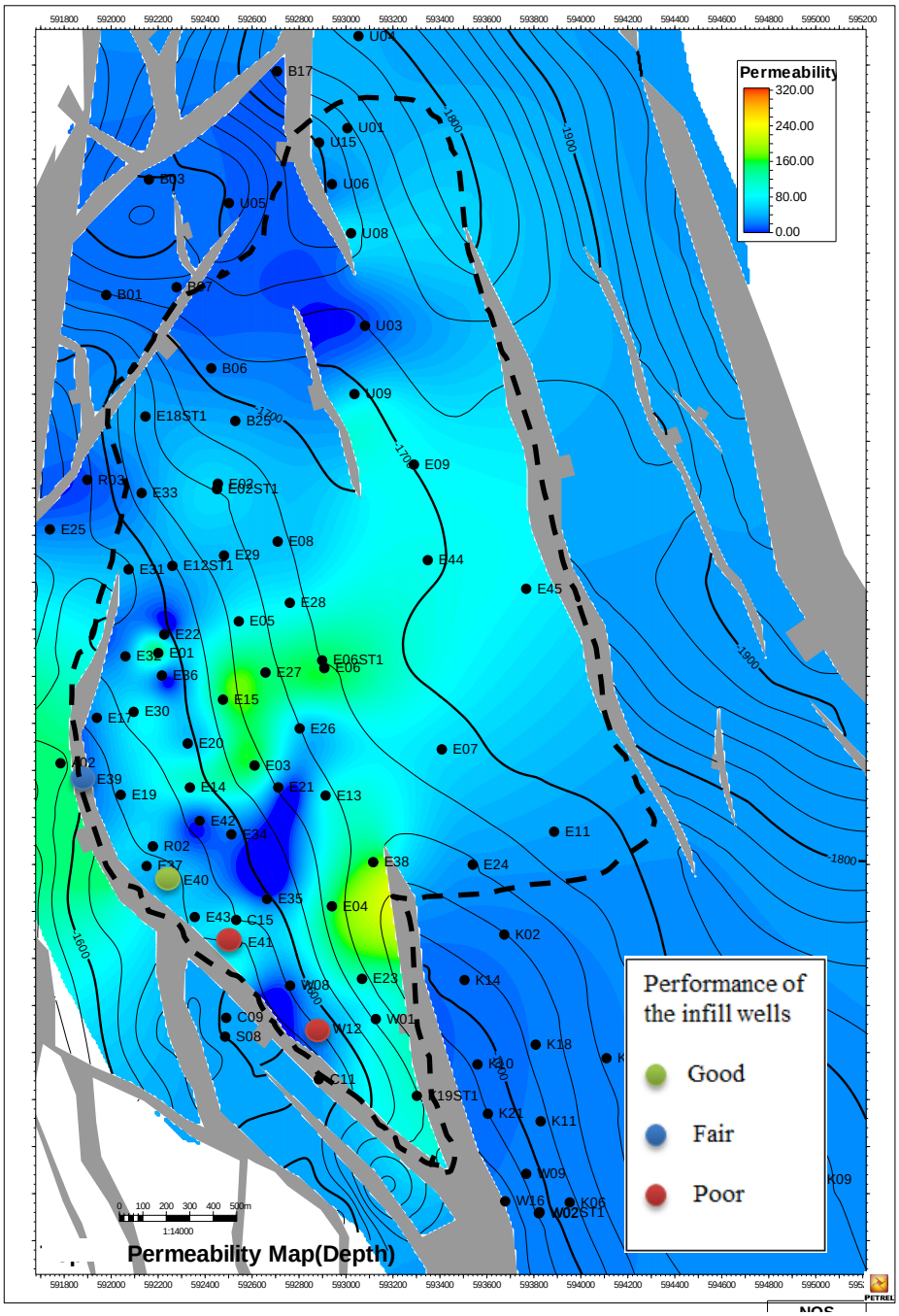

Figure 4.25 The permeability map overlaid with the locations of the 4 infill wells drilled in 2009

4.2.3.2 Validation with 10 infill wells drilled in 2007

For this scenario, all data obtained after 2007 are excluded from the analysis. The CRM's fitting period is selected to be from 2002 to 2006. All the maps, without the saturation map, are shown in Figure 4.26 - 4.29. The saturation is not meaningful in this case because the fitting period is too short leading to the elimination of the data from many wells.

The connectivity map (Figure 4.26) reveals that there were severe injection losses in several injectors, which is actually reasonable because of sparse well spacing at that time (2006). This caused an inefficient waterflood leading to the drilling of 14 infill wells after 2006. Overall, the performance of the infill wells corresponds with the gains. The good wells, E31, E32, E34, E37 and K19, were drilled in the low-gain areas while the poor ones, E36 and E38, were placed in the highly-dense gain areas. These areas were already well swept because of the good connectivities between the existing producers and injectors. This is verified by the actual production of these 2 wells that they were initially producing fluids with water cut of as high as 90 percent. However, it is not extraordinary that the results are still not perfect, i.e. some good wells like E31 and E37 are situated in the areas of lower gain than the best infill well, E32, are. This emphasizes the necessity to incorporate the reservoir characteristic maps into the analysis.

According to the permeability map (Figure 4.27), overall, the better infill wells were placed in the areas with higher permeability than the poorer ones. For instance, K19 and E37, which both are good wells, are located in the areas that have higher permeability than the area around W08, the fair one. Correspondingly, the area around E35, the poor one, has lower permeability than the area around W08. There were, however, some exceptions. E34, a good performance one, is located in the area with poor permeability while E38, the worst one, was situated in the good- permeability area. The

porosity map (Figure 4.28) mostly agrees with the permeability map. E38 was again placed in the area of high porosity. It seems like this property does not vary much because of the geological nature of the field, which is a clastic reservoir. It should be more useful for a reservoir that was deposited in the carbonate environment where the porosity can vary significantly because of the presences of vugs.

The thickness map (Figure 4.29) also shows agreement between the reservoir thickness and the infill wells' performance. Moreover, it provides an insight to the questionable E38 mentioned in the previous paragraph. Despite located in a high porosity and permeability area, the area surrounded E38 has extremely low net oil sand thickness (NOS) causing the poorest performance among all the infill wells. This area has low NOS because the sweep efficiency was good as revealed by the connectivity map (Figure 4.26). The interwell connectivities between the down-dip injectors, E24, E04 and E07, and the up-dip producers, E13 and E21, were good. As a result, the good peripheral flooding in this area causes oil to be well displaced by water to the producers leading to the high water saturation. Most reservoir layers here were already filled with water resulting in low oil sand thickness. This underlines the advantage of the combination of all maps for the analysis as doubtful scenarios from some maps may be explained by other maps.

Generally, all the data including the connectivity, the saturation, the porosity, the permeability and the thickness should be integrated simultaneously to obtain reliable results as demonstrated with the field case study here.

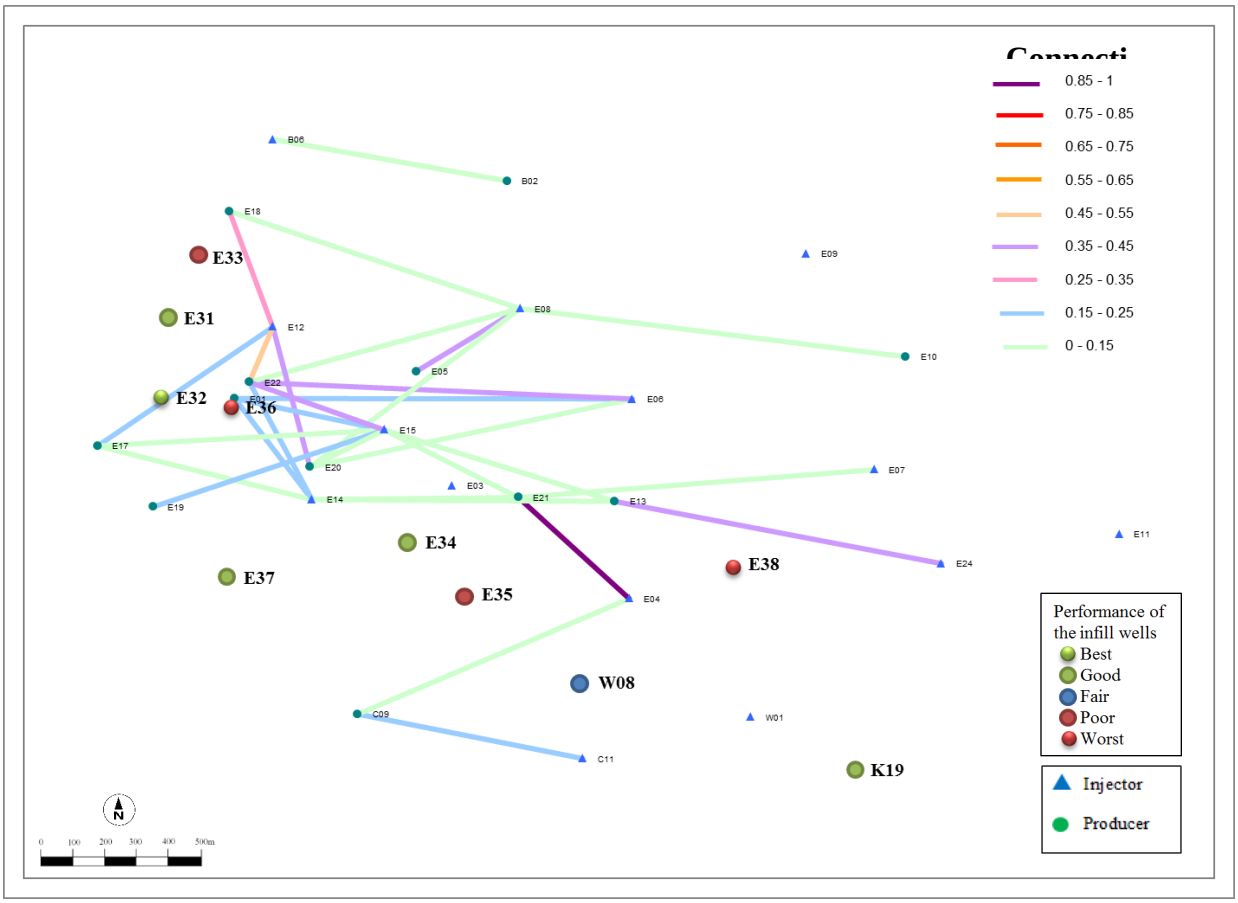

Figure 4.26 The normalized connectivity map overlaid with the locations of the 10 infill wells drilled in 2007

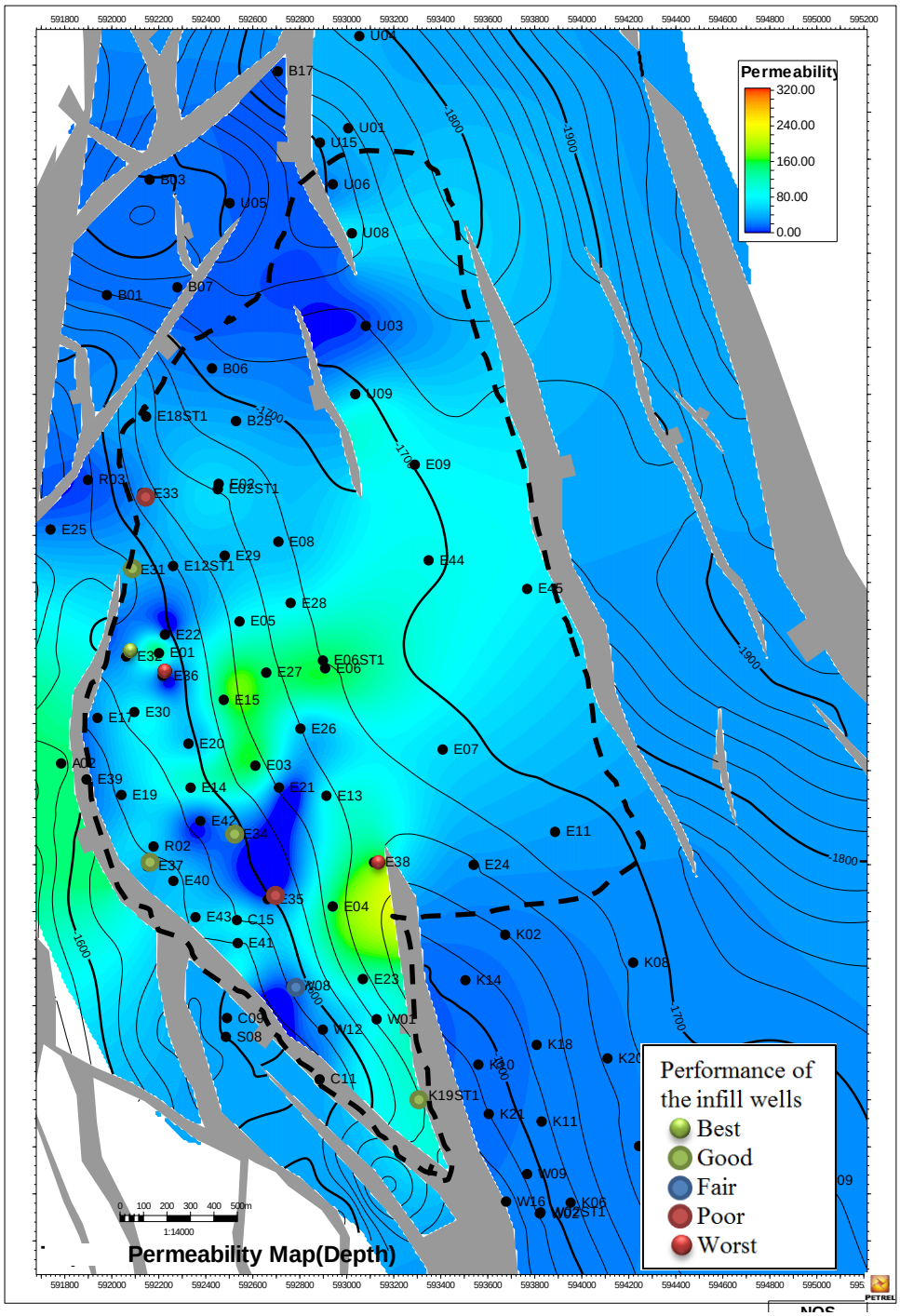

Figure 4.27 The permeability map overlaid with the locations of the 10 infill wells drilled in 2007

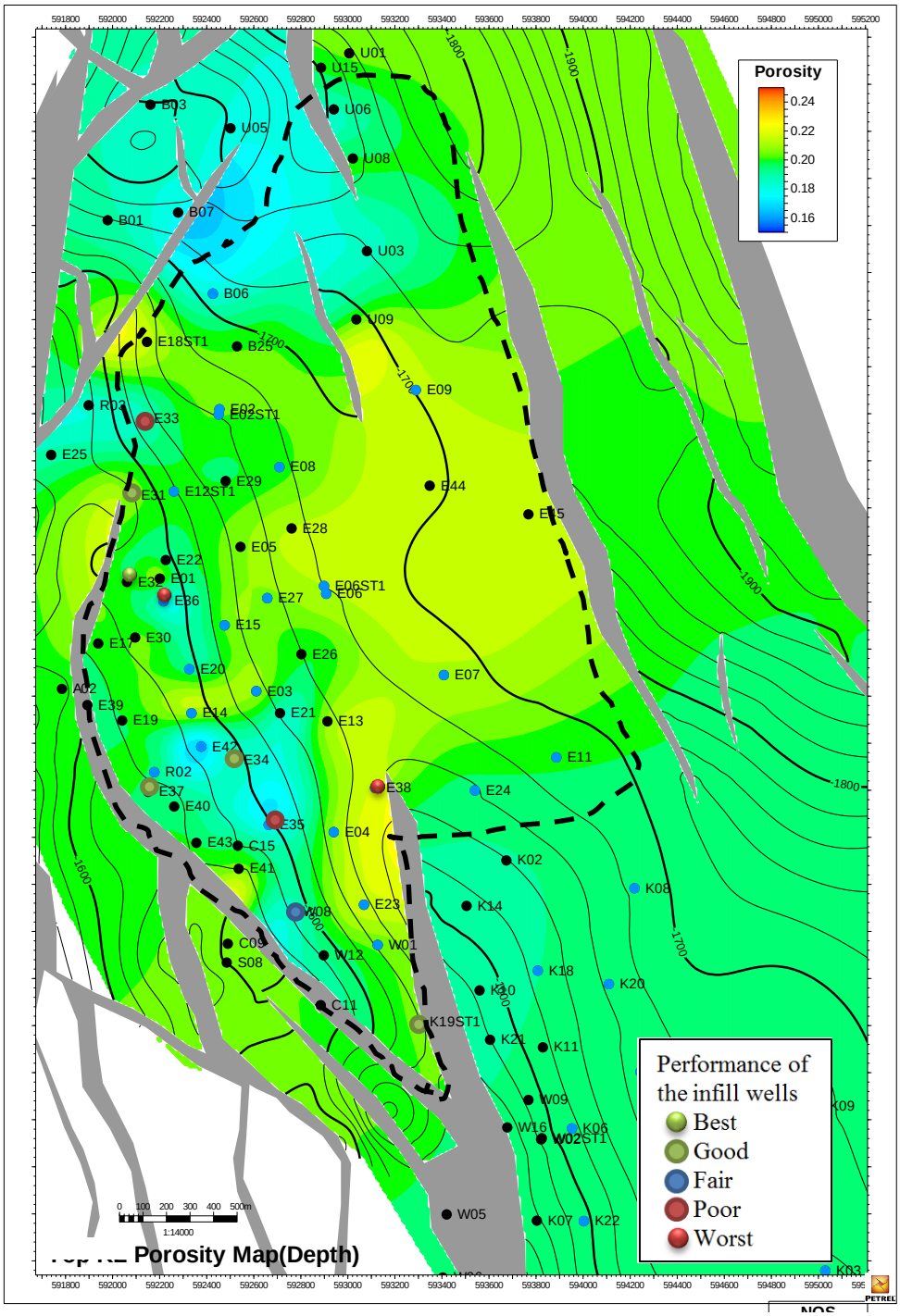

Figure 4.28 The porosity map overlaid with the locations of the 10 infill wells drilled in 2007

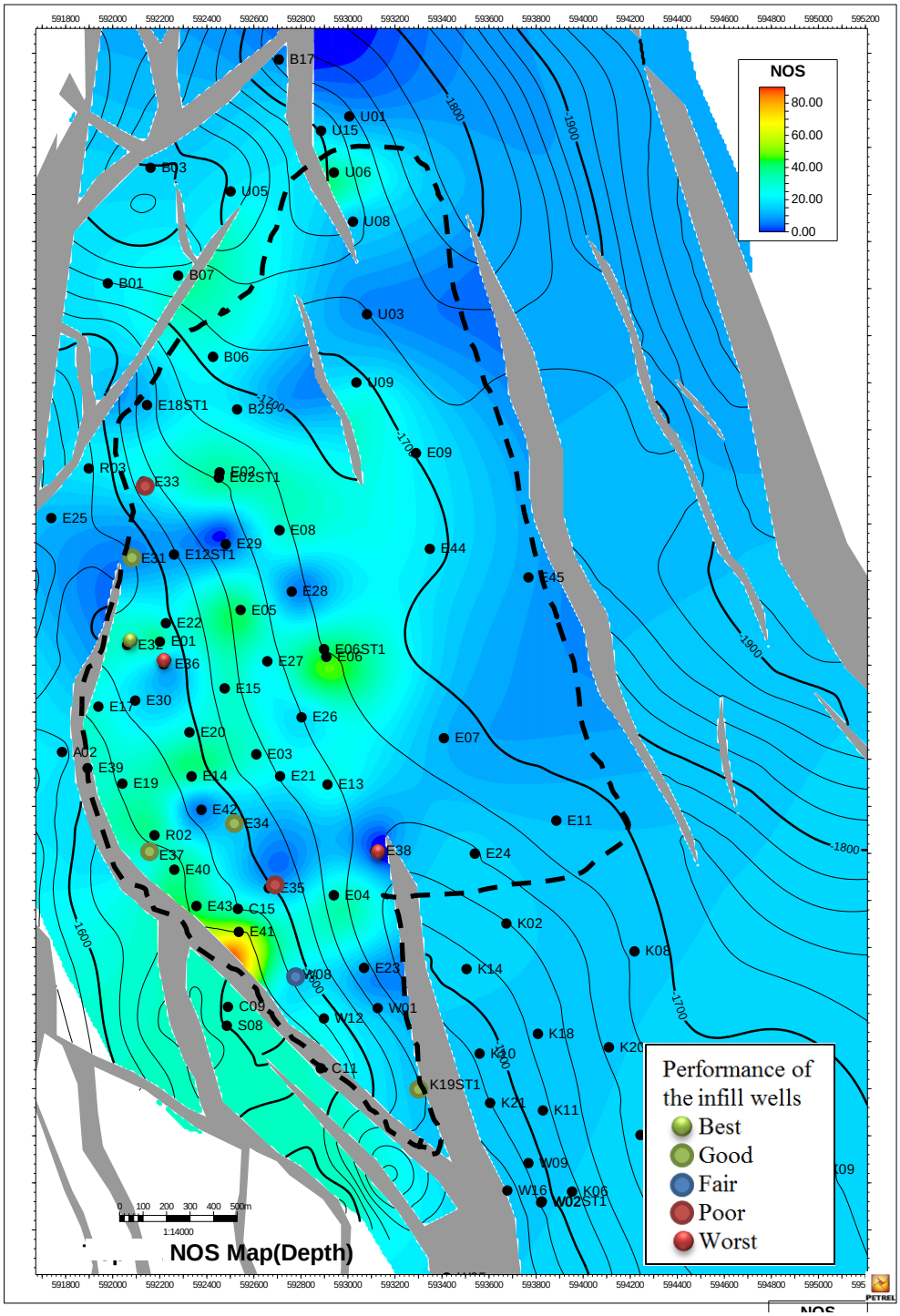

Figure 4.29 The thickness map overlaid with the locations of the 10 infill wells drilled in 2007

4.2.3.3 Evaluation of the predictive accuracy of the input parameters for the identification of potential infill locations

This section will provide a quantitative analysis of the predictive accuracy of all the input parameters, including the gain, saturation, thickness, porosity and permeability, to identify the potential infill locations as discussed in the previous section. The evaluation will be performed based on the obtained results of the infill wells drilled in 2007 and 2009 as explained in the previous sections. In addition, the analysis is carried out for all possible parameter combination scenarios consisting of single parameters and the combinations of 2 to 5 parameters.

4.2.3.3.1 Method

A rank statistic was used to quantify the accuracy of each scenario using the following procedures:

1. Sort infill wells (IFs) based on their actual performance. Hypothesizing that there are 4 infill wells drilled in 2005, namely, A, B, C and D. Based on 10-year cumulative oil production (N_p), their performance can be sorted as:

   A > B, C > D

   which means well A is the most successful infill well while well 4 is the worst.
2. Read the values of each parameter at the locations of these IFs. Unlike other parameters, for the gain, its density at each location was determined subjectively. The location that is adjacent to many dark-color gains is considered to have good reservoir continuity, which is not attractive for an infill well. Suppose there are 2 parameters to be analyzed: permeability and porosity. The wells are sorted in descending order based on the value for that parameter. For example:

For permeability: D > A > B > C

For porosity: B > A > C > D

which means the location that well D was drilled has the highest permeability compared to others.

3. Determine all possible scenarios from combinations of the parameters. The total number of scenarios $= \sum_{n=1}^{N_{pa}} \binom{N_{pa}}{n}$ where N_{pa} is the total number of parameters and $\binom{N_{pa}}{n}$ is the number of combinations of N_{pa} objects taken n at a time. For this example, there are 3 scenarios:

   Scenario 1: using only permeability to analyze the potential infill locations

   Scenario 2: using only porosity

   Scenario 3: using both permeability and porosity

   in which scenario 1 and 2 are called single-parameter scenarios while scenario 3 is a multiple-parameter scenario. For the scope of this research, the N_{pa} is 5.

4. Calculate the total error scores for each scenario, beginning with the single-parameter scenarios. The total error score is defined as the total number of wrong orders determined from all possible pairs. The higher the total error score, the less accurate the parameter or combination of the parameters suggests the potential infill locations. The following procedures explain this in detail:

   i. Match all possible pairs of IFs. The total No. of pair = $\binom{N_{IF}}{2}$ where N_{IF} = the number of infill wells. For this example, there are 4 wells so that there will be 6 pairs.

   ii. Compare the order of each pair to the order obtained from the actual performances (step 1).

      a) If the order is right, do nothing.

b) If the order is half-right; i.e. they should be equal but the parameter suggests that one is higher than another one, then add 0.5 to the error score.

c) If the order is wrong; i.e. one should be higher than another one but the parameter suggests that one is lower than another one, then add 1 to the error score.

For scenario 1 as an example, the first pair is A and B. The permeability suggests that A is higher than B corresponding to the actual performance; thus nothing added to the error score. Similarly, A and C are correctly arranged. On the other hand, D is higher than A based on the permeability, which is opposite of the order of the actual performance; thus adding 1 to the error score. For the pair of B and C, the permeability suggests that B is higher than C while the actual performance states that C is higher than B; thus adding 0.5 to the error score. Doing the same for all 6 pairs and ultimately, the total error score obtained is 3.5.

5. Repeat step 4 for all single-parameter scenarios. For this example, scenario 2 has the total error score of 1.5.
6. Consider multiple-parameter scenarios; calculate the total error scores for each scenario. For this example, there is only one multiple-parameter scenario, which is scenario 3.
    i. For each well, determine the rank score of each parameter. A well is given a descending rank based on the value for that parameter. The location of the well with the highest value is given rank 1 and so on. For example, the rank scores of permeability and porosity of well A are 2 and 2 because the

magnitudes of these properties at the location of well A are at the second place.

ii. Calculate the total rank score for that well by multiplying the rank scores of each parameter. The total rank score is defined as the number that combines all the effects from the considered parameters, in which for this case, are permeability and porosity. The higher the total rank score, the poorer the location is, as suggested by the considered parameters. The total rank score for well A is 4.

iii. Repeat step i and ii for all wells. This is illustrated in Table 4.4.

Well	Rank score of permeability	Rank score of porosity	Total rank score
A	2	2	4
B	3	1	3
C	4	3	12
D	1	4	4

Table 4.4 The total rank score for scenario 3

iv. Obtain the order determined by the combination of the parameters by sorting infill wells based on their total rank scores. According to this table, the combination of permeability and porosity suggests that the potential locations for infill wells are:

$$B > A, D > C$$

v. Repeat step 4 to calculate the total error score of each multiple-parameter scenario. The total error score for scenario 3 is 3.

7. Repeat step 6 for all multiple-parameter scenario. Finally, the total error scores for all possible scenarios are obtained. For this example, the result is summarized in Table 4.5.

Scenario	Total error score
1 (only permeability)	3.5
2 (only porosity)	1.5
3 (both permeability and porosity)	3

Table 4.5 The total error scores for each scenario

Based on the result of this hypothesized example, using only porosity is the most accurate method to identify the potential infill locations.

4.2.3.3.2 Results and Discussions

Using the method explained in the previous section, the total error scores for all possible scenarios, given 5 parameters including the gain, the saturation, the thickness, the porosity and the permeability, can be determined. The objective is to quantify the predictive accuracy of the parameters and their combinations. The accuracy increases with decreasing total error score. In addition, the base scenario is defined here to be a benchmark for the comparison. This scenario is created from the infill performances predicted by field personnel (the blue bar in Figure 4.17). An infill well with high pre-drilled reserves is expected to have good performance. The total error score is calculated from the order of infill wells arranged based on their performances.

The results for the 4 infill wells drilled in 2009 are presented in Figure 4.30. Note than the total error scores were normalized to be between 0 and 1. On the x-axis, $\lambda S_o \emptyset$ refers to the scenario of combining the gain, the saturation and the porosity to identify the potential infill locations. There are totally 31 possible scenarios for these 5 parameters, arranged on the x-axis from the smallest one to the largest five combinations of the input parameters. The horizontal line represents the total error score of the base scenario, which acts as the benchmark for the comparison. The scenario that has the total error score higher than that of the base scenario means the accuracy of using those parameters to

identify the potential infill locations is poorer than that of the prediction performed by field personnel.

Individually, CRM's outputs, the gain and the saturation are more accurate than the reservoir properties as indicated by the lower total error scores. The porosity alone seems unhelpful because the reservoir rock is clastic inferring that the areal distribution of the property is relatively uniform, unlike the carbonate system, where the porosity can differ significantly because of vuggy and moldic pores. Moreover, the average total error score of the 2-parameter scenarios is lower than that of the 3-parameter scenarios. This finding can be inferred that using more properties actually does not guarantee a more accurate result, especially when there are some properties (in this case, the porosity) that considerably misleads the interpretation. On the other hand, the most accurate methods are the combinations of S_o, $\lambda S_o h$ and $\lambda S_o k$. Generally, the combination of the relevant input parameters should increase the accuracy because they help each other to mitigate the errors caused from a single parameter.

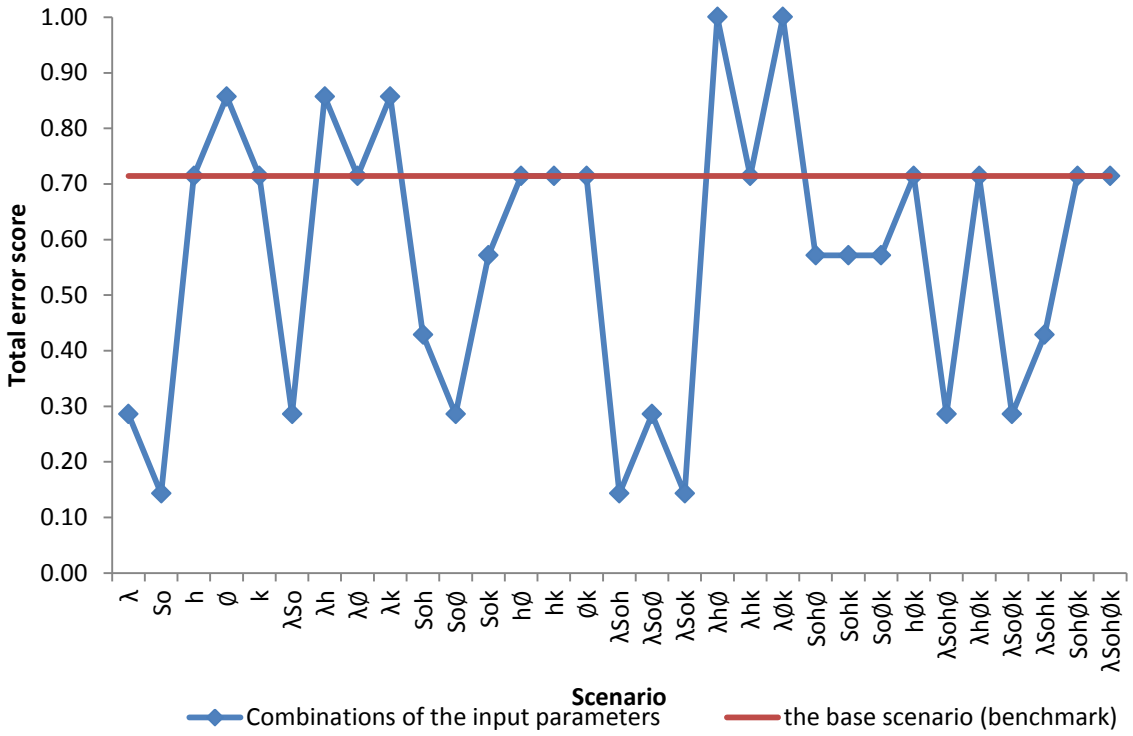

Figure 4.30 The total error scores of each scenario for the 4 infill wells (2009)

Next, the results for the 10 infill wells drilled in 2007 are presented in Figure 4.31. The oil saturation is not available for the analysis of this case resulting in fewer scenarios than the case of 4 infill wells. For this case, with the more wells, many scenarios provide better predictive accuracy than the base case. The average total error score is 0.7, while the value of the benchmark is 0.76. Likewise, the combinations of 3 to 4 parameters seem to provide more accurate results than the base case. Individually, the gain and the thickness outperform the permeability and the porosity in term of the predictive accuracy. As for the previous case, the porosity is the poorest parameter indicated by the highest total error score, emphasizing that it might not be useful for this field. In addition, the best scenario is the combination of the good individual ones, the

gain and the thickness. This observation certifies that the combination of appropriate parameters can yield the highest accuracy.

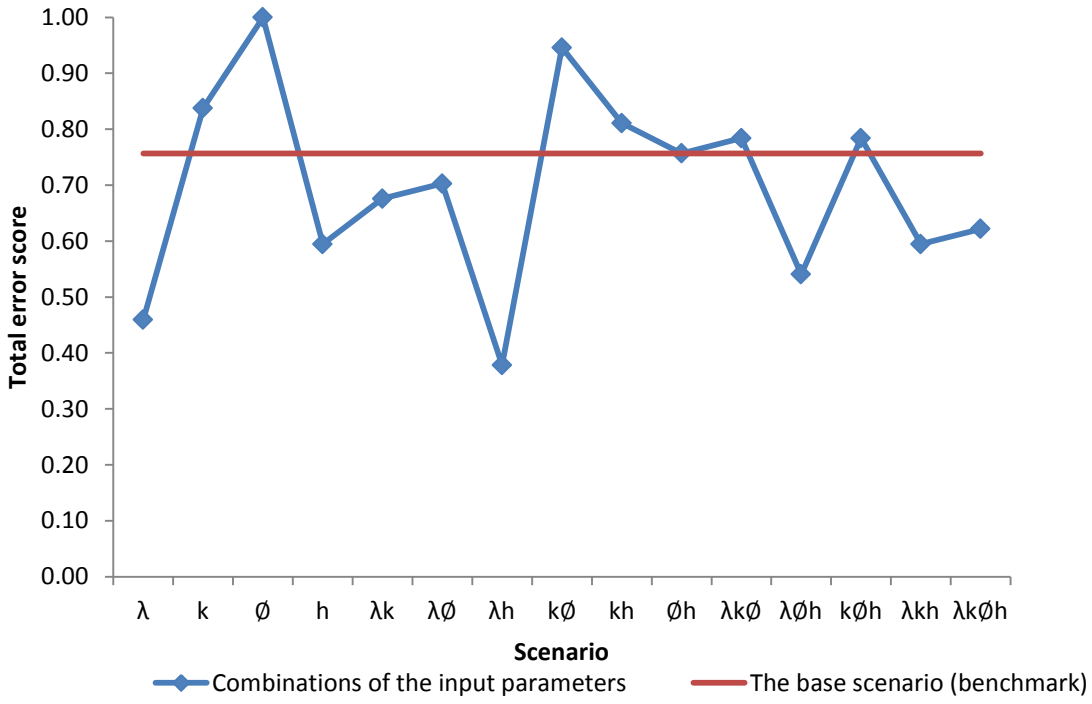

Figure 4.31 The total error scores of each scenario for the 10 infill wells (2007)

Chapter 5: Summary and Recommendation

The primary objectives of this research were to properly apply the CRMs to actual field data and to use the output from the CRMs to determine potential locations for infill producers. Ultimately, a novel method was established and successfully validated with actual infill wells' performance. This chapter presents a summary of this work and recommendations for future research in this area.

5.1 Summary

A significant amount of bypassed oil often remains in a mature waterflooded reservoir because of non-uniform sweep. Infill drilling is one of the most attractive options for increasing oil recovery because of its operational simplicity, low risk and promising results. Targeting proper infill location is a complex task and conventionally requires a comprehensive reservoir characterization program such as streamline simulation (SLS), integrating both geological and engineering data. Despite encouraging and robust output obtained from SLS, achieving a good and reliable model requires massive effort. This inspired the establishment of an alternative method, the CRM, which is fast, cheap, yet robust.

Firstly, the application of the CRM to an oil field in Southeast Asia led to the identification of several key challenges and the emphasis on examining the input data. Well interventions such as wireline and workover activities, disrupt the continuity of the production. Furthermore, additional perforations, zone changes and recompletion change well productivity indices; thereby violating current CRM assumption. Therefore, a well's production history must be examined to identify key events that can affect production rates, rather than an injection and FBHP changes. Generally, rate jumps or drops because

of primary recovery do not last long, and this was addressed by manually removing them from the fitting. The data of wells producing from electrical submersible pump (ESP) mostly have good quality for the CRM as this artificial lift tends to operate continuously with little interference. The issue of existence of free gas was handled by adding the free gas production into liquid production. On the other hand, the absence of the FBHP data was dealt within a straightforward way by substituting the surface well-head pressure (WHP) for FBHP as they are physically related and fluctuate up and down almost together.

The coupled two-phase CRM requires some additional input. The reservoir pore volume associated with each producer is determined from matching each well's historical water cut with Koval's equation. However, dealing with field data is more complicated as the trend often did not follow the theory because of early water breakthrough in a thief zone or poorly managed waterflood. The result reveals that the early-drilled wells tend to have larger drainage area than the late wells because of the larger production time. For the settings of the model's parameter, the selection of the fitting interval is one of the most critical steps. Fitting periods that should be avoided are during reservoir fill up; when the voidage replacement ratios were much greater than 1, high and unstable producing GOR, declining gross production rate that are unresponsive to injection. Nonetheless, a higher number of data points available for fitting will lead to better fitting quality. The radial limit should be determined based on the depositional environment of the reservoir, the well spacing and the depletion observed from RFT pressures.

For the results, overall, the CRM yield a good fit at both field and well levels. The quality of well by well matching seems to depend on the available number of data points of that well. It was observed that all wells with low r-square values have very limited available data for matching. The majority of the gain values, which is the key information

obtained from CRM, are less than one-third meaning that one injector generally provides support to several surrounding producers. They also reveal the good efficiency of the waterflood strategy as there are only 2 injectors having injection loss because of their remote down-dip locations. In addition, the gains are oriented equally in all directions except in east and northeast direction, which is reasonable as the reservoir is dipping toward the east.

It can be geologically inferred from the gain that the field is mildly anisotropic; there is no obvious preferential flow path in any specific direction. Moreover, field evidence such as the tracer tests, the RFT pressures and the wells' production history support the CRM results.

Most of the time constant values are in a good range of 20 to 2,000 days indicating that the reservoir conformed to the assumption of slightly compressible fluids. Most of the wells with large time constants are situated at the up-dip location, which is a gas zone; thus it is understandable that their control volumes are highly compressible. The remaining oil saturation provides insight to the analysis of infill drilling. The down-dip part of the reservoir has low potential as it has been peripherally flooded.

Synthetic case studies, which were designed to be anisotropic so that the oil can be trapped at the end of the simulation, showed that the areas with a high amount of bypassed oil are located between the producer and the injector in the direction of low permeability because the flooding is highly efficient in the direction of good connectivity. On the other hand, for the field case, historical infill wells' performances show that the method previously employed to predict the potential location of bypassed oil can be improved; hence it comes to the aim of this work to incorporate the CRMs, along with well logging data to identify proper infill locations. The hypothesis made here is that areas with low normalized gain, high oil saturation and high pore volume are attractive

for new infill producers. This was successfully validated with the actual infill wells' performance of this field. The combination of maps consisting of the connectivity, the saturation, the thickness, the porosity and the permeability maps, are analyzed simultaneously and qualitatively to see whether the potential areas identified by them correspond with the performance of the infill wells. The advantage of combining all maps for the analysis is that doubtful scenarios from some maps may be explained using information in other maps. Generally, the integrated examination of these data is theoretically expected to help locate the bypassed oil and provide an insight to the reservoir characterization and the waterflood performance. Ultimately, a proper infill location can be identified based on the good understanding of the reservoir.

Specifically, the analysis on this field found that the most accurate method is to combine S_o, $\lambda S_o h$ and $\lambda S_o k$ in order to come up with infill location. In addition, using more properties actually does not guarantee a more accurate result, especially when there are some properties that considerably mislead the interpretation. However, the combination of the relevant input parameters should increase the accuracy because they help each other to mitigate the errors caused from a single parameter. In other word, the potential area needs to have both poor reservoir continuity and good rock quality so that it is likely to yield a satisfying infill performance.

5.2 Recommendations for future work

1. The CRM's assumption of constant well productivity index (PI) for the whole fitting period is easily violated when applying to field data because of well activities. This work addressed the issue by manually removing the non-relevant data points. However, the CRM should be extended to theoretically handle the variable PIs.

2. The effect of removing the primary-recovery production data, free gas inclusion and the substitution of the flowing bottomhole pressure by the flowing wellhead pressure, should be quantified. The relationship of the amount of free gas presented in a reservoir and the degree of inaccuracy of the CRM's output should also be examined. In addition, the FBHP can be physically determined from the WHP using the existing multiphase flow correlations. One can attempt this in a small real field and assess its influence.
3. The sensitivity analysis on the model settings' parameters consisting of the fitting interval, the radial limit and the maximum number of injectors to which a producer can be connected, can be performed. Multiple realizations of the output are generated to evaluate the consistency of the obtained results. Furthermore, in some fields, the well productions are allocated down to the reservoirs. The CRM, which is generally applied to well data, should be also used with the reservoir-level data to evaluate the model's reliability.
4. Heterogeneity and geological features can be imposed on synthetic case studies to evaluate the effect on the identification of infill locations. Similarly, the CRM should be applied to a field that has a robust full-field finite-difference simulation available so that the potential areas identified by both techniques can be compared.
5. The concept of interference well testing, especially pressure-pulse testing, should be involved in the estimation of interwell permeability from CRM's time constant. Likewise, the solution to the diffusivity equation with the boundary condition of terminal constant pressure is expected to be related to this study.
6. The identification of infill locations using combinations of the CRM's output and reservoir characteristic maps can be extended to be performed quantitatively. Grids can be assigned to the considered area and the value can be given to each property.

For example, the grid cell that is more permeable than the other one should receive the higher score. The total score of each grid is determined by the combination of all relevant properties and thus can be ranked numerically.

REFERENCES

Al-Mudhafer, W. J. 2013. A Practical Economic Optimization Approach with Reservoir Flow Simulation for Infill Drilling in A Mature Oil Field. SPE 164612, presented at the North Africa Technical Conference & Exhibition, Cairo, Egypt, Apr., 15-17.

Albertoni, A. 2002. Inferring Interwell Connectivity Only From Well-Rate Fluctuations in Waterfloods. M.S. Thesis, The University of Texas at Austin, Austin, Texas.

Albertoni, A., and Lake, L. W. 2003. Inferring Connectivity Only From Well-Rate Fluctuations in waterfloods. *SPE Reservoir Evaluation and Engineering Journal,* **6**(1):6-16.

Beggs, H. D., and Brill, J. P. 1973. A Study of Two-Phase Flow in Inclined Pipes. 4007-PA SPE Journal Paper.

Cao, F. 2011. A New Method of Data Quality Control in Production Data Using the Capacitancce-Resistance Model. M.S. Thesis, The University of Texas at Austin, Austin, Texas.

Cao, F., Luo, H. and Lake, L. W. 2014. Development of a Fully Coupled Two-phase Flow Based Capacitance Resistance Model (CRM). Paper SPE 169486, presented at the SPE Improved Oil Recovery Symposium, Tulsa, OK, Apr., 12-16.

Can, B., and Kabir, C. S. 2012. Simple Tools for Forecasting Waterflood Performance. Paper SPW 156956, presented at the SPE Annual Technical Conference and Exhibition, San Antonio, TX, Oct., 8-10.

Carman, P. C. 1956. Flow of gases through porous media. Butterworths, London.

Corey, A.T. 1954. The Interrelation Between Gas and Oil Relative Permeabilities. *Producer Monthly* **19**(11):38-41.

Craft, B.C., Hawkins, M.F., and Terry, R.E. 1959. *Applied Petroleum Reservoir Engineering (Vol. 9).* Englewood Cliffs, NJ: Prentice-Hall.

Craig, F. F. 1993. *The Reservoir Engineering Aspects of Waterflooding.* SPE, Richardson, Texas.

Dehdari, V., Aminshahidy, B., and Tabatabaei-nejad, A. 2008. Well Spacing and Recovery Optimization of One of Iranian Oil Fields by Using Streamline and Reservoir Simulation. SPE 112985, presented at the SPE Western Regional and Pacific Section AAPG Joint Meeting, Bakersfield, CA., Mar.-Apr., 31-2.

Dinh, A., and Tiab, D. 2008. Interpretation of Interwell Connectivity Tests in a waterflooding system. SPE 116144.

Dinh, A., and Tiab, D. 2013. Analytical Determination of Interwell Connectivity Based on Flow Rate Fluctuations in Waterflood Reservoirs. SPE 164481.

Driscoll, V. J. 1974. Recovery Optimization Through Infill Drilling- Concepts, Analysis, and Field Results. SPE 4977.

Dykstra, H., and Parsons, R. L. 1950. The Prediction of Oil Recovery by Waterflood. *Secondary Recovery of Oil in the United States* **2**:160-174

Gentil, P. H. 2005. The Use of Multilinear Regression Models in Patterned Waterfloods: Physical Meaning of the Regression Coefficients. M.S. Thesis, The University of Texas at Austin, Austin, Texas.

Gould, T. L., and Munoz, M. A. 1982. An Analysis of Infill Drilling. SPE 11021, presented at the 57th Annual Fall Technical Conference and Exhibition of the Society of Petroleum Engineer of AIME, New Orleans, LA, Sep., 26-29.

Hagedorn, A. R., Brown, K. E. 1965. Experimental Study of Pressure Gradient Occurring During Continuous Two-Phase Flow in Small-Diameter Vertical Conduits. 940-PA SPE Journal Paper, presented at SPE 39th Annual Fall Meeting, Houston, Tx., Oct., 11-14.

Izgec, O., and Kabir, C. S. 2009. Establishing Injector/Producer Connectivity Before Breakthrough During Fluid Injection. Paper SPE 121203, presented at the SPE Western Regional Meeting, San Jose, CA, Mar., 24-26.

Jafroodi, N., and Zhang, D. 2011. New method for reservoir characterization and optimization using CRM-EnOpt approach. *JPSE* **77:**155-171

Kaviani, D. 2009. Interwell Connectivity Evaluation from Well Rate Fluctuations: A Water flooding Management Tool. Ph.D. Dissertation. Texas A&M University.

Kaviani, D., and Jensen, J. L. 2010. Estimation of Interwell Connectivity in the Case of Unmeasured Fluctuating Bottomhole Pressures. *JPSE* **90:**79-95.

Koval, E. J. 1963. A Method for Predicting the Performance of Unstable Miscible Displacement in Heterogeneous Media. *SPEJ* **3**(2):145-154.

Lake, L. W. 1989. *Enhanced Oil Recovery.* Prentice Hall, Englewood Cliffs, New Jersey.

Laochamroonvorapongse, R. 2013. Advances in The Development and Application of A Capacitance-Resistance Model. M.S. Thesis, The University of Texas at Austin, Austin, Texas.

Lee, K. H., Ortega, A., Ghareloo, A., and Ershaghi, I. 2011. An Active Method for Characterization of Flow Units Between Injection/Production Wells by Injection-Rate Design. *SPEREE***14**(4):433-445.

Liang, X., Weber, D. B., Edgar, T. F., Lake, L. W., Sayarpour, M., and Yousef, A. A. 2007. Optimization of Oil Production Based on a Capacitance Model of Production and Injection Rates. Paper SPE 107713, presented at the SPE Hydrocarbon Economics and Evaluation Symposium, Dallas, TX, Apr., 1-3.

Lolomari, T., Bratvedt, K., Crane, M., Milliken, W. J., and Tyrie, J. J. 2000. The Use of Streamline Simulation in Reservoir Management: Methodology and Case Studies. SPE 63157, presented at the SPE Annual Technical Conference and Exhibition, Dallas, TX., Oct., 1-4.

Mamghaderi, A., and Pourafshary, P. 2013. Water flooding performance prediction in layered reservoirs using improved capacitance-resistive model. *JPSE***108:**107-117

Moreno, G. A. 2013. Multilayer capacitance-resistance model with dynamic connectivities. *JPSE***109:**298-307.

Nguyen, A. P. 2012. Capacitance Resistance Modeling for Primary Recovery, Waterflood and Water-CO_2 Flood. Ph.D. Dissertation. The Unitversity of Texas at Austin, Austin, Texas.

Nguyen, A. P., Kim, J. S., Lake, L. W., et al. 2011. Integrated Capacitance Resistive Model for Resesrvoir Characterization in Primary and Secondary Recovery. Paper SPE 147344, presented at the SPE Annual Technical Conference and Exhibition, Denver, CO, Oct.-Nov., 30-2.

Nguyen, A. P., Lasdon, L., Lake, L. W., et al. 2011. Capacitance Resistive Model Application to Optimize Waterflood in a West Texas Field. Paper SPE 146984, presented at the SPE Annual Technical Conference and Exhibition, Denver, CO, Oct.-Nov., 30-2.

Sayarpour, M., Zuluaga, E., Kabir, C. S. and Lake, L. W. 2007. The Use of Capacitance-Resistive Models for Rapid Estimation of Waterflood Performance and Optimization. Paper SPE 110081, presented at the SPE Annual Technical Conference and Exhibition, Anaheim, CA, Nov., 11-14.

Sayarpour, M. 2008. Development and Application of Capacitance-Resistive Models to Water/CO_2 Floods. Ph.D. Dissertation, The University of Texas at Austin, Austin, Texas.

Sayarpour, M., Kabir, C. S., and Lake, L. W. 2009. Field Application of Capacitance-Resistance of Models in Waterfloods. *SPE Reservoir Evaluation and Engineering Journal,* **12**(06):853-864.

Sayyafzadeh, M., Pourafshary, P., and Rashidi, F. 2010. Increasing Ultimate Oil Recovery by Infill Drilling and Converting Weak Production Wells to Injection Wells Using Streamline Simulation. SPE 132125, presented at the CPS/SPE International Oil & Gas Conference and Exhibition, Beijing, China, Jun., 8-10.

Jahangiri, H. R., Adler, C., Shirzadi, S., Bailey, R., Ziegel, E., Chesher, J., and White, M. 2014. A Data-Driven Approach Enhances Conventional Reservoir Surveillance Methods for Waterflood Performance Management in the North Sea. SPE 167849, presented at the SPE Intelligent Energy Conference and Exhibition, Utrecht, Netherlands, Apr., 1-3.

Soroush, M., Jensen, J., and Kaviani, D. 2013. Interwell Connectivity Evaluation in Cases of Frequent Production Interruptions. Paper SPE 165567, presented at the 2013 SPE Heavy Oil Conference, Calgary, Alberta, Canada, Jun., 11-13.

Taware, S., Park, H. Y., Datta-Gupta, A., Bhattacharya, S., Tomar, A. K., Kumar, M., and Rao, H. S. 2012. Well Placement Optimization in a Mature Carbonate Waterflood using Streamline-based Quality Maps. SPE 155055, presented at the SPE Oil and Gas India Conference and Exhibition, Mumbai, India, Mar., 28-30.

Thiele, M. R., and Batycky, R. P. 2006. Using Streamline-Derived Injection Efficiencies for Improved Waterflood Management. SPE Reservoir Evaluation & Engineering, Apr.

Wang, W. 2011. Resesrvoir Characterization Using a Capacitance Resistance Model in Conjunction with Geomechanical Surfacr Subsidence Models. M.S. Thesis, The University of Texas at Austin, Austin, Texas.

Weber, D. B., Edgar, T. F., Lake, L. W., Lasdon, L. S., Kawas, S., and Sayarpour, M. 2009. Improvement in Capacitance-Resistive Modeling and Optimization of Large Scale Reservoirs. Paper SPW 121299, presented at the SPE Western Regional Meeting, San Jose, CA, Mar., 24-26.

Weber, D. B. 2009. The Use of Capacitance-Resistance Models to Optimize Injection Allocation and Well Location in Water Floods, Ph.D. Dissertation, The University of Texas at Austin, Austin, Texas.

Willhite, G. P. 1986. *Waterflooding*. SPE, Richardson, Texas.

Welge, H. J. 1952. A Simplified Method for Computing Oil Recovery by Gas or Water Drive. *Trans. AIME***195:**99-108.

Yousef, A. A., Gentil, P. H., Jensen, J. L., and Lake, L. W. 2006. A Capacitance Model to Infer Interwell Connectivity from Production and Injection Rate Fluctuations. *SPE Reservoir Evaluation and Engineering Journal,* **9**(5):630-646.

Yousef, A. A. 2005. Investigating Statistical Techniques to Infer Interwell Connectivity from Production and Injection Rate Fluctuations. Ph.D. Dissertation, The University of Texas at Austin, Austin, Texas.

Yousef, A. A., Jensen, J. L., and Lake, L. W. 2009. Integrated Interpretation of Interwell Connectivity Using Injection and Production Fluctuations. *Mathematic Geosciences,* **41**(1):81-102.